The T-shaped anisotropic molecule model: a unique perspective of the glass transition and gelation in low valence, directional, network forming liquids

Thesis by
Jennifer Elisabeth Witman

In Partial Fulfillment of the Requirements
for the Degree of
Doctor of Philosophy

1891

California Institute of Technology
Pasadena, California

2010
(Defended December 14th, 2009)

Dedication

To my Grandma-ma, Mary Elisabeth Stewart (1918-2009)

- *My admiration that she loved research, public service and teaching, may I grow to embrace this servant heart*
- *My appreciation that she travelled to family at all time, from her first trip to California to join my Grandfather as that greatest generation fought in the Pacific, to her visits to see me and encourage me in a much smaller struggle 60 years later*
- *My gratitude that she supported me in an illness that had overtaken the lives of her father, sister, and daughter. We rejoice together in modern medicine and, yes grandma-ma, I am still taking my meds.*

You have now joined all the saints before you with our Lord. Feel my hug.

Acknowledgments

I sincerely appreciate the philosophy of my advisor, Professor Zhen-Gang Wang. He views education in the broader sense of giving students freedom for personal development and discovery of vocation. His support of my decision to become a teacher and willingness to defer to an unconventional degree path means a great deal to me.

Professor David Tirrell has similarly given me the gift of exploration into a different side of scientific endeavor. Despite my short time with his group, trying my hand at laboratory research and passing along what I learned to others influenced my career decisions immensely.

The financial support of the NSF for a variety of programs has enriched my life in many ways. Starting from my high school 'Young Scholars' experience at Purdue, sending me for a field season in Antarctica, providing money for graduate work both through the CSEM and an individual fellowship and then creating wonderful material for me to use with my high school students, I hope I will prove a good return on investment.

My first professor will always have a special place in my heart. Thanks, Dad…I know you will always be there to help me with my homework. Mom, I am indebted to the many long hours of conversations, taxi driving, careful monitoring of my education experience and example of life-long inquiry. I also admire and seek to emulate your careful stewardship of your family, your lab, your home and the earth, awareness of your footsteps of all kinds.

Sisters-mine, you are my inspiration. Never stop holding me in account and reminding me of the Truth.

My gratitude to my Witman family, who has welcomed me as a daughter and sister, encouraged me unfailingly, and shares my passion for education.

The multitude people who have encouraged me and prayed with me during my work is too extensive to list. You know who you are…raise a toast for our joint accomplishment!

To my husband~ You make each day possible for me. Team Witman definitely earned this degree!

Abstract

Glass and gel formers exhibit unusual mechanical characteristics and amorphous phases which are highly dependent on their thermal history. We introduce a lattice model with T-shaped molecules that exhibits glassy and gel-like states without introducing artificial frustration. This system has a large number of degenerate energy minima separated by small barriers leading to a broad, kinetically-explored landscape. It particularly replicates valence-limited materials, which can form self-assembled materials with highly controlled physical properties. Despite its remarkable simplicity, this model reveals some of the fundamental kinetic and thermodynamic properties of the glass transition and of gel formation.

A dearth of low temperature experimental and simulation measurements has inhibited investigation in this field. We overcome this difficulty by using a modified Metropolis Monte Carlo method to quickly provide equilibrium samples. Then kinetic Monte Carlo techniques are used to explore the properties of the equilibrium system, providing a touchstone for the non-equilibrium glassy states.

Fully-dense simulation samples reveal a fragile-to-strong crossover (FSC) near the mean-field (MF) spinodal. At the FSC, the relaxation time returns to Arrhenius behavior with cooling. There is an inflection point in the configurational entropy, s_c. This behavior resolves the Kauzmann Paradox which is a result of extrapolation from above the inflection point. In constrast, we find that the s_c remains finite as $T \to 0$. We also observe different kinetics as the system is quenched below the FSC, resulting in non-equilibrium, amorphous states with high potential energy persisting for long periods of time. Simulation samples remain at non-equilibrium conditions for observation times exceeding those permitting complete equilibration slightly above the FSC. This suggests the FSC would often be identified as the glass transition without indication that there is true arrest or a diverging length scale. Indeed, our simulations show these samples do equilibrate if sufficient time is allowed. To elucidate the complex, interdependent relation time and length scales at the FSC will require careful consideration of the spatial-dynamic heterogeneity.

Dynamic mean-field simulations at high density and in the solvated regime reveal a rich range of morphological features. They are consistent with simulated and experimental results in colloidal systems. Stability limits of decreasing length scales beneath the phase separation bimodal coincide into a single curve, which terminates at the fully-dense MF spinodal, suggesting that gelation and vitrification are the same phenomena. Our work indicates that gelation is, therefore, a result of phase separation arrested by a glass transition.

Table of Contents

List of Figures

List of Notation

The symbols and variables listed below are presented in the order of appearance. Some differences do occur between the chapters for clarity in a particular Section and ease of discussion in context of the work of others. The most prominent example is the use of T^* in chapter 1 and T in all other Sections to refer to the dimensionless temperature (the superscript was dropped due to the large number of other temperatures specified).

Some of the symbols are overloaded with several definitions, with the hope that the context will distinguish which meaning is required. We continue the convention in the field of using β not only as in its normal thermodynamic usage but also as the exponent in stretched exponential function. This unfortunate symbolic overlap was particularly problematic for me as a novice, but is so ubiquitous in the literature as to be unavoidable.

In all the work, values were reported with respect to the non-dimensional temperature (${}^{T}\!/_{T_R}$ where $T_R = {}^{\varepsilon}\!/_{k} = 1$). Lower case use of thermodynamic variables indicates that they are the intensive (per site or 'vertex') quantity.

Symbol	Definition (Dimensionless)	Scaling
Abstract:		
s_c	Configuration entropy per site	$(kN^2)^{-1}$
T	Temperature	
Overview:		
T_g	Glass transition temperature	
Chapter 1:		

N	Number of sites along one axis which is our fundamental length scale($N\times N$ is total number of sites)	
$-\beta\varepsilon$	Dimensionless bond association energy	
i, j	Location on lattice	(N,N)
a	State of lattice site (orientation 1,2,3,4 or vacant 5)	
$\hat{p}_a(i,j)$	Occupancy of state a at location (i,j) (either 1 or 0)	
β	$(kT)^{-1}$ where $k$is the Boltzmann constant	k
βH	Hamiltonian of our system	
$\beta\eta$	Strength of isotropic interaction ($\eta = 0$ in all work)	
$q_{current\to new}$	Transition probability (generic form)	
ω	Attempt frequency (this is the fundamental time unit)	
E	Energy (internal energy)	k
$\vec{i}$	Two-dimensional coordinates	(N,N)
$\langle \vec{i},\vec{i}'\rangle$	Nearest neighbor sites	
$p_a(t;i,j)$	Probability of state a (used in mean-field calculation)	
$q(t;b\to a)$	Transition probability for rotation from state b to state a	
$q(t;c,\vec{i}'\leftrightarrow a,\vec{i})$	Transition probability for translation	
βf	Free energy per site	
ρ	Density (sum of occupied states per site)	
$\beta\mu$	Chemical potential per site	

βw	Grand potential energy per site	
$\theta(t-t_o)$	Correlation function	
τ	Relaxation time	ω^{-1}
β	Exponent in stretched exponent function	
τ_o	Vogol-Fulcher fit: characteristic relaxation	ω^{-1}
T_o	Vogol-Fulcher fit: critical temperature	
D	Volgol-Fulcher fit: fragility index	
$m(t-t_o)$	Time correlation 'order parameter' from mean-field calculations	
T_c	Critical temperature	
ν	Correlation length	N^{-1}
z	Dynamic scaling exponents	
T_k	Kauzmann Temperature	
ω	Diffusivity	
R^2	Mean-squared distance traversed during time t	$N^{-2}\omega$

Notation Changes for Sections outside of Chapter 1:

N	Total number of lattice sites
T	Dimensionless Temperature
'site'	'vertex' (we codified vertex for location vs molecule or site)

Notation Continued:

$\sigma_\alpha\left(\vec{i}\right)$	Orientation of molecule ($\alpha = 1,2,3$ or 4)	
m	One state of the entire lattice with all orientations specified	
k	Another state of the entire lattice with all orientations specified	
$\vec{x}_m$	Conformation coordinate of state m on the energy landscape	
$T_{mf,critical}$	Mean-field transition temperature	
$T_{mf,spinodal}$	Mean-field stability limit	
$q_{k\rightarrow m}$	Transition probability of moving from state k to state m	
p_m	Probability of a given state of the entire lattice with each molecules in a specific orientation	
$\vec{x}^*_{m\rightarrow k}$	Transition state between state m and state k	
$E^*_{m\rightarrow k}$	Energy of the transition state	k
C_v	Heat capacity	k
s	Entropy per site	$(kN^2)^{-1}$
T_{Cv}	Temperature at which the heat capacity is a maximum	
E_a	Arrhenius Fit: Activation Energy	
C	Adam-Gibbs Fit: Empirical fit constant	
J	Quadratic Fit: Empirical fit constant	
T_a	Quadratic Fit: Upper bound of cooperative relaxation	

	regime	
T_x	Quadratic Fit: Lower bound of cooperative relaxation regime	
$b\left(t;\left\langle \vec{i},\vec{i}\,'\right\rangle\right)$	Bond (1 present, 0 absent) along edge connecting near-neighbor vertices $\left\langle \vec{i},\vec{i}\,'\right\rangle$ at time t (defined by orientation of molecules at sites)	
$\phi_b\left(t-t_o\right)$	Bond autocorrelation function	
τ_{bond}	Bond relaxation time	ω^{-1}
$\sigma_\alpha\left(t;\vec{i}\right)$	Molecule at vertex $\vec{i}$ is in orientation α at time t (1 if present 0 if absent)	
$\phi_\sigma\left(t-t_o\right)$	Molecule-orientation autocorrelation function	
τ_σ	Orientation relaxation time	ω^{-1}
τ_c	Characteristic time	ω^{-1}
β	Stretching exponent	
$\Gamma(z)$	Euler gamma function	
$T_{\beta:fragility,\,onset}$	Highest temperature at which β is at its low temperature plateau	
$T_{\beta:FSC}$	Lowest temperature at which β is at its low temperature plateau	
γ	Cooling rate	ω
a,b,c,d	Empirical fitting constants	
T_{FSC}	Fragile-to-strong crossover temperature	
$T_{kMC,structure}$	Change in feature expectation value	

$\tau_{first\ change}$	Time scale for the molecule to change orientation for the first time	ω^{-1}
$\tau_{exchange}$	Time scale for fast and slow molecules to exchange mobility	
μ_{α}	Applied aligning field to skew to one alignment	k
ε_{mn}	Bond energies when they are not all the same	k
Appendix A:		
T_r	Reduced temperature	
Appendix B:		
p_c	Critical probability of bond occupation for percolation	
Appendix C:		
α	Order parameter indicating that either ┤, ├ or ┴, ┬ will be dominant on the lattice	
δ	Order parameter indicating that indicates left/right or up/down orientations are dominant	
Appendix D:		
ρ	Density of molecules on lattice	N
p_{α}	Probability that molecules are in a locally ordered domain	
p_b	Probability that molecules in an amorphous region	
βu_{random}	Internal energy per vertex of random (liquid or gas) state	kN^{-2}
βf_{random}	Free energy per vertex of random (liquid or gas) state	kN^{-2}
s_{random}	Entropy per vertex of random (liquid or gas) state	

$\beta u_{oriented}$	Internal energy per vertex of locally preferred oriented state	kN^{-2}
βf_{random}	Free energy per vertex of locally preferred oriented state	kN^{-2}
s_{random}	Entropy per vertex of locally preferred oriented state	
Appendix E:		
$r_{m \to k}$	Transition rate	ω
$\xi_{\max}$	Largest transition rate	ω
u	Random number (in this appendix only)	
n_m	Number of vertices that can change by the specific process m	
Appendix F:		
A_t	Observable	
σ	Variance (Appendix F only)	
Appendix G:		
E_{IS}	Inherent energy (internal energy)	k

Overview of Thesis

Amorphous materials are ubiquitous in our daily lives. As a high school teacher in the state of California, our curriculum acknowledges four states of matter: solid, liquid, gas and plasma. We give a nod to polymers and large biomolecules and move on. Inevitable when discussing materials in class, the items which catch students' eye are much more complicated. What is an LCD? Why are there different recycling codes, shouldn't we be able to mix it all together? What was that stuff they served down in the cafeteria today? It is wonderful to explain what we know and then challenge them to pursue open questions.

The center of this thesis is to develop an understanding of the characteristics and dynamics of amorphous materials. We are able to draw connections between two broad classes of glasses and physical gels by introducing a strikingly simple T-shaped molecular model on a two dimensional lattice. Having gained important insight into this relation, we then pursue more fundamental issues of the nature of the glass transition.

The focus of chapter one[1] is to identify and connect amorphous materials that are arrested on some time scale without invoking artificial frustration. The mean-field phase diagram of this model mimics those phase diagrams calculated for other systems[2] and seen in experiments[3]. Dynamic mean-field simulations demonstrate a wide variety of phases including liquid, solutions, glassy materials, foams and gels. Further evaluation demonstrated a kinetic preferred alignment and highlighted the large number of degenerate energy minima on the landscape. The calculated instabilities within the two phase region of the phase diagram converged along a line terminating in the fully-dense spinodal, suggesting a strong connection between gelation and the glass transition. Initial results of the dynamics of the simulations suggested the possibility of a return to strong behavior at the lowest temperature. We thus were able to define gelation in this model as phase separation arrested by vitrification. As we could investigate equilibrium at low temperatures, we noticed that there was behavior consistent with the fragile-to-strong crossover.

In the time between publishing our first paper[1] (chapter 1) and now as we are finishing work leading towards a second paper (chapter 2) several powerful conclusions were drawn in other research groups. In models capturing a wide range of experimental observations, from specific DNA tetramers[3] to silicon[4], a commonality was emerging. The controlling feature in the modeled potentials was the ability to suppress the isotropic portion allowing anisotropic forces to dominate[5]. This leads to local ordering which stabilizes the overall amorphous materials inducing dynamic arrest, observed as vitrification or gelation[2]. This suggests that the overall behavior of many of these materials can be reduced to generic descriptions of their valency[6, 7] .

However, as a field we are still bound by the fundamental difficulty encountered in simulation: computation time. Achieving low temperature results, particularly those which are able to avoid vitrification, will require the development of complex mechanisms to overcome difficulties in time scales in the potentials studied thus far[8]. Based on our success with this model in our initial work, we sought to overcome this difficulty. Placement of our T-shape molecules on a lattice naturally invokes the valence-limited potential with a computationally efficient Hamiltonian. We correctly postulated that using a combination of Monte Carlo simulations would allow us to investigate our system at the desirable low temperatures.

The second chapter is also formatted as an independent paper, although it includes a more extensive discussion relating to what may often be framed as future work in a dissertation.

Within this work, we concentrate on the glass transition in the fully-dense region. Our model allows us to quench the simulation samples to very low temperatures using a modified Metropolis Monte Carlo recipe. We can then apply the appropriate kinetic Monte Carlo approach to study the dynamics and structure of the equilibrium systems. This provides a backdrop against which we consider the temperature quench of simulation samples using the kinetic Monte Carlo method. Glassy states which persist for long lengths of time are documented. Overall, we see a clear signature of the fragile-to-strong crossover (FSC) at low temperatures. However, we do not observe evidence of a divergent length scale consistent with a thermodynamic critical point. We also find that the Kauzmann paradox is resolved by the change in the temperature dependence of the relaxation time at the fragile-to-strong crossover and, indeed, observe a positive configurational entropy as $T \rightarrow 0$. There is a dramatic change in the relaxation behavior at the FSC which would lead to a lower limit of the experimentally observable relaxation to equilibrium; however, this is not a fundamental kinetic arrest.

In seeking simplicity of explanation, we do not want to lose sight of the rich complexity and wide variety of glassy materials. However, with this in mind, we sally forth into an investigation of a simple model with surprisingly rich dynamics and thermodynamics.

1. Chapter 1: A Lattice Model of Vitrification and Gelation[1]

1.1. Introduction

There are natural parallels between the glass phase and physical gels (thermoreversible gels) as well as between vitrification and gelation. Recently there has been considerable interest in unifying these two classes of disordered materials. For example, theory and simulation predict the existence of both glass- and gel-like structures in colloidal systems[9-11]. These predictions are consistent with features found experimentally[12, 13]. In addition to structural similarity, dynamic observations have strengthened the conclusion that there is a relation between glasses and gels. Physical gels have associations with finite bond lifetimes (in contrast to chemically crosslinked gels). Experimental measurements of gelatin[14] and poly (vinyl alcohol) gels[15], both thermoreversible polymeric gels, have shown glass-like relaxation dynamics. Colloids with short-range attractions share this property and can form gels at high densities that exhibit glass-like kinetic arrest[16, 17] and relaxation properties[18]. In this work we use a lattice model occupied by T-shaped molecules to explore the relation between glasses and physical gels.

The glass state has been studied in great detail and the dynamics of many systems in addition to physical gels are analogous to those of a glass. Kauzmann, whose work was influential in the development of our current thermodynamic understanding of the glassy state, referred to the glass as one example of the 'torpid' state[19], a general category that includes linear polymers under flow and plastically deformed metals and crystals.

---

[1] *This chapter is reproduced with permission of the Journal of Physical Chemistry B from:* Witman, J.; Wang, Z.-G., A lattice model of vitrification and gelation. *Journal of Physical Chemistry B* **2006,** 110, (12), 6312-6324.
Copyright 2006 American Chemical Society

Additionally, a variety of other materials demonstrate dynamic behavior characteristic of glass-like states. These include such diverse examples as the polycrystalline structure of thin films, protein folding[20, 21] and granular material jamming[22].

Lattice models have been extensively used to explore both the structure and dynamics of the glassy state. Among the many examples it is useful to contrast two classes. The first consists of models whose Hamiltonians directly induce frustration. By construction, these models do not have fully satisfied alignment states. There are no configurations that satisfy all of the locally preferred low energy states. Ising spin glasses[23], in which the interactions are randomly assigned to favor parallel or antiparallel orientation, are classical examples. Conversely there are models whose rules of motion make the formation of macroscopic uniform phases unlikely. Falling under the umbrella of hierarchically constrained local dynamics, the evolution in time of these Ising-type models is restricted by the state of neighboring sites[24]. These include the Fredrickson-Anderson facilitated kinetic Ising models[25] and the East model[26]. In a similar manner the tiling model[27] and a recent model by Garrahan and Chandler[28] demonstrates glassy dynamics based on local dynamical rules, although the coarse-graining implicitly does not include the crystal state. Our model does not exclude ordered states, however unlike traditional liquids, these states have the same energy as satisfied yet inhomogeneous states.

One way to capture the features and behavior of amorphous solids on a lattice is to assign anisotropic interactions. Aranovich and Donohue have explored the role of anisotropy on molecular fluids[29]. Highlighting that most molecules and particles have anisotropic interactions due to steric limitations of arrangement and bonding constraints, they considered a variety of phase transitions including condensation, crystallization, and polymerization.

Developed concurrently are several other models of Ising-like lattice liquids and glasses that in some way restrict the number of nearest neighbors on the lattice leading to glassy features[30, 31]. In a similar manner, Del Gado et al. have employed a model in which monomers occupy a cubic lattice and are tetrafunctional, allowing for vacant sites within the network without energetic penalty[18]. The presence of telechelic monomers that can from a network with 'solvent' intuitively leads to a picture of a polymeric gel.

A minimal requirement for network formation in two dimensions is a trimer structure which allows junctions and branching. The Mercedes-Benz model [32, 33] (named for its resemblance to the famous logo) has three directional arms, each capable of supporting hydrogen bonding. There is an energetic balance between the advantageous formation of an open 'bonded' structure in which the arms of the monomers touch and a force favoring an incommensurate dense structure. This model has been studied in both on-lattice[33] and off-lattice[32, 34] formulations. Other on-lattice [35] and off-lattice models of water[36] distinguish between hydrogen bonds and Van der Waals forces determined by the relative orientation of the monomers. Our model features anisotropic interactions that lead to the number of bonds formed being smaller than the number of nearest neighbors. In addition to sharing this feature with geometrically constrained systems (e.g. colloidal particles with short range interactions), our model is naturally relevant to network forming liquids such as silica glasses[37] and water[38, 39], in which the interactions are due to directional bonds.

Gelation has commonly been associated with geometrical percolation. However, this condition is not sufficient to describe the transition in physically associating gels. These systems, which have bond life times comparable or shorter than the time scale of interest in experiments, may not exhibit solid-like character at the geometric percolation threshold[40, 41].

Further, simulations by Kumar and Panagiotopoulos show no change in a thermodynamic property at gelation, suggesting that gelation is not a higher order thermodynamic transition[42]. The specific molecular interactions yield rich behavior in some physical gels that does not conform to the percolation model[43].

We endeavor to link the glass transition and gelation within a lattice model that can encompass both glass and physical gel phases in appropriate relation to the liquid and solution phases. We investigate the properties of a lattice occupied by T-shaped molecules whose anisotropic nature leads to a wide variety of morphological states. We explore these states by using a dynamic mean-field simulation method that by construction evolves towards a free energy minimum as well as a Monte Carlo method. Glassy or gel-like behaviors are identified as corresponding to free energy minima associated with inhomogeneous and non-periodic structures[44].

Our primary concern in this work is to understand the thermodynamic and kinetic factors leading to such amorphous structures. We have also completed initial work investigating the dynamics of our model system. We propose that these amorphous, glass or gel-like structures arise as a result of the proliferation of a large number of such inhomogeneous free energy minima, which is intimately connected to an underlying spinodal of the uniform liquid or solution phase with respect to inhomogeneous fluctuations. However, the resultant structures depend on the ‘processing’ or quenching conditions. Therefore their origin is both thermodynamic and kinetic in nature. Our study suggests that a mechanism for gelation is incomplete phase separation in the two-phase region of the phase diagram arrested by the onset of glass transition.

1.2. T-shaped Molecule Model

We consider a two-dimensional square lattice of N x N sites. Each lattice site is either occupied by a 3-armed, T-shaped molecule, or is vacant, representing a solvent molecule. The T-shaped molecule can take any of the four orientations designated as *1, 2, 3* and *4* in Figure 1.2-1(a). The vacant state (not shown) is denoted as state *5*. Each arm of the T-shaped molecule is capable of forming an association (bond) of energy $-\varepsilon$ with the adjoining arm from a nearest neighbor molecule. The added level of complexity in our model arises from both the state of a site (vacant or occupied with orientation *1,2,3* or *4*) and the relative orientation of the molecule at that site with respect to its neighboring sites. This relative orientation determines the association state as the molecule is anisotropic.

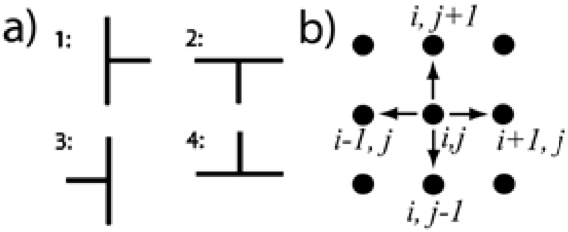

Figure 1.2-1: Definition of T-shaped model
(a) States of the T-shaped molecules on a square lattice. The model contains these four states and a fifth state (not shown) which represents a vacancy. (b) The relative orientation between site i,j and its nearest neighbors.

We will denote the occupancy of site (*i,j*) in state a by $\hat{p}_a(i,j)$ ($\hat{p}_a(i,j)=1$ if site (i,j) is in state a and 0 otherwise, and $\sum_{a=1}^{5}\hat{p}_a(i,j)=1$). The Hamiltonian of our system is written as:

$$\begin{aligned}
\beta H = &-\left(\frac{\beta\varepsilon}{2}\right)\sum_{i=1}^{N}\sum_{j=1}^{N}\Big\{\ \hat{p}_1(i,j)\big[\ \hat{p}_1(i,j+1)+\hat{p}_2(i,j+1)+\hat{p}_3(i,j+1)+\hat{p}_2(i+1,j)\\
&+\hat{p}_3(i+1,j)+\hat{p}_4(i+1,j)+\hat{p}_1(i,j-1)+\hat{p}_3(i,j-1)+\hat{p}_4(i,j-1)\ \big]+\\
&\hat{p}_2(i,j)\big[\ \hat{p}_2(i+1,j)+\hat{p}_3(i+1,j)+\hat{p}_4(i+1,j)+\hat{p}_1(i,j-1)+\hat{p}_3(i,j-1)\\
&+\hat{p}_4(i,j-1)+\hat{p}_1(i-1,j)+\hat{p}_2(i-1,j)+\hat{p}_4(i-1,j)\ \big]+\\
&\hat{p}_3(i,j)\big[\ \hat{p}_1(i,j+1)+\hat{p}_2(i,j+1)+\hat{p}_3(i,j+1)+\hat{p}_1(i,j-1)+\hat{p}_3(i,j-1)\\
&+\hat{p}_4(i,j-1)+\hat{p}_1(i-1,j)+\hat{p}_2(i-1,j)+\hat{p}_4(i-1,j)\ \big]+\\
&\hat{p}_4(i,j)\big[\ \hat{p}_1(i,j+1)+\hat{p}_2(i,j+1)+\hat{p}_3(i,j+1)+\hat{p}_2(i+1,j)+\hat{p}_3(i+1,j)\\
&+\hat{p}_4(i+1,j)+\hat{p}_1(i-1,j)+\hat{p}_2(i-1,j)+\hat{p}_4(i-1,j)\ \big]\ \Big\}\\
&-\left(\frac{\beta\eta}{2}\right)\sum_{i=1}^{N}\sum_{j=1}^{N}\ \hat{p}_5(i,j)\big[\ \hat{p}_5(i,j+1)+\hat{p}_5(i+1,j)+\hat{p}_5(i,j-1)+\hat{p}_5(i-1,j)\ \big]
\end{aligned}\tag{1}$$

For completeness we have included an isotropic interaction between the solvent molecules (or equivalently between the solute molecules by virtue of the occupancy constraint). In this work, we consider the case $\eta = 0$.

We have employed the following dynamic rules of motion for our model. The molecules can undergo both rotational and translational diffusion. During rotation a T-shaped molecule can interchange states *1,2,3* or *4* at a given site. We do not attempt to mimic the actual physical rotation of the T-shaped molecules and will thus allow a T-shaped molecule to rotate from a given state to any of the other states in a single time-step. For translational diffusion, we use Kawasaki-exchange dynamics[45] between a T-shaped molecule and a nearest neighbor solvent molecule as well as for self-diffusion, or exchange, of neighboring T-shaped molecules. In the fully-dense region of our phase diagram there is no fundamental difference between rotational and translational diffusion.

In this work we employ both the Metropolis Monte Carlo (MC) simulation technique[46] as well as the dynamic mean-field (DMF) simulation method[47]. Thus far, MC simulations have only been performed on a fully-dense lattice with no vacancies. The MC simulations proceed by selecting a site at random and then proposing a change in its orientation or an exchange with a nearest neighbor; this rule would be equally applicable where there are vacancies. The Metropolis recipe is used to determine whether this change is accepted.

The DMF simulations (to be discussed further in Section 1.3) can be considered a mean-field implementation of Monte Carlo dynamics[47]. However for computational purposes it is convenient to use the Barker form[48] of the transition probability , $q_{current \to new}$:

$$q_{current \to new} = \omega \frac{\exp(-\beta E_{new})}{\exp(-\beta E_{current}) + \exp(-\beta E_{new})} \qquad (2)$$

instead of the Metropolis form ($q_{current \to new} = \omega$ if $E_{new} < E_{current}$ and $q_{current \to new} = \omega \exp[-\beta(E_{new} - E_{current})]$ if $E_{new} > E_{current}$). In equation 2, ω is an attempt frequency (which can be different for the rotational and translation moves) and $E_{current}$ and E_{new} are respectively the energy of the system in its current state and new state. As in the MC simulations, the new state reflects both orientation change and nearest neighbor exchange. The dynamics in the DMF evolution of the singlet density at each lattice site follow a steepest descent path into a free energy minimum.

1.2.1. Role of Anisotropic Interactions

The anisotropy of the model, which allows for orientational disorder and mimics bonding and steric constraints, plays a strong role in the type of quenched structures we observe. The organizing feature of this model is the presence of a non-bonding side or 'back'. Before exploring the phase diagram in detail it is helpful to consider some of the phases the lattice can adopt. In our DMF simulations (to be described later in Section 1.3) we can identify whether a particular site was strongly oriented and would persist in that state over time.

These sites are shown in dark black in the figures. Sites that are not strongly oriented appear in grey. Sites that are most probably solvent molecules are represented as blanks.

In the fully-dense limit, without solvent, the molecules must be arranged in pairs back to back in order for the lattice to be satisfied. Otherwise there is an associating end presented to a non-bonding side. These satisfied structures can be crystal-like (Figure 1.4.5-1(a)) or amorphous (Figure 1.4.5-1(b)) depending on the pattern of the pairs. The amorphous structures can also contain unsatisfied sites at which not all arms form bonds with their neighbors. These sites are still liquid-like in that they retain equal probability to arrange in any orientation.

In other regions of the phase diagram the back of the molecule points towards the solvent. This gives the molecule a self surfactant character. The molecules can be arranged in phase separated, highly satisfied states (Figure 1.5.5-1) or in gel-like states (Figure 1.5.5-2 and Figure 1.5.5-4). In observing gel-like structures, two features are clear. The first is that the structures involve at least a pair of molecules that form ladder-like structures. The second is that there are unsatisfied sites located at the junctions of the fibrils. Gel-like features are observed under a wide range of conditions. The particular characteristics of the gel-like state, for example the fibril length and width, can be varied by altering the simulation conditions.

1.3. Dynamic Mean-field Simulations

The dynamic mean-field (DMF) simulation technique is a deterministic method for evolving the singlet mean-field probability, p_a, of the lattice sites from a given initial condition[47]. It is similar to the dynamic density functional methods for molecular[49] and polymeric fluids[50]. Given the dynamic rules for a lattice model, the DMF equations of motion are obtained from a local mean-field approximation of the master equation corresponding to those rules. The DMF simulation method has formulations for both conserved and non-conserved order parameters. The governing equations and detailed balance conditions for both cases were derived in the reference[47]. Below we present the application of these equations to our current model.

1.3.1. Dynamic Mean-field Equations

The probability that a lattice site (*i,j*) will be in state a at time *t* is given by $p_a(t;i,j)$. Our master equation encompasses both rotational diffusion and translational diffusion. The overall probability that a molecule will be found in a particular orientation (states *1,2,3* and *4*) on the lattice is not conserved. However the number of molecules on the lattice remains constant, requiring conserved motion. These two forms of motion are captured in the master equation under the mean-field approximation given by:

$$\begin{aligned} p_a(t+1;\vec{i}) &= p_a(t;\vec{i}) + \sum_{b\neq a}\left[q(t;\vec{i};b\to a)p_b(t;\vec{i}) - q(t;\vec{i};a\to b)p_a(t;\vec{i})\right] \\ &+ \sum_{\langle \vec{i},\vec{i}'\rangle}\sum_{c\neq a}\left[q(t;c,\vec{i}\leftrightarrow a,\vec{i}')p_c(t;\vec{i})p_a(t;\vec{i}') - q(t;a,\vec{i}\leftrightarrow c,\vec{i}')p_a(t;\vec{i})p_c(t;\vec{i}')\right] \end{aligned} \tag{3}$$

for the first four states (*a=1-4*) and:

$$\begin{aligned} p_5(t+1;\vec{i}) &= p_5(t;\vec{i}) \\ &+ \sum_{\langle \vec{i},\vec{i}'\rangle}\sum_{c\neq 5}\left[q(t;c,\vec{i}\leftrightarrow 5,\vec{i}')p_c(t;\vec{i})p_5(t;\vec{i}') - q(t;5,\vec{i}\leftrightarrow c,\vec{i}')p_5(t;\vec{i})p_c(t;\vec{i}')\right] \end{aligned} \tag{4}$$

for the solvent. The summation in equation 3 over *b* includes states *1-4* and the summation in both equations over *c* includes all states. We use the vector $\vec{i}$ to denote the two dimensional coordinates and $\langle \vec{i},\vec{i}'\rangle$ indicates that $\vec{i}$ and $\vec{i}'$ are nearest neighbor sites. $q(t;b\to a)$ is the transition probability for rotation from state *b* to state *a*. The transition probability for translation, $q(t;c,\vec{i}\,'\leftrightarrow a,\vec{i})$, involves exchanging the states between site $\vec{i}$ and its nearest neighbor $\vec{i}\,'$. Consistent with the mean-field approximation at the singlet density level, these transition probabilities can be written simply as[47]:

$$q(t;a\rightarrow b)=\omega_1\frac{\exp[-\beta E_b(t;\vec{i})]}{\exp[-\beta E_a(t;\vec{i})]+\exp[-\beta E_b(t;\vec{i})]} \tag{5}$$

and

$$q(t;a,\vec{i}\leftrightarrow b,\vec{i}\,')=\omega_2\frac{\exp[-(E_a(t;\vec{i}\,')+E_b(t;\vec{i}))]}{\exp[-(E_a(t;\vec{i})+E_b(t;\vec{i}\,'))]+\exp[-(E_a(t;\vec{i}\,')+E_b(t;\vec{i}))]} \tag{6}$$

In our calculation we take ω_1 to be 1/6 and ω_2 to be 1/24. Also, the temperature of our system is always taken to be that of the final condition resulting in 'instantaneous' quenches. The energy appearing in the transition probabilities is given by $E_a(t;\vec{i})=\dfrac{\partial H}{\partial p_a(t;\vec{i})}$, where H is the mean-field energy of the system (equation 1) with the fluctuating $\hat{p}_a(t;\vec{i})$ replaced by the average $p_a(t;\vec{i})$. As an example:

$$\begin{aligned}E_1(t;i,j)=\frac{\partial H}{\partial p_1(t;i,j)}=\frac{-\varepsilon}{2}\big[&p_1(t;i,j+1)+p_2(t;i,j+1)+p_3(t;i,j+1)+p_1(t;i,j-1)\\&+p_3(t;i,j-1)+p_4(t;i,j-1)+p_2(t;i+1,j)+p_3(t;i+1,j)+p_4(t;i+1,j)\big]\end{aligned} \tag{7}$$

where we reintroduce the two-dimensional lattice coordinates to emphasize the relative orientation of the T-shaped molecules with respect to the direction of its nearest neighbors.

The master equation will evolve with time until it reaches a stationary state. This stationary state is a result of detailed balance which is given by:

$$p_a(\vec{i})q(a\rightarrow b)=p_b(\vec{i})q(b\rightarrow a) \tag{8}$$

and

$$q(c,\vec{i}\,'\leftrightarrow a,\vec{i}\,)p_c(\vec{i}\,')p_a(\vec{i}\,)=q(a,\vec{i}\,'\leftrightarrow c,\vec{i}\,)p_a(\vec{i}\,')p_c(\vec{i}\,) \tag{9}$$

By virtue of the choice of the transition probabilities which satisfy detailed balance, the DMF equations will evolve the system towards an equilibrium or metastable equilibrium state. Thus, the stationary solutions of the DMF equations correspond to free energy minima. Glassy or gel-like phases are identified as inhomogeneous, non-periodic, stationary solutions of the DMF equations. Although the DMF equations cease to evolve at these stationary solutions, and hence would lead to complete structural arrest, such a result is a manifestation of the deterministic nature of the mean-field equations. In the presence of random thermal motion, the system would continue to evolve through activated processes by jumping out of the local free energy minima. Nevertheless, the *existence* of such free energy minima indicates structural arrest on some short time scales and hence signals a change in the character of the dynamics of the system. Therefore, in addition to describing the temporal evolution of the system at the mean-field level, the DMF simulation technique provides a useful method for searching and locating these inhomogeneous free energy minima.

1.4. Fully-dense System: Liquid, Crystal and Glass Phases

In this Section we consider the behavior of the fully-dense system (where there is no solvent or state 5) under the mean-field approximation. We start with an overview of the phase behavior in this region before proceeding calculate the transition temperature between the liquid and the vitrified phases as well as the spinodal of the liquid phase. With this analysis as a guide we then use DMF simulations to characterize the response of the liquid to fluctuations and investigate the morphology of the solid.

1.4.1. Overview of Phase Behavior

In the fully-dense region (p_5=0) the lattice can assume a liquid phase or a solid configuration. At high temperatures there is an equal probability that the molecules will be found in any of the four states (p_1=p_2=p_3=p_4=1/4); we identify this state with the liquid phase. At sufficiently low temperatures, the T- shaped molecules at most of the lattice sites become strongly oriented in one of the four orientations. A simple mean-field calculation predicts a first-order transition from the liquid state to these locally oriented solid states. Mean-field theory also predicts a spinodal for the liquid state below which a metastable liquid can no longer exist. As this spinodal signals the spontaneous appearance of inhomogeneous free energy minima, we associate it with the ideal glass transition from this model. The crystalline state in this model– an alternating bilayer structure– is a peculiar state. Unlike many physical glasses, the crystalline state in our model has no energetic advantage over other amorphous configurations. Its appearance is a result of a particular kinetic path. For our purpose, the existence of this crystalline state has no special significance. There are a vast number of equivalent lowest energy states that have all the arms bonded or satisfied (more details will be given in Section 1.6.1).

1.4.2. Transition between the Liquid and the Vitrified States

Instantaneously quenched from the high temperature liquid to the low temperature crystalline or glassy states, the T-shaped molecule at an individual lattice site transitions from having an equal probability of being oriented in any of the four states to strongly preferring one state. Characterization of the glass-like configurations requires specifying the spatial probability distribution of the molecule orientation of the full lattice. As this is analytically intractable, we make a simplifying approximation that each site is dominated by one particular orientation, and all the other orientations have equal probabilities. Furthermore, we assume that the probability of the dominant orientation is the same for all lattice sites (although the dominant orientations at different lattice positions need not be the same). While the validity of these assumptions is not immediately obvious, our DMF simulation confirms that the vast majority of sites have the same bias toward a dominant local orientation and that the subdominant orientations have approximately equal probabilities.

Taking the dominant probability to be p_1, we can write an approximate free energy per site for the solid state as:

$$\beta f_{solid} = -\tfrac{1}{2}\beta\varepsilon\left(3p_1^2 + 12p_1p_2 + 21p_2^2\right) + p_1 \ln p_1 + 3p_2 \ln p_2 \qquad (10)$$

where we have made use of our assumption $p_2 = p_3 = p_4$. In this calculation we do not distinguish between the crystal-like and the glass-like solid states because we neglect the details of the structure on the lattice. Therefore this free energy also describes the bilayer crystalline structure described in Section 1.4.5[51].

The equilibrium state is obtained by minimizing the free energy with respect to these probabilities. Phase transition occurs when this free energy equals that of the liquid with unbiased orientation distribution:

$$\beta f_{liq} = -(9/8)\beta\varepsilon - \ln 4 \qquad (11)$$

We find a first-order transition at $\beta\varepsilon = 3\ln 3$ with the solid state having $p_1 = 3/4, p_2 = p_3 = p_4 = 1/12$ at the transition.

1.4.3. Stability Limit of the Uniform Liquid Phase

Because the transition from the uniform liquid to the solid phase is first-order, the formation of the solid phase from a metastable liquid involves a nucleation barrier. It is therefore possible to supercool the liquid below the freezing temperature. However, this supercooling can only proceed as far as the spinodal, or metastability limit of the liquid. Beyond this limit the uniform liquid becomes unstable with respect to an infinitesimal inhomogeneity in the probability distributions, i.e., an inhomogeneous structure will form spontaneously. Each of these inhomogeneous(amorphous) structures corresponds to a local free energy minima. Since in the mean-field picture there are no activated events, a system, having reached one such free energy minimum, is permanently trapped there. This consideration motivates us to identify the spinodal as the mean-field signature for an 'ideal' glass transition. In this sense the spinodal temperatures can be likened to the Kauzmann temperature T_k, the lowest temperature for the onset of the glass transition. We note that other authors have previously hinted at the connection between the liquid spinodal and an ideal glass transition[52-54]. This conclusion has been explicitly demonstrated in the case of block copolymer microstructural glasses[55]. In reality, because of thermal fluctuation, the system can fall into these amorphous states earlier than the spinodal, as well as escape them and diffuse between minima[39].

The spinodal of the liquid can be easily obtained by examining the second derivative of the free energy expression Equation 10. Setting this derivative to zero, we find that the spinodal occurs at $\beta\varepsilon = 4$. This value agrees with a more systematic calculation by finding the lowest eigenvalue of the second derivative matrix of the full mean-field free energy function as calculated in Section 5.3.

1.4.4. Correlation in the Liquid State

With the theoretical analysis of the mean-field behavior as a guide, we now proceed to examine the system in the fully-dense phase using the DMF simulation. While the equilibrium probability of a site being in each of the four orientations is equal in the liquid state, the anisotropy of the interactions leads to nontrivial spatial correlations. Within mean-field theory, these correlations can be examined by the response of the system to a small localized perturbing field. Figure 1.4.4-1 shows the probability profile for the four different states on the *i* and *j* axes when site (0,0) is perturbed by a field of magnitude 0.0001β that favors state *1*. The system is a liquid at $\beta\varepsilon = 3.92, \rho = 1.0$.

Because the field at the origin (0,0) favors state *1*, the probability of this state at site (0,0) is enhanced at the expense of the other three states. More reflective of the anisotropy of the interaction are the probability of the states next to (0,0). For example, state *1* is depleted both to the left and to the right, whereas states *2*,*3* and *4* are enriched to the right. The site (-1,0) is particularly interesting since state *3* is enriched while all other states are suppressed. These trends, as well as the special symmetry of the profiles along the j axis, can all be rationalized by the energetic preference to have the arms of the molecules pointing to each other and not to have the arm of a molecular facing the back of another.

The effects of the field at site (0,0) diminish as we move far from the origin, manifesting as damped small oscillation with respect to the bulk value. A correlation length can be defined as the length scale for the decay of the probability profiles to their bulk value; the correlation length shows the characteristic square-root divergence with the proximity to the spinodal as expected from the mean-field behavior. However, the numerical prefactor turns out to be unusually small, the correlation length reaching only a few lattice spacings when T is within one percent of the spinodal.

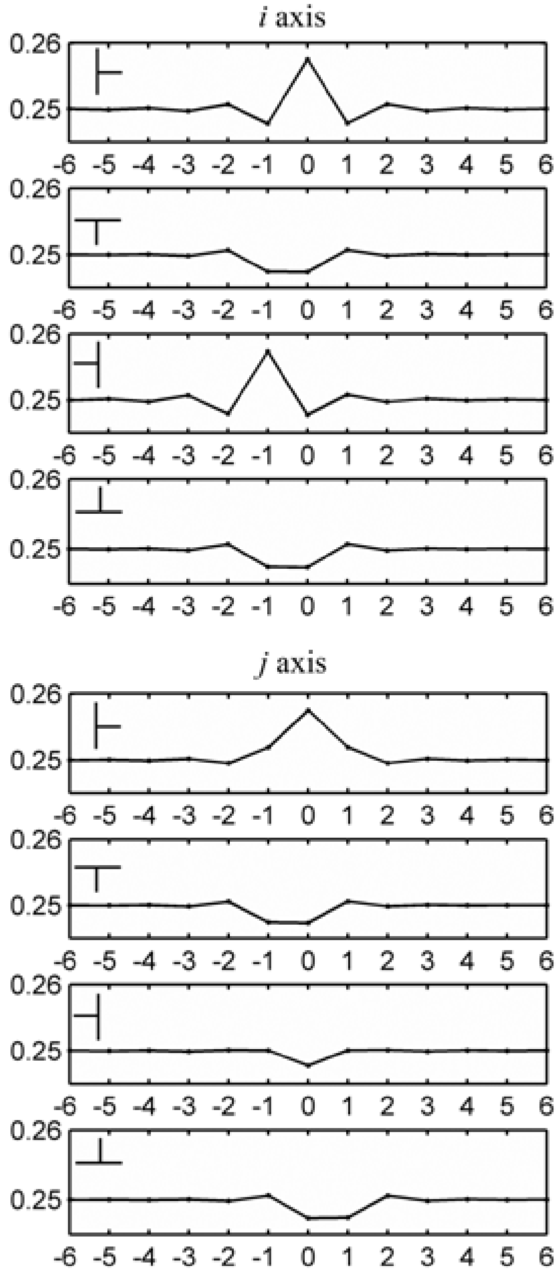

Figure 1.4.4-1: Result of small applied force in the liquid state
The probability of being in each state as a function of position along the i and j axis after a small pinning force of magnitude 0.0001β favoring state 1 is applied at site (0,0) to a fully-dense lattice. The unperturbed liquid-like state at βε=3.92, ρ=1 has an equal probability (0.25) of being in each state.

1.4.5. Vitrification in DMF Simulations

We can investigate the morphology of the solid-like state using DMF simulations. Starting with the isotropic liquid state at high temperature where the four orientations are equal on all lattice sites, we quench the system instantaneously to a lower temperature. Since the DMF equations are deterministic, we add small random perturbations in the probabilities to provide the initial driving force for setting the equations into motion. Above the liquid-solid transition temperature, we find that the lattice of probabilities relaxes back to the isotropic liquid state. For sufficiently small perturbations, it is possible to supercool the liquid below the transition temperature. However, at some temperature between the transition and spinodal temperatures, a sufficiently large local perturbation will be able overcome the nucleation barrier and induce growth of the solid phase. Figure 1.4.5-1(a) shows a typical configuration of the crystalline state obtained from a shallow quench past the coexistence temperature. In this configuration, all the molecules on the lattice are satisfied; each associating end group is paired.

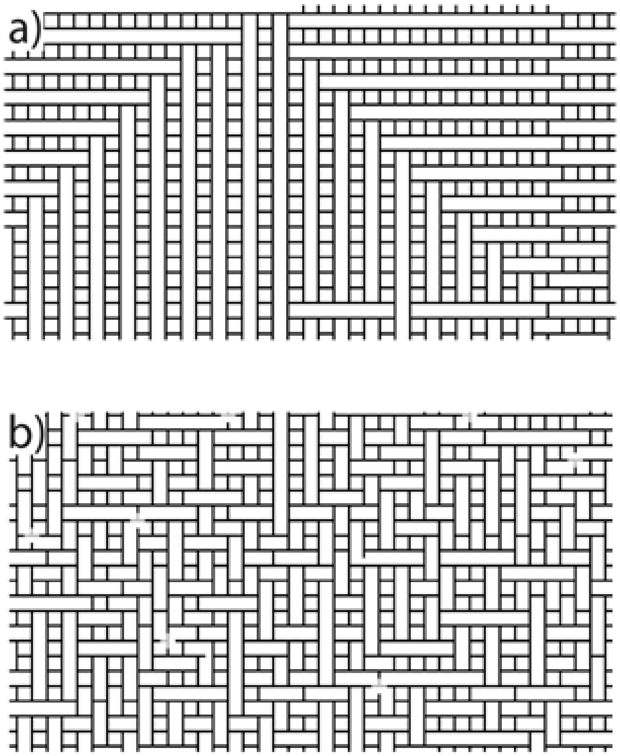

Figure 1.4.5-1: DMF simulation results for the fully-dense state
(a) Crystalline State ($\beta\varepsilon = 3.7$, $\rho = 1$) and (b) Glassy State ($\beta\varepsilon = 4$, ρ=1). Both simulations were started from a liquid state with small perturbations before instantaneously quenching to the final conditions. The black molecules are strongly oriented in the indicated direction. The grey molecules indicate that the site has equal probability of being in any of the four orientations. The orientation at these sites is chosen randomly in the figure.

The formation of a crystal-like phase when a small number of nucleation sites exists is a kinetic phenomena, not a thermodynamic one. Fully bonded amorphous states share the same entropy and energy. The tendency to form a crystalline region arises from the propensity to bury the ‘back’ or non-bonding side of the molecule. Figure 1.4.5-2 shows the evolution of a crystalline state in frames (a-f). As described in Section 1.4.4, the response of a liquid to a fluctuation is anisotropic; this has a strong influence on the kinetics of orientation surrounding a nucleation site. Consider for a moment one nucleation event, for example the molecule at lattice site *(i,j)* oriented in state *3* with a probability that upsets the metastability of the system (a). The initial bias will tend to orient its neighbor to the right in the opposite direction, state *1*, (b), as this orientation presents the largest probability for all the arms of the neighboring sites to be bonded.

The surrounding sites of this initial pair experience an environment that has strong orienting properties. The pair above the nucleus now will experience a strong tendency to align one of their associating ends with the associating ends pointing downward from the initial sites. To take best advantage of the energetics, the new pair will align in the same direction as the previous pair. This initiates the formation of a lamella (c).

From the sides of this initial lamella will evolve lamella oriented in the orthogonal direction (d). Again, the organizing feature is the anisotropic non-bonding side. As the growth occurs in an outward manner, eventually the different domains of lamella begin to influence the growth of each other (e). At the interSection there are a variety of satisfied orientations that can be adopted (f).

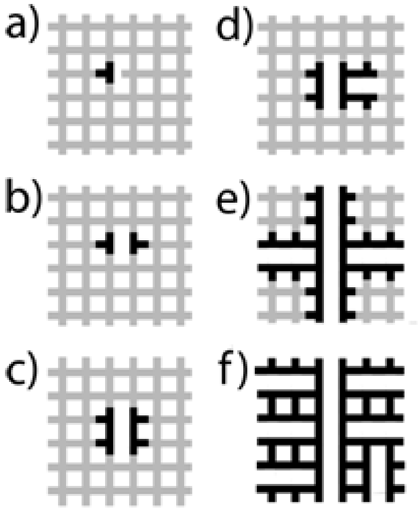

Figure 1.4.5-2: Progression of the DMF simulations from a nucleation point.
The oriented (solid-like) T-shaped molecules are shown in black while the grey T-shaped molecules represent those which are not oriented (are liquid-like).

When the system is instantaneously quenched to a temperature past the spinodal, spatial inhomogeneities in the probability distribution grow spontaneously. Unlike the isolated nucleation events that occur between the coexistence temperature and the spinodal, the simultaneous growth of all instabilities leads to heterogeneous microenvironments. The thermodynamic driving force for the T-shaped molecules to form associating bonds with their neighbors becomes sufficiently strong such that most or all adopt a preferred orientation. The T-shaped molecules attempt to maximize the number of bonds by choosing the locally optimal orientation determined by their microenvironments. The orderly growth of crystal-like structures at higher temperatures is replaced by simultaneous formation and growth of bonded clusters, which eventually grow to a large network. The resulting structure appears very amorphous without clear crystalline ordering. In this structure most sites are satisfied, i.e., their three arms are held strongly by bonds formed with their neighbors. However, because the structure results from the uncoordinated formation of associating bonds driven by the local needs of the molecules, some molecules may be left unsatisfied. These sites are shown in grey in Figure 1.5.5-1(b). While one orientation is chosen randomly at each of these sites for the purpose of illustration, these grey sites retain their liquid character ($p_1 = p_2 = p_3 = p_4$).

1.5. Solvated Phases: Gel-like Structures with Glassy Features

In this Section we explore the variety of morphologies that are observed when solvent (state 5) is present. We start with a discussion of the role that the solvent plays in the system and an investigation of the high temperature solution state. We follow this by a calculation of the mean-field phase diagram and our analysis of the spinodals. Finally we present simulation results that highlight the role of the glass transition in arresting phase separation.

1.5.1. Role of Solvent in Phase Behavior

When solvent is present, the interplay between phase separation and vitrification generates a variety of morphologies, including uniform solutions, phase separated droplets and a range of gel-like structures such as foam-like, networked and fibril-like morphologies. Which of these structures is observed in the simulation depends closely on the quench conditions.

We observe the solution phase above the coexistence line. The solvent and the T-shaped molecules are equally distributed over the lattice. The solute has an equal probability of being in any of the four states ($p_a(i,j) = \rho/4$ for $a = 1,2,3,4$ and $p_5(i,j) = 1 - \rho$). At lower temperatures the lattice will phase separate into solvent-rich and solute-rich phases. The solute-rich phase can either be an isotropic liquid phase or be in a glassy state depending on the concentration and temperature.

The interface between solvent- and solute-rich phases plays an important role in the local, morphological organization. The solute prefers to orient in such a way that its non-bonding side is adjacent to the solvent. This orients the molecule so that the associating groups are pointing towards the denser, solute-rich region, whether this region is still solution-like or has adopted a glassy configuration. The anisotropic nature of the T-shaped molecule causes it to behave as a surfactant at the interface between the T-shaped molecule rich phase and the solvent.

1.5.2. Mean-field Phase Diagram

We calculate the equilibrium phase diagram using the simplest approximation involving the singlet density. Although higher order approximations can be constructed without too much difficulty, we choose this level of approximation so as to be consistent with the level of mean-field approximation in the DMF simulation.

In the absence of orientational order, the liquid-liquid coexistence curve can be easily obtained. Assuming equal probability of the solute being oriented in each of the four orientations ($p_1 = p_2 = p_3 = p_4 = \rho/4$), the free energy per site is simply

$$\beta f = -(9/8)\beta\varepsilon\rho^2 + \rho\ln(\rho/4) + (1-\rho)\ln(1-\rho) \tag{12}$$

This is similar to the Bragg-Williams free energy for a lattice gas[56], the factor of 1/4 inside the logarithm having no effect on the phase diagram[57]. Equation 12 predicts a symmetric phase diagram with a critical point at $\beta\varepsilon = 16/9$.

For sufficiently low temperatures, we expect the high-density phase to be the vitrified phase with locally broken orientation symmetry. Since the free energy of the lamellar crystalline state is identical to that of the glassy state in our approximate treatment of the glassy phase in the fully-dense state, we will not distinguish between these two states here either. For the purpose of constructing the phase diagram, we will characterize the glassy phase the same way we characterize the fully-dense case ($p_1 > p_2 = p_3 = p_4$). This characterization amounts to a uniform dilution approximation, in which the effect of the solvent is simply to change the normalization of the probabilities from $\sum_{a=1}^{4} p_a = 1$ to $\sum_{a=1}^{4} p_a = \rho$. Under this approximation, the free energy of the glass-like state becomes,

$$\begin{aligned}\beta f_{ran} = &-(1/2)\beta\varepsilon\left[3p_1^2 + 4p_1(\rho - p_1) + (7/3)(\rho - p_1)^2\right] \\ &+ p_1\ln p_1 + (\rho - p_1)\ln[(\rho - p_1)/3] + (1-\rho)\ln(1-\rho)\end{aligned} \tag{13}$$

where the last term accounts for the entropy due to the presence of solvent.

Using Equation 13, the probability of the dominant orientation is obtained by minimizing the free energy with respect to p_1. The coexistence between the glassy state and the isotropic liquid or gas phases is calculated by equating the chemical potential ($\beta\mu = (\partial\beta f / \partial\rho)$) and the grand potential density ($\beta w = \beta f - \beta\mu\rho$). The phase diagram is shown in Figure 1.5.2-1 with a triple point at $\beta\varepsilon \approx 3.37$, $\rho \approx 0.97$.

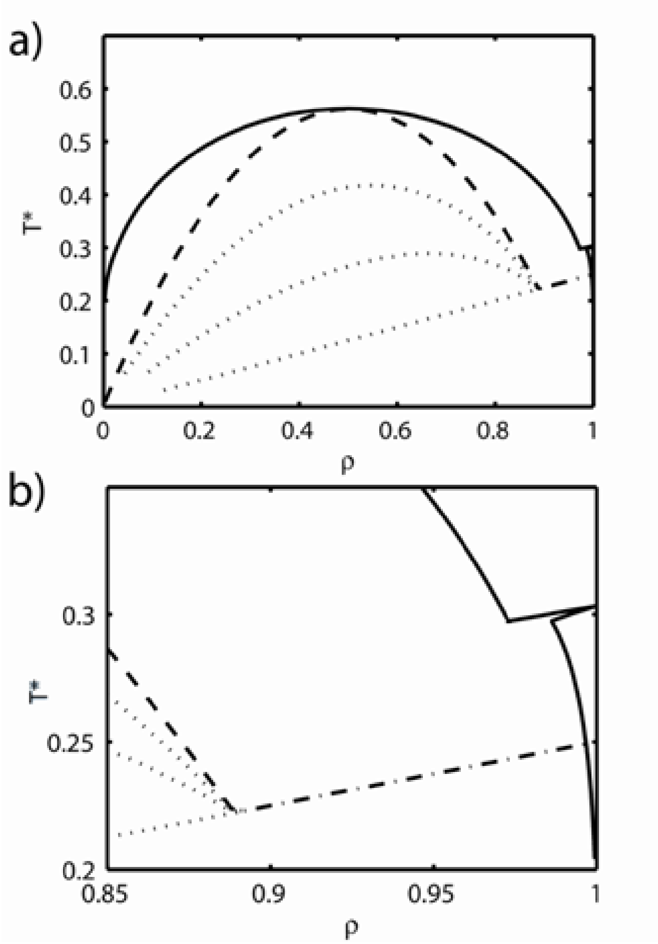

Figure 1.5.2-1: Mean-field phase diagram
(a) Phase diagram: binodal (solid line), macroscopic spinodal (dashed line) local ordering spinodal (dot dashed line), cascade of spinodals within the liquid-liquid spinodal (dotted lines). $T^* \equiv (\beta\varepsilon)^{-1}$ is the dimensionless temperature; (b) an expanded view of the high solute density region around the transition temperature for the glass-like phase.

1.5.3. Analysis of the Spinodals

As in the fully-dense case, the spinodal plays an important role in determining the thermodynamic and kinetic behavior of the system when solvent is present. With the DMF equations of motion, it is possible to perform a linear stability analysis of the uniform state and determine the linear rate of growth of the unstable modes that are consistent with the dynamic rules of the model. For simplicity, however, here we will examine the issue of stability based purely on a consideration of the free energy. The spinodal or limit of metastability is determined by evaluating the matrix of the second derivatives of the free energy:

$$F^{(2)}[a,i,j;a',i',j'] \equiv \frac{\partial^2 F}{\partial p_a(i,j)\partial p_{a'}(i',j')} \tag{14}$$

where F is the Helmholtz free energy as a function of the spatially varying singlet probabilities. We construct the matrix explicitly on a 16×16 lattice and diagonalize the matrix to find its eigenvalues. The vanishing of the lowest eigenvalue defines the spinodal. The result is shown in Figure 1.5.2-1.

Inside the liquid-liquid coexistence, we have the usual spinodal of the uniform liquid with respect to macroscopic phase separation (dashed line). In the high density region, there is another spinodal which corresponds to the limit of stability of the uniform liquid with respect to spatially inhomogeneous probability distribution on length scales of the size of the lattice spacing (dot-dashed line). This spinodal is the extension of the one occurring at $\beta\varepsilon = 4$ in the fully-dense state. As we decrease the temperature inside the envelope of the macroscopic spinodal, additional instabilities set in that represent progressively smaller length scales (dotted lines). We represent the onset of these new unstable modes by a family of curves as they move down the temperature. We note that while both the liquid-liquid coexistence curve and the macroscopic spinodal curve are symmetric, these higher modes of instability become skewed towards high density, presumably reflecting the tendency for orientational ordering. The most striking feature of this cascade of instabilities is that they converge to an extension of the spinodal of the uniform liquid with respect to local orientational ordering as temperature decreases. These higher instabilities will be crucial for determining the morphology of quenched structures in the two-phase region. We note that the phase behavior implied by our phase diagram is very similar to the general phase diagram of a physical gel, lending confidence to our assertion of gel-like features[58].

1.5.4. Correlations in the Solution Phase

As in Section 1.4.4, we measure the correlation in the system via the introduction of a small biasing field to a single site. Due to the anisotropy of the system, the resultant probability profile is again different for each state. In Figure 1.5.4-1, we show the profiles for each state along the *i* and *j* axis for a solution at $\beta\varepsilon = 1.7$ near the critical point of $\beta\varepsilon = 16/9$. For these calculations we use the grand canonical ensemble and set the chemical potential so that the unperturbed solution is kept at a density of $\rho_c = 0.5$ solute. We bias the probability of state *1* to be higher at site *(0,0)* by introducing a field of magnitude 0.01β at that site.

Overall there is an increase in solute density near the site of the perturbation. However, the self-surfactant characteristic of the molecule results in a very different probability profile when solvent is present as compared to the fully-dense liquid. In the negative *i* direction the perturbation has almost no effect on the probability profile whereas the profiles are remarkably symmetric along the *j* axis. This significant asymmetry between the positive and negative *i* directions as well as between the *i* axis and *j* axis foreshadows the inhomogeneous solid-like features at lower temperatures.

A correlation length can be similarly defined from the site of the perturbation. Again, a mean-field square root divergence with proximity to the critical temperature is obtained. In comparison to the fully-dense case, however, at the same relative distance to the critical point, the correlation length is significantly longer here.

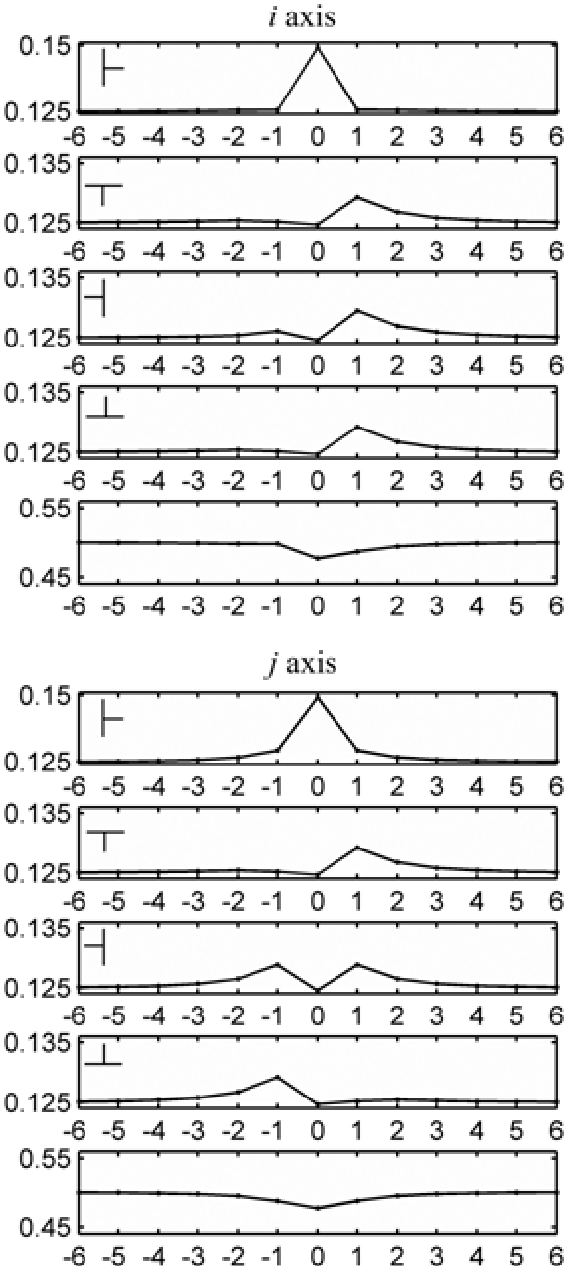

Figure 1.5.4-1: Result of small applied force in the liquid state
The probability of being in each state as a function of position along the *i* and *j* axis after a small pinning force with magnitude 0.01β favoring state *1* is applied at site *(0,0)* to a solution. The unperturbed solution-like state $\beta\varepsilon$=1.7, ρ=0.5 has an equal probability (0.125) of being in each rotational state of the solute and 0.5 of being solute (state *5*).

1.5.5. DMF Simulations: Gelation as a Result of Arrested Phase Separation

In the two phase region, a wide range of structures is observed. The results of a stepwise quench in which the lattice is equilibrated at successively lower temperatures show very different characteristics than those of a lattice that is quenched to the same conditions in one step. In order to illustrate this effect, we first present the results of a quench of the system that is equal parts T-shaped molecules and solvent.

When the simulation is taken from the 'high' temperature solution phase to just below the liquid/liquid coexistence curve, it phase separates without any (orientational) ordering. Both the solute-rich phase and the solvent-rich phase retain liquid character. If we further quench this structure to below many spinodals but at a temperature such that the solute-rich phase is above the triple point, we observe the formation of a layer of oriented molecules at the interface (Figure 1.5.5-1(a)). This film occurs at all of the solute-rich phase boundaries. The bulk of the molecular rich phase retains the expected liquid-like character. Small droplets of solvent-rich phase have developed within the initial solute-rich droplet. If this system is cooled further so that the solute-rich phase is below the triple point, then the solute-rich phase solidifies into a glass-like structure (Figure 1.5.5-1(b)). The presence of small, solvent-rich voids within the glassy droplet suggests a very dense gel-like structure.

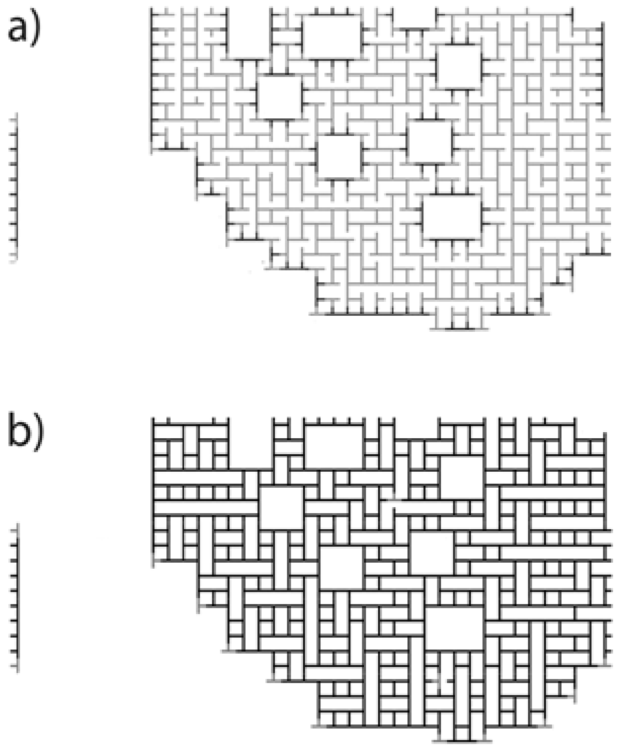

Figure 1.5.5-1: DMF simulation results at $\rho = 0.5$
(a) Phase separated droplet shows the self-surfactant character of the molecules. A simulation in the solution state was initially, instantaneously quenched to $\beta\varepsilon = 2$ and allowed to equilibrate, before instantaneously quenching to a final temperature of $\beta\varepsilon = 3$ and (b) Glassy droplet was successively equilibrated from a solution to $\beta\varepsilon = 2$, $\beta\varepsilon = 3$ and then, as shown, at $\beta\varepsilon = 4$. Sites shown in grey are not oriented but instead retain their liquid character.

If we plunge the system with equal parts molecules and solvent below many spinodals and near or below the triple point, we observe networked gel-like structures. Figure 1.5.5-2(a) presents a dramatic example of the highly ramified structure that is the result of an instantaneous quench. The structure is very different from that of the more step-wise quenched Figure 1.5.5-1(b) despite resulting from simulations at the same final conditions. Experimentally, such differences in features are closely dependant on the 'processing conditions'[59]. Our model replicates a wide variety of morphologies by changing the quench conditions and volume fraction of molecules.

Overall, if we quench a simulation in very small increments from the solution phase, we allow for phase separation to proceed unhindered. However, at some temperature below the triple point the phase separation transitions from liquid/liquid separation to liquid/solid separation. The solid phase is a disordered, glassy phase and the simulation is structurally arrested. As the simulation is further cooled small voids of solvent rich phase will accumulate within the molecular rich phase. The resultant structure is a very dense gel. In a similar manner if we quench from the solution phase directly to below the triple point the phase separation is arrested by the onset of the solid phase. However, since there is not sufficient time for liquid/liquid phase separation before the onset of vitrification, the structure is much less dense and has a networked characteristic.

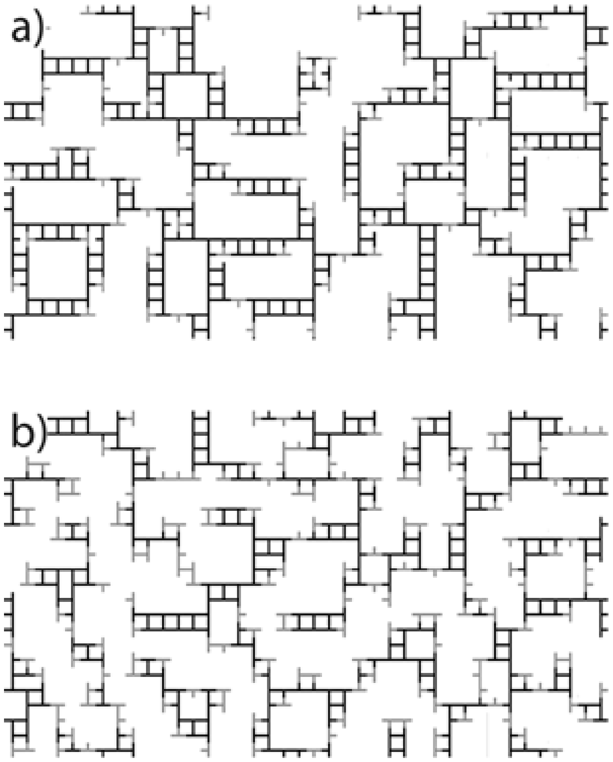

Figure 1.5.5-2: DMF simulation results at ρ=0.5

(a)A gel that results from a simulation instantaneously quenched from a solution state to $\beta\varepsilon = 4$ and (b) A gel quenched from a solution state to a lower temperature $\beta\varepsilon = 10$. Sites in grey retain their liquid-like character.

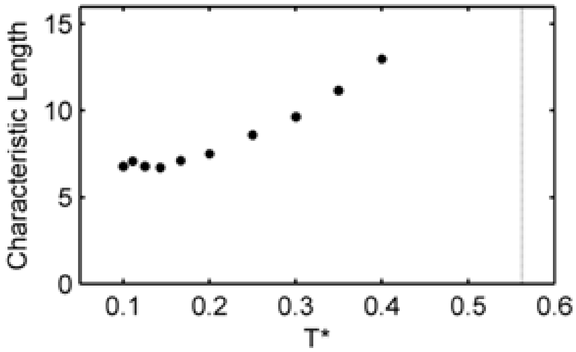

Figure 1.5.5-3: DMF simulation results at ρ=0.5: the characteristic length (defined as 2π over the peak position of the circularly average structure factor) as a function of the quench depth given in dimensionless temperature $T^* \equiv (\beta\varepsilon)^{-1}$. The data are the result of averaging over 40 simulations of an 80 by 80 lattice. The dotted line indicates the critical temperature.

The length scale of the gel depends on the quench depth. We compare an instantaneous quench to a moderate temperature (Figure 1.5.5-2(a)) with a quench to a very low temperature (Figure 1.5.5-2(b)). Although the system is initially at the same identical liquid conditions, the deeper quench results in a smaller feature size. We can quantify the length scales of the gel by examining the peak position of the density-density structure factor[60]. As can be noted in Figure 1.5.5-3, there is a clear trend towards a smaller characteristic length with temperature. This is consistent with our analysis of the cascade of spinodals in Section 1.5.3; the instability with respect to spatial inhomogeneity shifts to smaller length scales as temperature decreases.

More precisely, however, the observed dependence on the temperature is a consequence of both thermodynamic and kinetic factors. It is well known that in spinodal decomposition the most unstable mode has a wavelength inversely proportional to the square root of the distance to the critical temperature[61]. In a simple binary mixture, coarsening occurs beyond this initial growth of the most unstable mode. However in our system, once the concentration of the T-molecule rich phase becomes sufficiently high, vitrification sets in which arrests any further domain growth. The deeper the temperature quench, the smaller the length scale of the initial instability, and hence the smaller the length scale at which the system gets arrested. The decrease in length scale with deeper quench was observed in a colloidal gel system studied by Dinsmore and Weitz[13].

We note that there is an interesting transition between coarsening to macroscopically phase separated states at temperatures just below the critical point and developing ramified microstructures at lower temperatures (still above the triple point). We speculate that this transition reflects the tendency toward inhomogeneous structures at finite length scales associated with the lower spinodals which are more of microphase separation than of macrophase separation in nature.

Simulations at similar temperatures but at higher volume fraction of molecules demonstrate other features of the gel-like structures that can be formed. At these higher concentrations, we can form dense gels that span the space of the simulation. Figure 1.5.5-4(a) is a result of a two step quench. While the solvent rich voids are of the same scale as the glassy droplet in Figure 1.5.5-1(b), this structure more resembles a foam. As before, when the simulation is quenched directly it results in a more networked structure with smaller mesh sizes (Figure 1.5.5-4(b)).

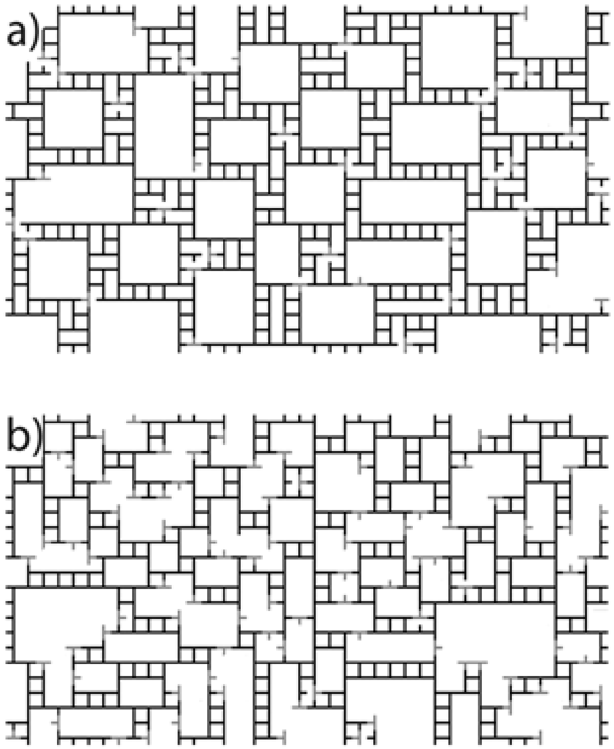

Figure 1.5.5-4: DMF simulation results $\rho = 0.65$
(a) A two step quench starting with the solution phase instantaneously quenched to $\beta\varepsilon = 3$ and allowed to equilibrate before being quenched to $\beta\varepsilon = 5$ and (b) A single step quench from the solution state directly to $\beta\varepsilon = 5$.

Exploring the portion of the two phase region at low volume fraction of the T-shaped molecules, we observe the formation of suspended small droplets and fibrils. Given enough time to first phase separate under liquid/liquid conditions before quenching below the triple point, small droplets of glass form. On the other hand, if quenched quickly ladder-like fibrils result. These suspended structures could be due to the lack of a cluster diffusion mechanism in our dynamics; it is not clear, however, that when such a mechanism is included these droplets and fibrils would aggregate or coalesce. As the surfaces of these structures have relatively few unbonded association sites, even if the droplets or fibrils were to come into contact they might not aggregate. For the suspended structures to aggregate or coalesce, internal restructuring is required, which is greatly inhibited by the vitrification of the solute below the triple point[62]. Therefore, since these structures still correspond to local free energy minima we include them in the class of gel structures in our consideration, even though they lack the connectivity of a space-spanning network usually associated with gels.

It has long been noted that gel formation in the two phase region is highly dependant of the conditions of formation, much to the chagrin of experimentalists. De Gennes observed that incomplete phase separation due to an effective change in solvent quality during polymer association and slow kinetics of solvent diffusion lead to heterogeneous gels[63]. Our model also results in heterogeneous gels; however in our case the inhibition of phase separation is due to kinetic arrest arising from the formation of a glassy state in the solute rich regions.

We develop a picture of the phase behavior of these systems being arrested in a metastable state by the onset of glass-like structure. This incomplete phase separation, though driven by the thermodynamic conditions, represents a kinetic phenomenon. The features that we observe are determined by the confluence of the thermodynamic and kinetic conditions.

1.6. Structural Relaxation in the Glassy State

Thus far, we have been focusing on the thermodynamic and structural properties of our system. The diversity in morphologies observed in the gelation regime highlights the critical role of kinetics as well. In this Section, we study the structural relaxation in the fully-dense phase. Our discussion has been focused on the mean-field phase diagram and structures obtained with the DMF simulations. Within this framework, once the system finds itself in a local free energy minimum, no relaxation is possible from this state. However it is possible to study the relaxation in the liquid state as the system is cooled. We explore the relaxation of the system in the fully-dense case by examining the energy landscape features and the relaxation mechanism at low temperatures. We also include results from both DMF and MC simulations that show dynamics characteristic of glass forming systems.

1.6.1. Features of the Energy Landscape

The energy landscape paradigm has become an important guide to consider the thermodynamic signatures of glasslike systems [for reviews see 38, 64-66]. An unusual feature of our model is the exponentially large number of states in which all the associating sites are satisfied. The lamellar crystalline state is but one of these states (Figure 1.4.5-1(a)). A lower bound on the number of ground states in the fully-dense case can be estimated by the following argument. We note that a foursome of molecules can be organized in two energetically equivalent ways which present to the neighbors of this grouping the same number of associating sites (Figure 1.6.1-1(a-b)). A fully satisfied lattice can be created by using this foursome as the repeating units in either of these two states. Thus on a lattice of size n there are $2^{n/4}$ satisfied configurations. This is a lower bound as more complex repeating units can be used to generate the lattice (Figure 1.6.1-1(c)) and there can also be structures that cannot be created using any repeating units.

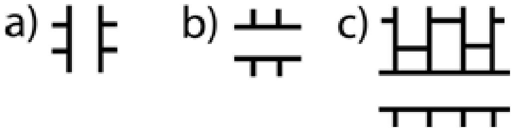

Figure 1.6.1-1: Determining the number of ground states
(a,b) two basic building blocks from which we can demonstrate that there are an exponential number of ground state configurations; (c) additional state not accounted for in the previous estimation

As the temperature in a glass forming liquid nears the glass transition T_g ,it has been empirically noted that the stretched exponential functional form, $\theta(t) = \exp[-(t/\tau)^{\beta}]$, fits both experimental and simulation measurements of the structural relaxation well. The dramatic increase of relaxation time upon cooling in fragile glasses can be described well by the Vogel-Fulchur (VF) equation, $\tau/\tau_o = \exp[D/(T - T_o)]$ with the value of D being the 'fragility index'[67].

The large degeneracy of the minima in the free energy landscape, together with the relatively low barriers separating the minima (in the sense that the rearrangements can be made by breaking a small number of bonds) implies fragile liquid behavior. However at sufficiently low temperatures, the relaxation mechanism involves creating isolated unpaired bonds, with a well defined energy scale (see Section 1.6.4 for more discussion). This suggests an Arrhenius dependence of the relaxation with temperature which is associated with strong liquid behavior. Therefore we expect that our systems will exhibit fragile-liquid characteristics at higher temperatures and strong-liquid characteristics at very low temperatures.

1.6.2. Relaxation in DMF Simulations

The DMF simulation technique described in Section 1.3 is employed for temperatures above the spinodal to observe relaxation of small and random perturbations back to a uniform liquid state. To quantify the relaxation behavior, we define an order parameter:

$$m(t - t_0) = \frac{\sum_{i=1}^{N}\sum_{a=1}^{4}\sqrt{\left(p_a(i;t) - 0.25\right)^2}}{\sum_{i=1}^{N}\sum_{a=1}^{4}\sqrt{\left(p_a(i;t_0) - 0.25\right)^2}} \tag{15}$$

The decay of this function is found to be well fit by a stretched exponential form $m(t-t_o)=\exp-\left(\frac{t-t_o}{\tau}\right)^{\beta}$. Figure 1.6.2-1 shows the behavior of the exponent β and characteristic time τ as a function of temperature.

We find that as the temperature decreases, β decreases significantly from one, as is characteristic of a fragile liquid[68]. At the same time, the dependence of the relaxation time with temperature is well fit described by the VF equation. Remarkably, the least square fit to the data in Figure 1.6.2-1 results in $T_o \cong 0.24$, very close to the theoretically predicted mean-field spinodal, implying an 'ideal' glass transition at this temperature [69]. To see if this observed relaxation could be more a reflection of a critical slowing down rather than glassy dynamics, we have also fitted the relaxation time τ into $\tau=\tau_o\left|\frac{T}{T_C}-1\right|^{-2\nu z}$ where ν and z are respectively the correlation length and dynamic scaling exponents; the mean-field values $\nu=1/2$ and $z=2$ are used[70]. We find that the fit is quite poor (not shown).

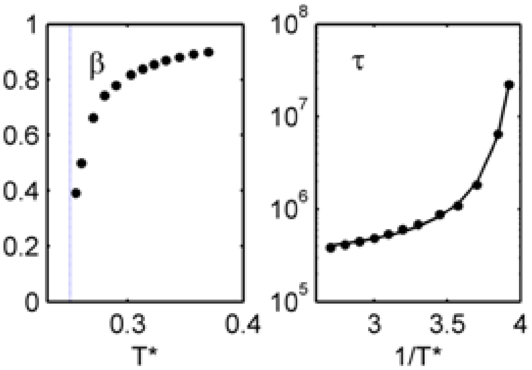

Figure 1.6.2-1: Glassy dynamics shown in DMF simulations
a stretched exponential functional form is fit to the relaxation of the order parameter (equation 15) The figures show the temperature dependence of the stretching exponent β and characteristic time τ.

1.6.3. Relaxation in MC Simulations

To investigate relaxation without the restriction of the mean-field approximation, MC simulations are performed. The rules of motion are described in Section 2. Simulations are equilibrated at each temperature over many MC steps (each step is defined as one randomly proposed move in configuration space that may or may not be performed)[71] We then perform 1.6 x 10^6 MC steps on the initial configuration and track the correlation function $\theta(t-t_o)$ defined as the fraction of sites on a lattice which have not undergone any transition to other states from time t up to t_0. We repeat this procedure 10 times and average the resulting correlation functions. We then fit $\theta(t-t_o)$ with a stretched exponential form and repeated the process. The temperature dependence of β and τ are shown in Figure 1.6.3-1. Note the small increase in β at the lowest temperatures; this may reflect the approach to the strong liquid limit (this will be discussed further in Section 1.6.4). Our results are similar to that of a simulation for liquid silica which found that the material behaved thermodynamically as a ‘fragile’ liquid at high temperature while a ‘strong’ liquid at low temperatures[72].

When the VF equation is fit to the relaxation time as a function of temperature, we find $T_o \cong 0.07$ which is well below the mean-field spinodal temperature. This is a consequence of activated events allowing for exploration of the energy landscape below the onset of inhomogeneous energy minima. As in experiments, the glass transition is a kinetic phenomenon defined by the relaxation time of the system. As equilibration at very cold temperatures takes an exceedingly long-time, and since our main focus in this present work is illustrating some structural and thermodynamic properties, we have not yet evaluated temperatures as low as T_o found from the VF fit; these calculations will be performed in the future.

Overall these MC simulation shows dynamics that reflect a 'stronger' liquid than that observed with DMF simulations. Various explanations of deviations of T_o from T_k – which are generally greater for 'stronger' liquids than they are for more 'fragile' liquids– have been proposed[68, 73]. The fundamental reason appears to be decoupling of the thermodynamics (distribution of energy minima) and kinetics (details of the depth of the well around the minima) on the landscape[74]. Thus it is not surprising that the MC simulations which reflects both thermodynamics and kinetics would reveal different results than those of the DMF simulations which involve the thermodynamics alone.

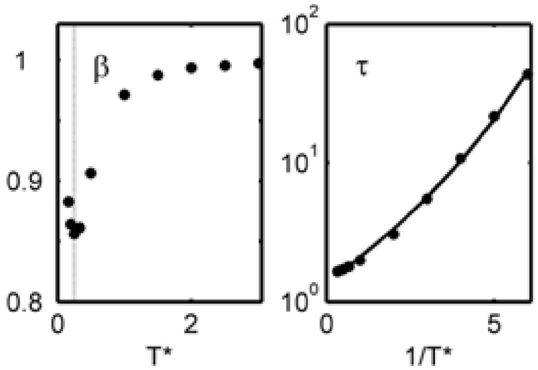

Figure 1.6.3-1: Glassy dynamics shown in MC simulations
a stretched exponential functional form was fit to the averaged relaxation of the correlation function. The figure shows the values of the stretching exponent β and the characteristic time τ.

1.6.4. Relaxation Mechanism at Low Temperatures

The landscape features of our model imply a different relaxation mechanism than commonly associated with structural relaxation in supercooled liquid as it approaches the glass transition which usually involves hopping between deep free energy minima separated by large, energetic barriers[65, 69, 75, 76]. In our model, proceeding from one ground state to another involves only a small energy penalty. All that is required is for one molecule to rotate, breaking a pair of bonds. This pair of unsatisfied T-shaped molecule can then diffuse over the lattice, changing the state of the system at each time step, until they annihilate themselves by finding another unpaired T-shaped molecule. We can directly observe this behavior in our MC simulations. At low temperatures, the concentration of such unpaired molecules is roughly $\exp(-\beta\varepsilon)$. The area per unpaired molecule is thus $\exp(\beta\varepsilon)$. Assuming this molecule diffuses freely with a diffusivity ω, the area visited in time t is proportional to the mean-square distance traveled by the molecule $R^2 \sim \omega t$. The system will have relaxed from its initial configuration if an unpaired molecule has visited an area of the size of the area per unpaired molecule. Thus the relaxation time is simply $\tau \sim \omega^{-1} \exp(\beta\varepsilon)$[77]. While this argument does not predict the time dependence of the relaxation dynamics, it shows that the slowing down of the dynamics as temperature decreases is due to the decrease in the number of (essentially isolated) 'mobile' (i.e., unpaired) molecules. This is a very different process than that of an activated process on a landscape with deep energy minima, which often requires concerted or facilitated motion. Instead of the glass or gel being the result of high energy barriers, in our model they result from the multiplicity of energetically degenerate states.

The temperature dependence predicted from the low temperature argument is Arrhenius. Thus at very low temperatures, our model should behave like a strong liquid; this is consistent with the upward turn of the stretching exponent β as temperature is decreased at very low values and the observation that the right-most data for the characteristic time τ on the semilog plot (Figure 1.6.3-1) appears to approach a straight line.

1.7. Conclusions

The strength of this lattice model lies in its simplicity and its ability to capture a wide range of morphological behavior without imposing an artificial constraint that causes the system to be frustrated. In our model, amorphous vitrified (glass or gel-like) structures arise not because of frustration but because of the ready availability of a large number of inhomogeneous free energy minima; this observation is consistent with the recent thermodynamic picture of structural glasses resulting from self-generated randomness as a result of a large number of degenerate ground states[78-81]. Although nontrivial, glassy dynamics do not require the existence of a large number of inhomogeneous free energy minima, however the existence of such minima necessitates a change in the dynamics. Shifting from liquid-like to glass-like, relaxation of the system now requires leaving the free energy minima through thermal activation. In the DMF simulations, which do not allow for thermal fluctuations, the dynamic transition temperature occurs at the mean-field spinodal. When activated motion is possible in the MC simulations, the dynamic transition temperature is lower than the spinodal. However, it is important to note that both simulations exhibit glassy behavior at low temperatures.

An important result of this work concerns the nature of the gel phase and its relationship to the glass phase. Various authors have noted the similarities between these two classes of materials[17, 82-84]. Our model allows us to explore this relationship. From the structural and thermodynamic point of view, both states of matter result from the proliferation of a large number of inhomogeneous free energy minima, which are ultimately connected to the underlying mean-field spinodals with respect to inhomogeneous structural fluctuation. In our model, the glassy state is obtained as a result of the quenching of the liquid phase in the high density, one-phase region of the phase diagram below the temperature for the appearance of an exponentially large number of inhomogeneous free energy minima. The gel state can be viewed as an extension of the glassy state into the two phase region, or equivalently as an incomplete phase separation arrested by the onset of glass transition. The length scale of the gel phase is determined primarily by the most unstable, i.e. fastest-growing, mode – a deeper quench leads to a network with smaller mesh size. The arrest of phase separation is a result of the system having reached a state of local free energy minimum. At such free energy minima, the deterministic thermodynamic driving force vanishes; further evolution of the structure must require overcoming free energy barriers. Such a relaxation mode is very different from the coarsening process in a typical phase separating binary fluid; in our case the relaxation of this structurally arrested state is more properly described as an aging process.

The behaviors exhibited by our model relate well to those of colloidal gels in particular. Colloidal gels are akin to a solvated glass that has short range attractive interactions[17, 84], a feature that we capture in our model. The decrease in the characteristic length scale with quench depth lends further credence to this correlation. While it might be surprising that this is the case given the isotropic nature of a colloidal particle, we believe that this suggests that the steric constraints on the system are fundamentally similar to an anisotropic interaction in a lattice model. Indeed, a two dimensional square lattice model in which each site can only form up to three attractive interactions with its nearest neighbors is identical to our T-shaped molecule model.

Our model can be extended in several directions. First, as alluded to in the model description, it is straightforward to add an isotropic term that either favors or disfavors nearest neighbor contacts between the solute molecules. The latter type would suppress the critical temperature, possibly making it lower than the glass transition in the fully-dense case. The resulting phase diagram would appear closer to the phase diagram for colloidal particles with short-ranged attractions[17]. Second, it is possible to construct three-dimensional versions of the model. Besides the obvious fact that most systems are in three dimensions, the mean-field approximations are more accurate in three dimensions than in two. Finally, exploring the dynamics of the solvated state should prove interesting and help investigate the gelation transition as it relates to vitrification. We plan to pursue these directions in the future.

Acknowledgment: This research was supported in part by the National Science Foundation through the Center for the Science and Engineering of Materials.

2. Chapter 2: The Glass Transition: Comparison of the Supercooled Liquid and the Kinetically Arrested Glass

2.1. Introduction

Interest in valence-limited materials is growing, due to both their unique behaviors and their potential to form self-assembled materials with highly controlled physical properties. Despite length scales which differ by orders of magnitude, from atomic[4, 85, 86] and molecular [5, 72, 87] fluids to polymeric[88] and colloidal systems[7], these materials share common structural and dynamic features. They are all characterized by intermolecular potentials in which anisotropic interactions prevent high density conglomerates, instead allowing for more open and organized network formation[7]. These potentials describe unique and important molecular materials such as water, silica[89] and silicon[4]. The 'lock and key' specificity of natural motifs allows DNA[3, 90] and proteins[3, 91] to form anisotropic, networked structures. Directional anisotropic interactions can also be an emergent characteristic in systems after a conformational change. Examples include polymer-grafted nanoparticles[92] and low-molecular mass gelformers[93], proteins and DNA which assemble into fibers[8]. Additionally, the phase diagrams of a subset of these systems, those that form gels[3, 13, 29, 90, 94, 95, (Appendix D)], seem to be influenced primarily by the specific number of possible nearest neighbors[6], suggesting that design of novel materials can be predicted from general principles. Our strikingly simple T-shaped molecular model captures the behavior of this diverse class of materials well[1].

The phase diagram presented in our previous work demonstrated that valence-limited systems can form a wide range of materials influenced not only by the equilibrium characteristics, but also by kinetic arrest. The T-shaped molecular model includes simple liquids, gels, glasses, foams and colloidal solutions in different regions of the phase diagram dependent in part on the quenching conditions. We use the term 'molecule' to describe our elementary bonding unit; however, our model could equivalently represent an abstraction of an atomic, molecular, polymeric or colloidal system. As we seek to understand this class of materials, we must grapple with the thermodynamic and kinetic features of dynamic arrest in the high density region. Particularly, we need to consider the nature of the glass transition as it pertains to this system.

All materials, under the appropriate experimental conditions, can be supercooled below their normal melting temperature and arrested in an amorphous state on the observed timescale. Many material properties change as the glass transition temperature, T_g, is approached due to a dramatic slowing in the molecular motion and an increase in the relaxation time, τ. One of the most interesting features of supercooled liquids is that the relaxation processes become non-exponential. Near T_g the response function, $\phi(t)$, is well fit by the Kohlrausch-Williams-Watts (KWW) equation:

$$\phi(t) = e^{-\left(t/\tau\right)^{\beta}} \tag{1}$$

The value of the stretching exponent β generally decreases from 1, or simple exponential behavior, as the temperature is lowered. This behavior is also observed in gel forming materials[96].

The temperature dependence of τ near T_g has often been used to classify glass formers[64]. 'Strong' materials show nearly linear behavior on an Arrhenius plot of $\log(\tau)$ as a function of inverse temperature. Conversely, 'fragile' materials exhibit non-linear, super-Arrhenius, activation energy growth as the temperature decreases[67]. Usually, fragile liquids have a smaller value of β than strong liquids[97].

At high temperatures, simple liquids are Arrhenius in nature. As they are quenched, they reach a temperature, T_{onset}, below which there is the onset of a more fragile regime. In a number of systems there is an apparent return to Arrhenius behavior at very low temperatures referred to as the fragile-to-strong crossover (FSC)[3, 5, 72, 89, 98-102]. In addition to these dynamic properties, it has been shown that there is an inflection point in the configurational entropy, $s_c\left(T\right)$, near T_{FSC}. If we were to extrapolate the $s_c\left(T\right)$ from temperatures above the FSC, then we would find a finite temperature or 'Kauzmann' temperature, T_K, at which $s_c\left(T_K\right)=0$. Below T_K, the entropy of the liquid would be less than that of a crystal resulting in a violation of the third law as $T\rightarrow 0$[19], commonly known as the 'Kauzmann Paradox'[38]. However, the inflection point may avoid this result, instead leading to $s_c\left(T\right)>0$ for all temperatures[89]. Valence-limited systems have also been also shown to have C_v maxima, or inflections in $s_c(T)$, at all densities in the phase diagram. Whether this universally reflects a structural change is not clear[7]; however, there is compelling evidence that structural changes in colloidal systems with patchy interactions are related to the maximum in heat capacity[40, 91].

We have previously identified two factors that contribute to the rich phase behavior of the T-shaped model: local arrangements that lead to stable structures on microscopic length scales and degenerate energy minima on the potential energy landscape (PEL). Degenerate ground states are a general characteristic of limited valency systems[7]. Under the PEL paradigm[103, 104], a system is described as a point moving along a hyper-dimensional surface. If the simulation sample is at equilibrium, the probability that the system will occupy a specific location on the PEL is determined only by the thermodynamics. In both equilibrium and arrested systems, the transition states between minima on the surface defines the motion kinetics and as well as the dynamic response.

A variety of explanations have been posed for the origin of the FSC transition. As in the case of the glass transition, we can broadly group these descriptions into those with a kinetic basis and those which suggest an underlying thermodynamic cause. From either perspective, a rough overview is coming to light. Couched in the perspective of the PEL, near T_g the energy required to overcome the energetic barriers between minima becomes significant. Additionally, the system may be unable to explore the full landscape due to the lack of mobility of near-neighbors, reducing the configurational entropy. The confluence of these effects leads to super-Arrhenius temperature dependence in this regime. At the lowest temperatures, the system becomes energetically trapped or structurally frustrated in a single basin or region of basins such that configurational entropy is nearly temperature independent. Only energetic terms contribute to the relaxation time dependence on temperature, which becomes Arrhenius again. Strong glass properties such as simple exponential behavior of the correlation function, appear to be connected to elementary local independent process of bond breaking[7]. Inherent in this description is a reduction in configurational entropy as the exploration of the surface becomes limited, and regions may become inaccessible.

Kinetically constrained descriptions of glassformers describe facilitated motion of the molecule based on the mobility of the near-neighbors. Above T_{FSC} hierarchical dynamics dominate, requiring multiple near-neighbors to obtain certain configurations before moving. At lower temperatures only infrequent single, isolated activation steps lead to diffusive motion[28]. The higher temperature dynamics are thus the result of cooperative motion, leading to fragile characteristics, while the lower temperature dynamics are the result of individual rearrangements and, thus, return to diffusive motion and strong behavior. From this viewpoint, it is the kinetics of the model that lead to the thermodynamic and structural properties[28]. It is interesting to note that this model depends on the formation of defects which at low temperature have a concentration proportional to the energy, matching our prediction for the T-shape model[1].

Alternately, it has been noted that there are a vanishing number of defects at low temperature in network glass formers, often with a dramatic threshold or 'cutoff' of the density of states at the FSC[89]. This suggests that the PEL has a large gap between higher temperatures, where there are many locally metastable configurations, and low temperatures with limited configurations that met bond requirements. This observation may be a result of a buried phase transition[105]. Of particular note is a speculated buried liquid-liquid coexistence line in systems with potentials that facilitate both a high density isotropic liquid phase and a low density networked liquid phase[5, 36, 106]. The 'Widom line', which is a continuation of the coexistence line past the critical point and into the one phase region of the phase diagram, reflects the asymptotic convergence of response functions close to the critical point due to their common reliance on the correlation length. A system crossing the Widom line upon cooling will not demonstrate the discontinuity in the measured characteristics associated with a phase transition, but will still exhibit a dramatic change. The result is that the response function maximum, in our case C_v, marks thermodynamically the FSC[5, 72]. It has been suggested that different classes of glass formers may be characterized by the shape and magnitude of C_v as well as its relative location with respect to the melting temperature of the liquid[107].

An example of a buried liquid/liquid phase transition can be found, in valence controlled atomic glass formers (e.g. in MD simulations of a modified Stillinger-Weber potential[85] for tetrahedral silicon[4], as well as in a germanium experimental system[86]) where there is a liquid/liquid transition such that the coexistence shifts from a single liquid metastable with respect to the crystal phase to two liquids, one of which is structurally similar to the crystal. This liquid immediately crystallizes resolving the Kauzmann paradox[4].

It has been postulated that there is a phase transition in trajectory space, as opposed to configurational space[108]. The premise is that the order parameter that should be evaluated is the trajectory of a system on the configuration manifold of the PEL. As the system becomes increasingly correlated in motion on the PEL, a first-order phase transition takes place between trajectories that remain ergodic and those that are non-ergodic[108, 109]. While no thermodynamic variables are specifically causal to this transition, there is a direct relationship to the features of the PEL[108]. Along a similar line of thought, tree representations of the PEL have been helpful in evaluating pathways towards low energy minima[110]. Wales and Bogdan created the discontinuity or tree graphs for several Lennard-Jones (LJ) potentials to demonstrate the entropic funneling could direct the state of the system, as is reflected in the heat capacity calculations[110].

Spatial heterogeneity with regard to dynamic phenomena has been well documented in both simulations and experiments of glassy systems[87]. The correlation functions of glass-like materials are often well described by a stretched exponential fit, pointing to the likelihood of a superposition of relaxation phenomena. This leads to the assumption of different local environments which would accommodate this range in values. Empirically, the Vogel-Tammann-Fulcher (VTF) is often used to describe the temperature dependence of the dynamics for fragile glasses:

$$\tau = \tau_o e^{\left(\frac{D}{T-T_o}\right)} \tag{2}$$

It is mathematically equivalent to the Williams-Landel-Ferry equation used in polymer science[64, 111]. The accuracy of this fit in so many systems suggests that the presence of a characteristic temperature T_o, at which the relaxation time would diverge, has a physical origin. This result inspired an early theory by Adam and Gibbs[69], which defines the glass transition as a loss of ergodicity due to growing cooperatively rearranging regions, described by the size of energy fluctuations required to allow a group of particles to collectively relax into their local equilibrium. Other more recent theories and models build on this work, utilizing some form of spatial partitioning of the system[27, 68]. There is growing experimental and theoretical evidence that material dynamics are very different in regions only a few nanometers apart at temperatures near the glass transition. An excellent review of spatial heterogeneity by Ediger[97] captures a variety of results from experimental and simulated systems, as well as potential explanations. Of note, it is not clear whether the spatial heterogeneity is a result or cause of the dynamic heterogeneity. There is no apparent structural cause for these cooperative regions as a liquid is supercooled. X-ray and neutron scattering studies only show small changes in local packing even in samples with viscosity changes of 12 orders of magnitude[97]. Our model gives us insight into the spatial dynamics of a prototypical example of valence-limited glasses, hopefully lending further information towards this fundamental question.

Within this chapter we extend our work with the T-shaped molecule model to include not only structural, but also dynamic information collected from simulation samples. A paucity of low temperature measurements hinders attempts to understand the fragile-to-strong Crossover (FSC)[102, 112]. Exploration of valence-limited systems have also been inhibited by the inability to access low temperatures[113]. Our work, which captures low temperature supercooled equilibrium states as well as kinetically arrested states, sheds some light on these questions. After defining the model in the appropriate context in Section 2, we describe the simulation methods used in Section 3. We then analyze the equilibrium liquids structure and dynamics in Section 4, and compare these with the kinetically arrested, non-equilibrium, glass formers reported in Section 5. In Section 6, evidence of structural heterogeneity in the equilibrium system is presented. We end this chapter with a discussion of our results to date and a brief summary of our conclusions.

2.2. Definition of T-shaped Molecule Model

The T-shaped molecule occupies the vertex, located at $\vec{i}$ on a square lattice, a model we previously described[1]. Each T-shaped molecule, σ_α, has three bonding sites which lie in a plane, resulting in 4 possible orientations, $\alpha = 1, 2, 3$ or 4. When the T-shaped molecules at two neighboring vertices, $\langle \vec{i}, \vec{i}\,' \rangle$, are oriented such that they each have bonding sites along the same edge, we define the resulting connection to be a bond which leads to a favorable energetic interaction. Else, there is no interaction.

Our simulation samples are in the fully-dense region of the phase diagram where every vertex is occupied by a molecule. While the density of T-shaped molecules (1 per vertex) is a conserved quantity, the density of bonds is not. Instead, the density of bonds is strongly influenced by the temperature. In the limiting case of high temperature, the bond density is 9/8 per vertex on a square lattice[114]. As the temperature goes to zero, the bond density approaches 3/2 per vertex.

For convenience and clarity, we restate the Hamiltonian for the fully-dense lattice:

$$\beta H(t) = {}^{-\beta\varepsilon}\!/_{2} \sum_{\langle \vec{i},\vec{i}\,' \rangle} \sigma_\alpha\left(t;\vec{i}\right)\sigma_\gamma\left(t;\vec{i}\,'\right) \tag{3}$$

where

$$\sigma_\alpha\left(t;\vec{i}\right)\sigma_\gamma\left(t;\vec{i}\,'\right) = \begin{cases} 1 \text{ if both molecules have bonding} \\ \quad \text{sites along the shared edge } \left\langle \vec{i},\vec{i}\,' \right\rangle \\ 0 \text{ otherwise} \end{cases} \tag{4}$$

the Greek subscripts indicate the orientation of the molecule($\alpha = 1,2,3$ or 4), t indicates that the orientation may be different at different times, and the sum is over all shared edges (near-neighbors pairs). The temperature is expressed in reduced units $T^* = \left(\beta\varepsilon\right)^{-1}$. We omit the asterisks in the following text for convenience. All simulation samples studied are 128 vertices by 128 vertices with periodic boundary conditions. This is much larger than any spatial correlation found within the simulation samples themselves.

In previous work (Section 1.4.3)[1], we reported the transition temperature under the mean-field approximation as $T_{mf,critical} = (3\log 3)^{-1}$ with the supercooled stability limit of $T_{mf,spinodal} = 1/4$. In the following sections and discussion, we will identify other temperatures of interest. However, these transition temperatures provide a reference point during our work.

2.3. Simulation Methods

The glass transition is, by its very nature, controlled by the interplay of the thermodynamics and kinetics of the material. One powerful description of this interrelation is the energy landscape paradigm. We can visualize all possible states of the lattice as defining a hyper-dimensional PEL (albeit discrete) in conformational space. A specific state of the system (our simulation sample) m is located on the PEL at the conformation coordinate $\vec{x}_m$, where $\vec{x}_m \equiv \left\{ \sigma_{\alpha_1}\left(\vec{i}_1\right), \sigma_{\alpha_2}\left(\vec{i}_2\right), \cdots, \sigma_{\alpha_N}\left(\vec{i}_N\right) \right\}$. The numerical subscripts specify individual molecules, σ, in orientation α and location $\vec{i}$ on the square lattice. The energy at $\vec{x}_m$, E_m ,is defined by the Hamiltonian and motion along the surface to a new coordinate $\vec{x}_k$ occurs by the change in orientation of a single molecule.

The energy at each state, however, only defines the intrinsic thermodynamics of the system. We must also incorporate the appropriate transition probabilities $q_{k \to m}$ between states such that at long-time ($t \to \infty$) the probability that a simulation sample is found in state m, p_m, reflects the canonical distribution. (All our simulations were performed using the canonical ensemble with our simulation samples coupled to a thermal bath.) In Section 2.3.1, we will find that there are many choices of $q_{k \to m}$ which could satisfy the requirement and lead to the appropriate distribution. We employ two different Monte Carlo (MC) simulation techniques with their associated transition probabilities in our work.

The first is a modified Metropolis MC recipe, as described in Section 2.3.2, with which we indentify the low temperature 'equilibrium' conditions. If we wish to explore the kinetic properties of our model and collect dynamic information, we must also define the physically appropriate transition states $\vec{x}^{*}_{m \to k}$ for our model. The choice of $q_{k \to m}$ is now further restricted to incorporate the energetic impact of these transition pathways. Residence time kinetic Monte Carlo (kMC) incorporating both the use of the landscape description to find the transition probabilities and a technique to improve the speed of the simulation is described in Section 2.3.3. Further description of these methods can be found in Appendix E.

2.3.1. Master Equation

As the equilibrium probabilities are not known *a priori*, we use the master equation formalism such that any initial distribution explores conformation space according to the dynamic path[115]:

$$\frac{dp_m(t)}{dt} = \sum_k q_{k\to m} p_k(t) - \sum_k q_{m\to k} p_m(t) \tag{5}$$

The transition probabilities, $q_{k\to m}$, specify the rules of motion along the landscape from $\vec{x}_k$ to $\vec{x}_m$. At long-times, steady state should be reached, so the left hand side of (5) must go to zero and the probabilities $p_k(t)$ and $p_m(t)$ adopt their equilibrium value. This results in the condition of detail balance with:

$$q_{k\to m} \exp\left(-\beta E_k\right) = q_{m\to k} \exp\left(-\beta E_m\right) \tag{6}$$

We notice that the choice of transition probabilities is not unique. As is often the case, even our simple model does not result in an analytically tractable master equation. Instead, we find the dynamic and equilibrium properties by creating a lattice ‘sample’ and using Monte Carlo (MC) simulations to evolve this sample in time[46, 116].

2.3.2. Metropolis Monte Carlo Simulations

As mentioned above, two different MC simulation methods were employed for these studies. First, a modified Metropolis recipe[117] was employed for equilibration of the lattices. Under the modified Metropolis algorithm, the probability of acceptance is a comparison of the initial and final states only. Although the rate of change of breaking a single bond increases exponentially with decreasing temperature, all transitions to lower or degenerate energy states are accepted (see Figure E-1). The acceptance rate for this method was sufficiently large to cool to very low temperatures relative to the predicted mean-field transition. Thus, the method allows for a simulation sample to explore a large number of configurations quickly from a computational stance.

In our implementation, we challenge an individual molecule with a random transition from its current orientation to a new orientation chosen at random. The acceptance of the new orientation or return to its original orientation completes the move. We define one Monte Carlo step (MCS) to be equal to the same number of challenges as there are vertices on the lattice. However we select the molecule for the move randomly, so in one MCS not every vertex on the lattice may be challenged. While the time step for each Monte Carlo attempt under this recipe does not have an explicit connection to real time, and therefore the dynamics do not have a clear definition, we note at equilibrium the distribution of states is expected to be canonical and the conditions of detail balance is met[118, 119]. We consider the Metropolis results to represent the true equilibrium description of the system, an assumption supported by results (see Section 2.4.1).

2.3.3. Kinetic Monte Carlo Simulations

In addition to the two conditions described by (5) and (6), extracting dynamic details via residence time kinetic Monte Carlo (kMC) simulation- also known as the ‘n-fold method’- requires us to define the conformational surface between $\vec{x}_m$ and $\vec{x}_k$ for all states m and k [118]. The transition state energy, $E^*_{m\to k}$ at $\vec{x}^*_{m\to k}$ describes the energy barrier to the change in state. The transition probabilities $q_{m\to n}$ reflect the potential energy difference between $\vec{x}_m$ and $\vec{x}^*_{m\to k}$

$$q_{m\to k} = \omega \exp(-\beta(E^*_{m\to k} - E_m)) \tag{7}$$

where ω^{-1} becomes the fundamental time scale which encompasses all faster relaxation process due to thermal vibrations within the energy well that our coarse grain model neglects. Conveniently, because each state is linked via the rotation of a single molecule $\sigma_\alpha\left(\vec{i}\right)$, we define $E^*_{m\to k} - E_m$ as the number of bonds that specific molecule had at state m, which must be broken to move to the new state. Notice that there is no impact of the final orientation of that molecule on the transition probability. This choice also meets the requirements of detail balance.

The traditional importance method, proposing a new state and then accepting, or rejecting, that move based on comparison with a random number, is inadequate at low temperature because of the large number of rejected moves[46]. Instead, we found the n-fold, or residence time [118, 120, 121], technique to be very effective. In this technique, every event is accepted and the time between events is weighted by the total probability of moves.

2.4. Supercooled Liquid: Investigation of Equilibrated Samples

Using the modified Metropolis recipe, we are able to quench to very low temperatures, creating simulation samples which are in an equilibrium state. We use the term equilibrium to denote samples which reflect path-independent quantities, which are characterized by the current conditions regardless of previous temperature history. In this section, we will present results that establish that the MC samples are at equilibrium, and then use these equilibrated samples as the initial point for both thermodynamic and kinetic calculations.

We note that while we can calculate a first-order, mean-field liquid to solid transition temperature $T_{mf,binodal}$, the significance of the melting temperature and the order of the actual transition are not clear from the outset. One objective is to ascertain the differences between the equilibrium behavior and the non-equilibrium behavior. For the purposes of this work and consistency with other sources, we will refer to all simulation samples as supercooled liquids without regard to the implication of metastability with respect to a solid. In a similar fashion, all simulation samples that deviate from equilibrium at long-time, as described in Section 2.5, will all be classified as glasses without specific demonstration of dynamic arrest.

2.4.1. Equilibrium Results from Metropolis MC Method

The simulation samples that are quenched initially via the Metropolis recipe do indeed appear to reflect an equilibrium state, with similar energetic and structural length scales of low temperature simulation samples that are quenched with the kMC method. The Metropolis recipe does not provide dynamic information, but does search the PEL more rapidly because there is no energetic barrier for transition beyond the difference in the number of bonds in initial and final states. If we are able to access a large number of configurations during our simulation time, then we have the ability to meet the conditions of equilibrium described by equation (6). We noted that the measured acceptance rate, the percent of MCS that represents motion on the PEL, remains sufficiently high even at low temperature implying that we are, indeed, capable of meeting this requirement.

While we cannot formally prove that these simulations are truly the equilibrium state, evidence points to reproducible results that, excluding the initial decay, do not change in energy over long simulation periods. For all results in this section, each simulation sample was created at a unique, random, initial condition equivalent to $T \to \infty$. They were then 'quenched' by using the final temperature during all simulation moves. The samples were relaxed for at least 10^6 MCS before any data was reported. In previous work[1] we found that the Metropolis MC simulation samples had a relaxation time of less than 10^2 MCS for samples as low as T=0.18 (refer to Figure 1.6.3-1). This gives us confidence we had reached the low energy equilibrium state for each temperature. Ten separate measurements of the internal energy density, u, were recorded at intervals of 1000 MCS, from which the average was then calculated. This was repeated for a second independent simulation run with the same quench conditions but a different initial configuration. Both sets of data are reported in Figure 2.4.2-1. Two additional series following the same protocol were generated but omitted in our figure as they were not used for the fitting of u. None of the energy values differed by more than 1%.

Additionally, the simulation samples' path independence- that is, whether the states could be completely defined by the current conditions regardless of previous thermal history- was also investigated. In the stepwise method, a sample was equilibrated at high temperature, then 'quenched' to the next cooler temperature, where it was equilibrated and the process repeated (temperature steps followed those reported in Figure 2.4.4-1, so individual data points could be compared). This procedure provided a set of simulation samples that is not distinguishable from those generated during the direct quench.

As seen in Figure 2.4.2-1, the samples also approach the high-and-low temperature energy limits, as we would expect. In Section 2.4.3, we indicate the presence of the crystalline state (long range enrichment in either orientation 1 and 3 or 2 and 4) as primarily a kinetic phenomena. We note that in the absence of a crystal with lower free energy, any of the degenerate minima would be the equivalent thermodynamic equilibrium state[122]. Thus, our calculation of the configurational entropy in Section 2.4.2, which indicates that the entropy remains positive as the temperature goes to zero, is consistent with the absence of a unique state with the lowest energy. The structural ordering documented in Section 2.4.3, which occurs due to the anisotropic nature of the molecules, is not representative of a unique equilibrium state.

2.4.2. Configurational Entropy

There are several different methods to calculate the heat capacity, and thus entropy, for a simulation sample. As the model is defined on a lattice and each molecule has a discrete number of orientations, the only entropy present in our system is the configurational entropy. If our system is at equilibrium, we can use the thermodynamic relationships

$$C_V \equiv \left.\frac{\partial U}{\partial T}\right|_V, \quad s(T) = s\big|_{T=\infty} - \int_T^{\infty} \frac{C_V}{T} dT \qquad (8)$$

where C_v is the heat capacity per site and s is the entropy per site. The entropy density at infinite temperature can be easily found using the Boltzmann definition, $s\big|_{T=\infty} = \log(4)$ as there are 4 orientations at each site.

Alternately, we could measure the heat capacity directly from our simulation results because we can measure the fluctuations in the energy, via the variance of the internal energy, as

$$C_V \equiv \frac{\left\langle \left(U - \langle U \rangle \right)^2 \right\rangle}{kT^2} \tag{9}$$

However, because of the statistical inefficiency of using the variance of the internal energy (see Appendix F), we chose to fit the data to an arbitrary function that can be differentiated analytically using Eq. (8). Hyperbolic functions were chosen because the energy has both a high and low temperature asymptote (polynomial and simple exponential expansions cannot take advantage of the two known values). We found that

$$\begin{aligned} u &= -9/8 - 3/8\left((a)\tanh\left(b/T \right) + (1-a)\tanh^2\left(c/T \right) \right) \\ &= -9/8 - 3/8\left((0.468)\tanh\left(0.375/T \right) + (1-0.468)\tanh^2\left(0.256/T \right) \right) \end{aligned} \tag{10}$$

describes our data well, with a small number of variables (note the -9/8 and -3/8 are set by the asymptotes).

In Figure 2.4.2-1 (a), we plot the data with its fit (equation (10)). As mentioned above, we use the analytic derivative of equation (10) to calculate the specific heat, shown in *(a)inset*. To insure that this choice does not deviate in a systematic way, the variance of the energy measured directly from the simulation samples employing equation (9) is shown with black dots (●). Additional confirmation is given by the close alignment of the slope of the line segment connecting adjacent energy measurements marked by the red stars (*). The entropy per site calculated from the integration of C_V / T and knowledge of the high temperature limit is shown in Figure 2.4.2-1 (b).

The equilibrium conditions generated by this Hamiltonian require that there be a peak in the heat capacity at some temperature, T_{Cv}. We draw this conclusion by considering the functional shape of the internal energy per site, u. In the high temperature limit, the thermal energy will overwhelm any resistance from bonds and explore the entire energy landscape. Thus, the internal energy will be equivalent to the energy of the random state ($u = -9/8$). As this condition is asymptotic as $T \rightarrow \infty$ and the energy decreases upon cooling, the function is by nature concave down above T_{Cv}. As a sample cools (under conditions slow enough to maintain equilibrium) towards absolute zero, the molecules will preferentially align towards a bonded condition. Therefore $u \rightarrow -3/2$ as $T \rightarrow 0$ and below T_{Cv} the internal energy function is concave up. We find this description to be consistent with all simulated conditions in this study. The maximum heat capacity occurs at $T_{Cv} = 0.21$ (recall $T_{mf,spinodal} = 0.25$).

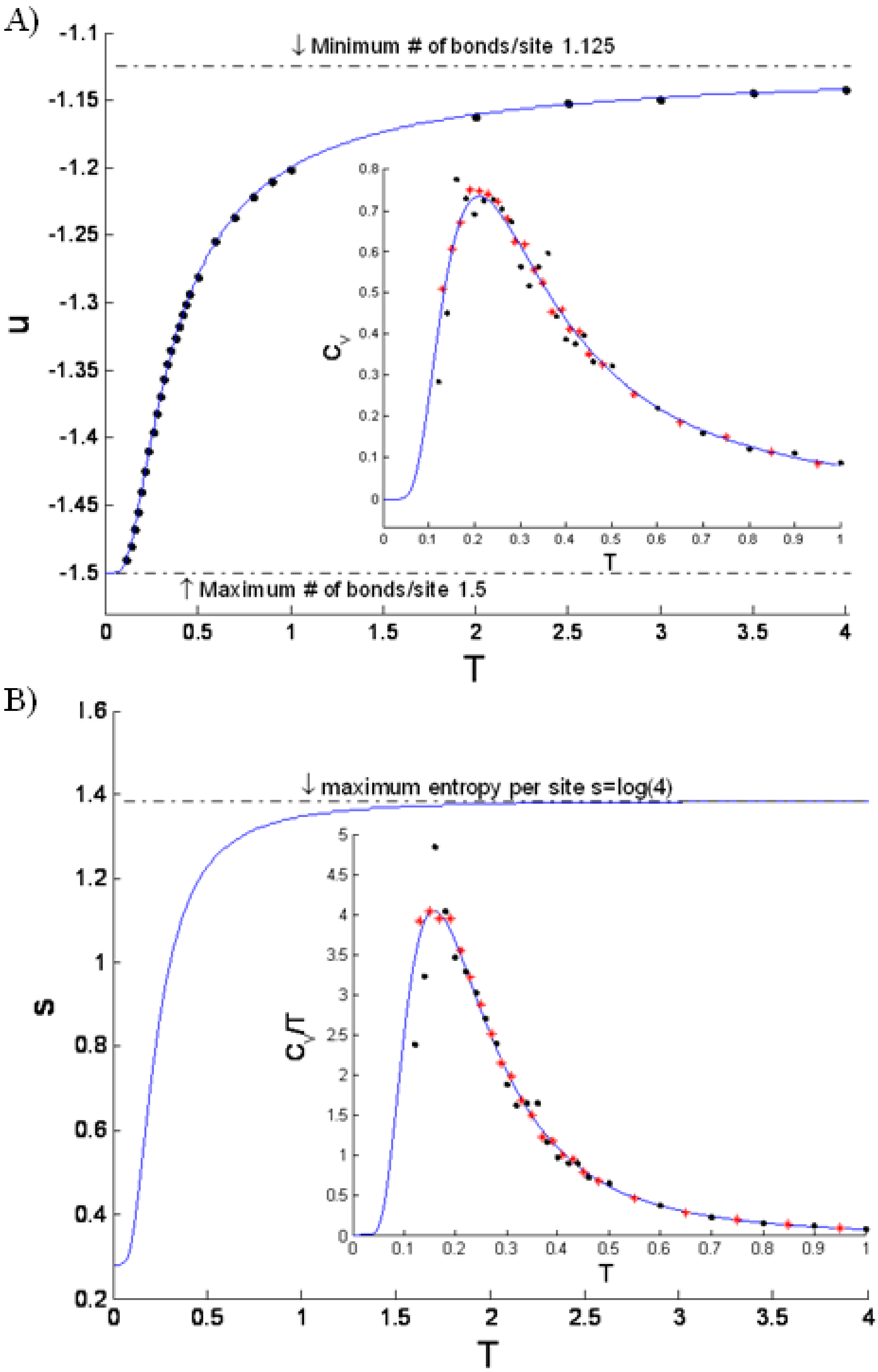

Figure 2.4.2-1: Thermodynamic features of the 'supercooled' liquid

(A) u as a function of T. The data (●) was fit to an arbitrary analytic function(—). The inset shows C_V calculated by three methods: (●) variance of the energy, (*) slope of the line segment connecting adjacent energy measurements, (—) the analytic derivative. (B) s (—) calculated from the integration of C_V/T and knowledge of the high temperature limit.

We note that the greatest error in calculating entropy occurs in the low temperature measurements, when relaxation times are the longest, as one would expect. Computational limitations have precluded other investigations from achieving low temperature results[123]; we are fortunate to have a simple model and technique to overcome this difficulty. However within this error our calculations still suggest a positive residual entropy, a result that has also been found in an experimental system[124]. This quantity can only be reasonably extrapolated from low temperature equilibrium conditions. There is very active research into the applicability and definition of thermodynamics and statistical dynamic quantities in the immediate vicinity of $T = 0$, which are beyond the scope of this work[125, 126].

If the configurational entropy of the glass does not go to zero as temperature goes to zero, the extrapolated inversion of the liquid and crystal entropies is not thermodynamically mandated. This provides a resolution to the 'Kauzmann Paradox' for our system without the need for a thermodynamic or dynamic event at lower temperatures. Indeed, it questions the universal applicability of the assumption that one may calculate the 'ideal glass transition' based on extrapolations of the configurational entropy to $s_c = 0$.

2.4.3. Structure

Because of the system anisotropy, there is noticeable ordering as the temperature is lowered. The anisotropic nature of the molecules leads to the formation of 'back-to-back' pairs so that the non-bonded sides of the molecules face each other. Structures in the same direction as the long axis of the molecule are formed. The result is local enrichments of molecules whose long axis is oriented in the same direction ($\alpha = 1,3$ or $\alpha = 2,4$). Measurements of simulation samples at different temperatures show a pronounced increase in the size of these domains at colder temperatures.

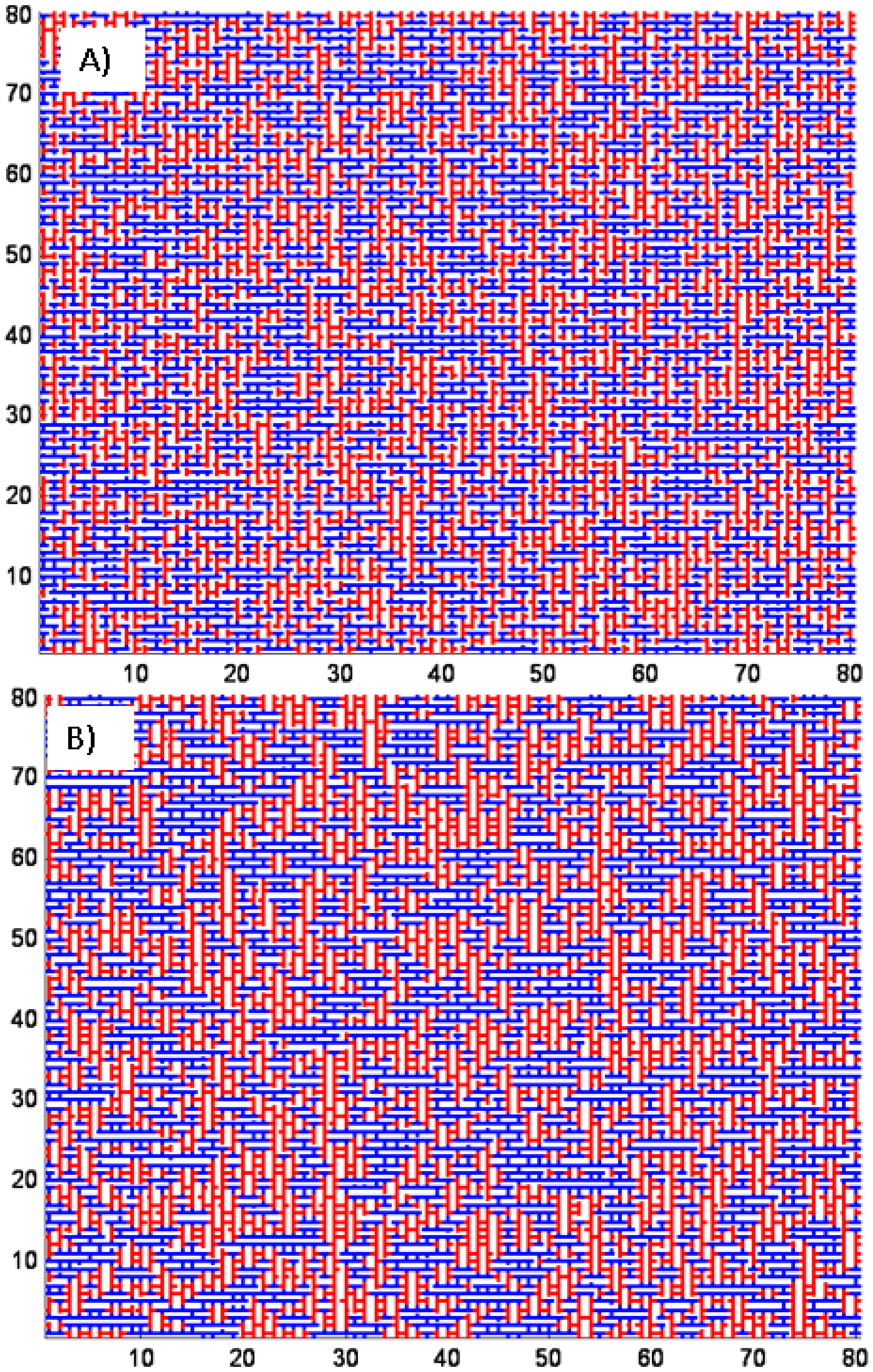

Figure 2.4.3-1: Representative snapshots of simulation samples
Supercooled liquid simulation samples at (A) T=1.0 and (B) T=0.20 . Coloring is a guide to the eye to distinguish orientations 1 ├ and 3 ┤ from 2 ┬ and 4 ┴ .

Given that there is a kinetic preference for an aligned system (described in Section 1.4.5), which we intuitively relate to the ordered crystalline state, why do we not observe the macroscopic crystal in the MC samples? When we used the dynamic mean-field (DMF) simulation to cool a sample which had a small fluctuation at a temperature very close to the transition temperature, we indeed did see a crystalline structure[1]. The nature of the DMF simulation as a method of steepest decent is such that once it finds one energy minimum, it does not continue to explore the configuration space. The small kinetic preference toward the alignment leads to formation of a long range structure when only a single disturbance is introduced. In contrast, either form of the MC simulation permits the sample to explore a wide range of energy minima at this temperature, most of which have minimal ordering. (Due to the anisotropic nature, there is ordering on a small-length scale congruent with the need for the 'back-to-back' alignment for bond formation.) Recently Ediger et al. [127] posited that the kinetic rate of crystallization is proportional to the rate of discovery of crystalline configurations on the PEL. In our model, the overwhelming number of non-aligned minima would make crystallization unlikely.

We are able to see clear regions with local enrichments of molecules whose long axis is oriented in the same direction ($\alpha=1,3$ or $\alpha=2,4$). These regions grow with decreasing temperature, despite their kinetic origin, due to the stabilization of the bonds within their boundaries. Rotation of a molecule to a different orientation would raise the energy of the simulation sample by at least one bond, possibly two.

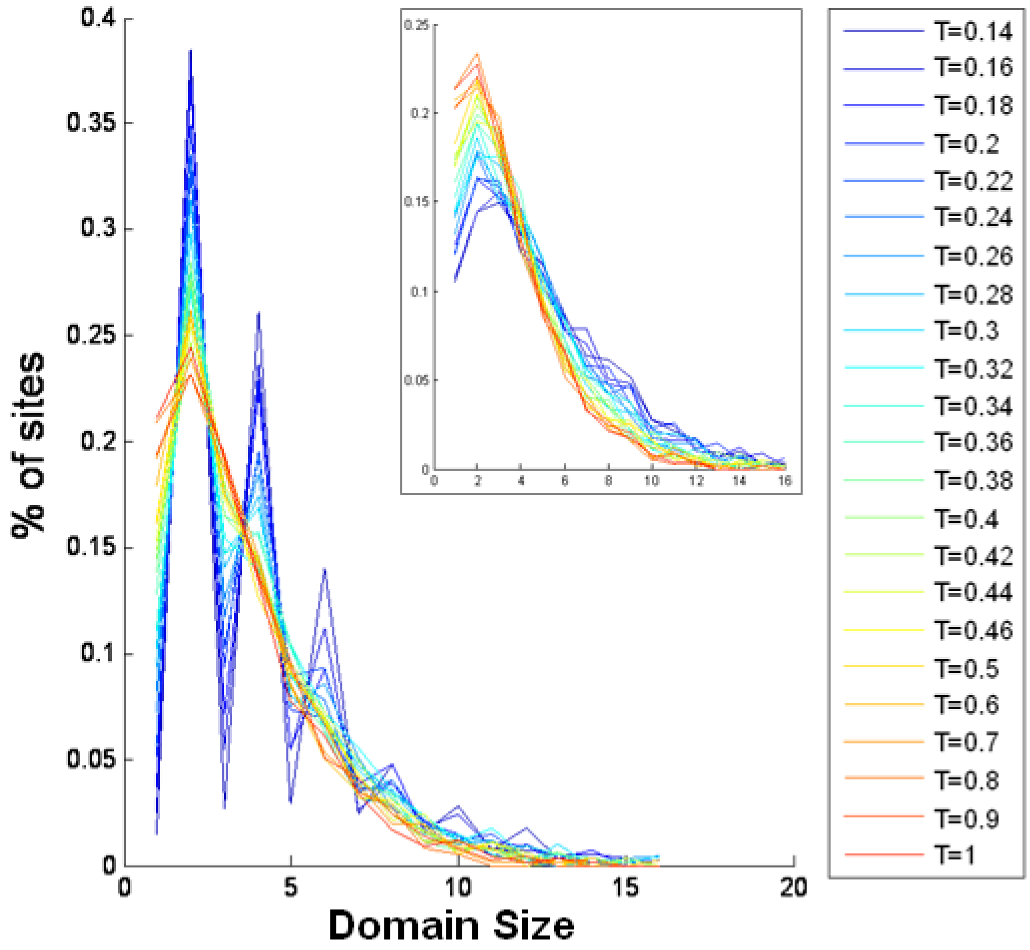

Figure 2.4.3-2: Distribution of domain size at different temperatures
The anisotropic ordering is pronounced when the length of rows/columns in the enriched regions are measured in the direction of the long axis (inset: domain length measured in perpendicular direction).

The local enrichments demonstrate the model's tendency toward reversible self-assembly. Indeed, a number of other anisotropic or limited valence models and materials share this characteristic that local homogeneous patches stabilized by a network of intermolecular bonds (e.g.7, 90 and references therein). Due to the small length scale of these regions with respect to the lattice spacing, measurements along the axis in a linear direction are significantly more revealing than the traditional radial distributions and structure factors. We have chosen the expectation value of the domain size, or length scale of local enrichment of either the 1├ and

3 ┤ or 2 ┬ and 4 ┴ orientation, as a convenient representation of the degree of orienting. In Figure 2.4.3-3 we can clearly see that there is an onset of increased orientation at approximately $T_{structure} = 0.5$, but that there does not seem to be any signature of divergence in this length scale as $T \to 0$. It is important to note that there are approximately an equal number of molecules in each orientation within a sample during the duration of the simulation. The locally oriented regions do not necessarily indicate an underlying phase transition due to a symmetry breaking in orientation.

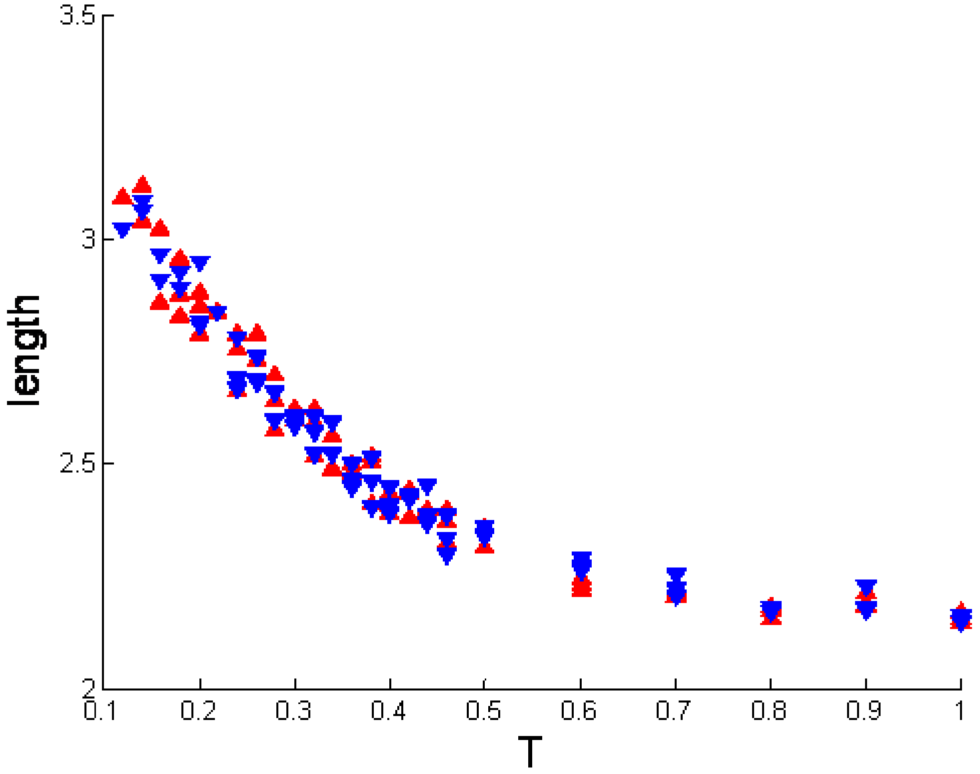

Figure 2.4.3-3: Expectation value of the domain size at different temperatures
The expectation value of the linear distribution in the direction of the long axis(▲) and perpendicular to the long axis(▼)

2.4.4. Relaxation Time

We employ the relaxation time as proxy for rheological measurements of the material's viscous character. Among many possible choices for the relaxation time, we explore the relaxation time for two autocorrelation functions within this work. The bond autocorrelation function, $\phi_b(t-t_o)$, comparing the bonding state of the lattice at time t to that at the time t_0 defined as:

$$b\left(t;\left\langle \vec{i},\vec{i}\,'\right\rangle\right)=\begin{cases}1:\ \text{bond along edge } \left\langle \vec{i},\vec{i}\,'\right\rangle \text{ at } t\\ 0:\ \text{no bond along edge } \left\langle \vec{i},\vec{i}\,'\right\rangle \text{ at } t\end{cases}$$

$$\phi_b(t-t_o)=\frac{\left[\left\langle b\left(t_o;\left\langle \vec{i},\vec{i}\,'\right\rangle\right)b\left(t;\left\langle \vec{i},\vec{i}\,'\right\rangle\right)\right\rangle-\left\langle b\left(t;\left\langle \vec{i},\vec{i}\,'\right\rangle\right)\right\rangle^2\right]}{\left[\left\langle b\left(t;\left\langle \vec{i},\vec{i}\,'\right\rangle\right)^2\right\rangle-\left\langle b\left(t;\left\langle \vec{i},\vec{i}\,'\right\rangle\right)\right\rangle^2\right]} \tag{11}$$

We also simultaneously evaluated the molecule-orientation autocorrelation function,

$$\sigma_\alpha\left(t;\vec{i}\right)=\begin{cases}1:\ \text{if molecule at vertex } \vec{i} \text{ is in orientation } \alpha \text{ at time } t\\ 0:\ \text{otherwise}\end{cases}$$

$$\phi_\sigma(t-t_o)=\sum_{\alpha=1}^{4}\frac{\left[\left\langle \sigma_\alpha\left(t_o;\vec{i}\right)\sigma_\gamma\left(t;\vec{i}\right)\right\rangle-\left\langle \sigma_\alpha\left(t;\vec{i}\right)\right\rangle^2\right]}{\left[\left\langle \sigma_\alpha\left(t;\vec{i}\right)^2\right\rangle-\left\langle \sigma_\alpha\left(t;\vec{i}\right)\right\rangle^2\right]} \tag{12}$$

The structural resistance and solid-like features in our simulation samples are provided by the bonding structure. As has been observed in other models[3], the local structure can reinforce the bonding along a specific edge, $\left\langle \vec{i},\vec{i}\,'\right\rangle$. Thus, a bond may break and reform quickly, returning to the original structure and not suggesting actual progress towards relaxation. Further, in our model several different orientations of the molecule at a specific site may result in the same local bonding characteristics. The results for the orientation and bond relaxation functions were very similar. As the bonding state defines the thermodynamics and as we also use bonding to describe the structural correlation functions, we choose to report the bond relaxation function results here. Later, in Section 2.6 we will refer to the orientation times.

We evaluated the equilibrium relaxation time, τ, for the simulation samples that were created by quenching from an initial random state (infinite temperature) to the final temperature and equilibration for more than 10^6 MCS with the Metropolis method. Following equilibration, the data for the autocorrelation functions was collected using kMC simulations. As described earlier, it is important that we consider the transition states to capture appropriate motion on the energy landscape when we are directly evaluating any function involving time dependence.

There are many ways to characterize the relaxation time from the autocorrelation function results. For this work, the use of the integrated relaxation time, or mean relaxation time, is preferred because it incorporates both the influence of the characteristic time, τ_c, and the stretching exponent, β. We calculated the relaxation time by first fitting the autocorrelation function with the stretched exponential equation, $\phi(t) = e^{-\left(t/\tau_s \right)^{\beta}}$. The Euler gamma function then allows us to calculate the integral.

$$\begin{aligned} \phi(t) &= e^{-\left(t/\tau_s \right)^{\beta}} \\ \tau &= \int_0^{\infty} e^{-\left(t/\tau_s \right)^{\beta}} dt = \left(\tau_s/\beta \right) \Gamma\left(1/\beta \right) \end{aligned} \qquad (13)$$

It also provides a clear connection to the relaxation time calculated by a single exponential relationship. In the simple exponential relaxation function, the relaxation time remains the same when integrated over the interval, $\phi(t) = e^{-t/\tau}$ or $\tau = \int_0^\infty e^{-t/\tau} dt$ [38]. We found that in all cases the stretched exponential provided a better fit than a single exponential function.

The values of τ and β are reported in Figure 2.4.4-1. We monitored the decay of the correlation function and fit the data to each measurement separately to ensure that the simulation sample was exploring similar regions of the PEL and that we did not neglect a longer timescale. As the error of the integrated relaxation time τ was small (each measurement is reported separately and at most temperatures the symbols overlap), we have confidence that the reported values reflect the actual relaxation times. On the other hand, there was a larger variation in β (Figure 2.4.4-1 *inset*). Other authors often report β as nearly independent of temperature, noting that the change in the vicinity of T_g is minimal[3]. It has been noted that the value of β is very sensitive to the fitting method[128, 129]. We considered different ways to fit the data, particularly whether to include or exclude very short or long-time processes. Compared to the variance in values of τ or β between quenches at the same temperature, neither truncated data set had fitting parameters which were significantly different.

The value of β can be used as an indicator of the kinetic fragility as it represents the non-exponential movement of the simulations sample on the PEL. Indeed a dramatic change in β upon a return to simple exponential relaxation is given as the hallmark of the fragile-to-strong crossover (FSC) in a spin facilitated kinetic Ising model[129]. Despite the spread of our measurements, since we are considering the FSC, it is interesting to note that the simulation samples become more fragile as the temperature is lowered to $T_{\beta:fragility,\ onset} \approx 0.5$. The value of β then stabilizes until it begins to increase at $T_{\beta:FSC} \approx 0.26-0.24$. Again, however, the specific temperatures are difficult to establish.

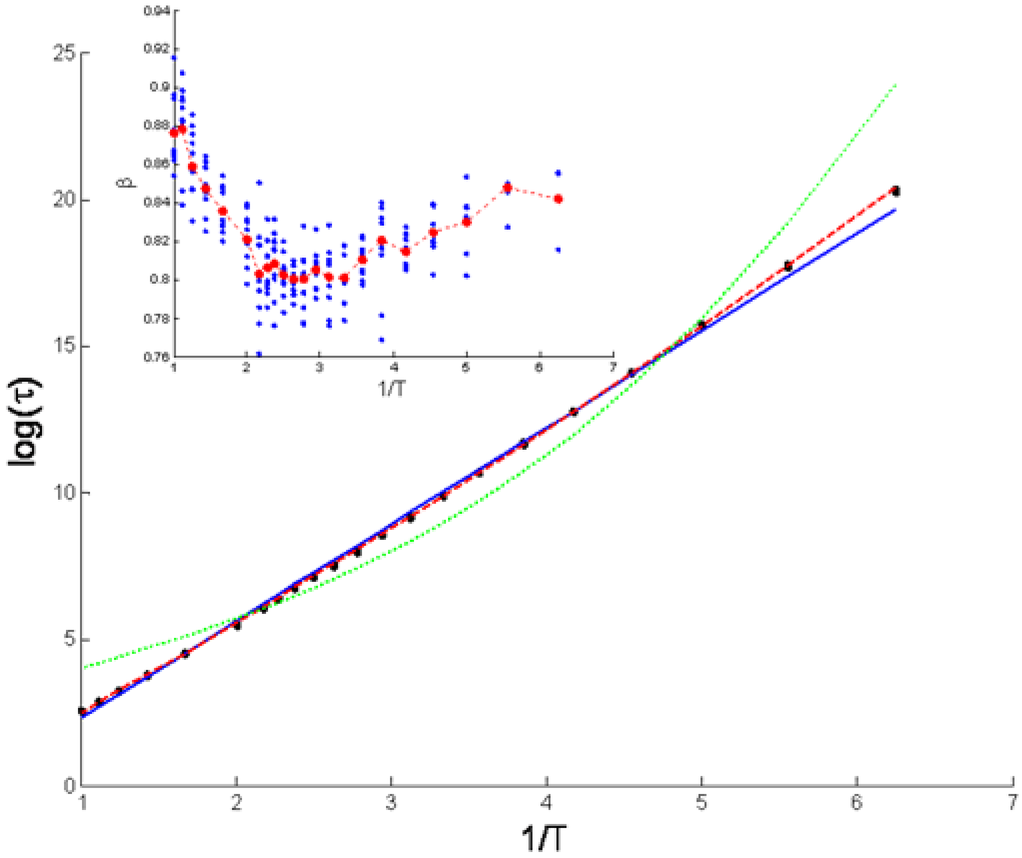

Figure 2.4.4-1: The integrated relaxation time of supercooled simulation samples
The points (•) are independent fits of relaxation runs (4 at T=0.16, 3 at T=0.18, 8 at T=0.20, 10 for all other) which overlap closely on this scale. The data is fit in to the (—) Arrhenius, (--)Vogel-Fulchur and (•••) Adams-Gibbs equations. Inset: shows the (•) values of the stretched exponent β, (•) the average value and (--) as a guide to the eye. Note that while x-axis is 1/T, to match the main plot for convenience to the reader, the y-axis on the inset is linear.

The integrated relaxation time as a function of temperature was fit with four functions. As expected from the implied cooperative relaxation, the Vogol-Tammann-Fulchur function(VTF):

$$\tau = \tau_o e^{\left(\frac{D}{T-T_o}\right)} = 0.656 e^{\left(\frac{2.85}{T-0.023}\right)} \tag{14}$$

fit the complete data set better than an Arrhenius function:

$$\tau = \tau_o e^{\left(E_a/T\right)} = 0.368e^{\left(3.32/T\right)} \qquad (15)$$

We notice that the activation energy, E_A, in the Arrhenius fit is 3.32, which is slightly larger than that which would be required to break three bonds. In regions of the system which are fully satisfied, change in orientation of a monomer requires that three bonds be broken. This represents the highest energy barrier to local relaxation. Whereas, at higher temperatures samples have a smaller bond density, the largest energy barrier may be circumvented by longer pathways over the PEL, there will be a time penalty for this diffusive motion. Therefore, while the energy scale is appropriate for both scenarios, the details of the relaxation mechanism remain unknown.

With the thermodynamic calculations made before, we are able to evaluate the fit of the Adam-Gibbs[69] (AG) equation. This equation, and the theory on which it is based, was inspired in part from the excellent empirical fit of the VTF function. If we postulated that there is a physical significance to T_o, the singularity suggests a divergent relaxation time consistent with the ideal glass transition. T_o is often then equated with Kauzmann temperature T_K.

The configurational entropy, calculated at each temperature as shown in Figure 2.4.2-1, is known, so it is not a degree of freedom in our fit for the AG equation:

$$\tau = \tau_o e^{\left(C/TS_c\right)} = 13.6e^{\left(1.89/TS_c\right)} \qquad (16)$$

The fit is relatively poor. However, if we restrict the fit to a smaller region closer to the expected glass transition, as is commonly done[128], the fit greatly improves (not shown).

Recent work suggests that the AG should also fit well if extended above the activated regime, where the s_c has little dependence on temperature[123].

Alternative relationships are also being actively proposed as the source of the relaxation behavior and the nature of T_g is investigated. Recently, Elmatad et al. proposed a quadratic fit, which could be used to collapse an impressive range of data from structural glass formers[112]. We could use this functional form to fit our data, either over the entire temperature range,

$$\tau = \tau_o e^{\left(\left(J/T_a\right)^2\left(\left(T_a/T\right)-1\right)^2\right)} = 1.48 e^{\left(\left(3.32/2.28\right)^2\left(\left(2.28/T\right)-1\right)^2\right)} \tag{17}$$

or alternately over an arbitrary subset of temperatures (no fits are shown). The physical rational behind this functional fit, based on the activation energy required to relax a domain of a particular size, limits its application to temperatures where the system movement on the energy landscape is dominated by activated, cooperative motions ($T < T_a$). Likewise, it will no longer apply when the temperature is further cooled ($T < T_x$) returning to motion without correlated transitions. The authors expected that below T_x the relaxation dynamics would return to an Arrhenius form. We did not find unique choices of T_a and T_x while attempting to fit this function to our relaxation data. However, our data is consistent with a transition into a cooperative, fragile, relaxation regime, followed by a return to Arrhenius, strong, behavior at even lower temperature, as demonstrated elsewhere.

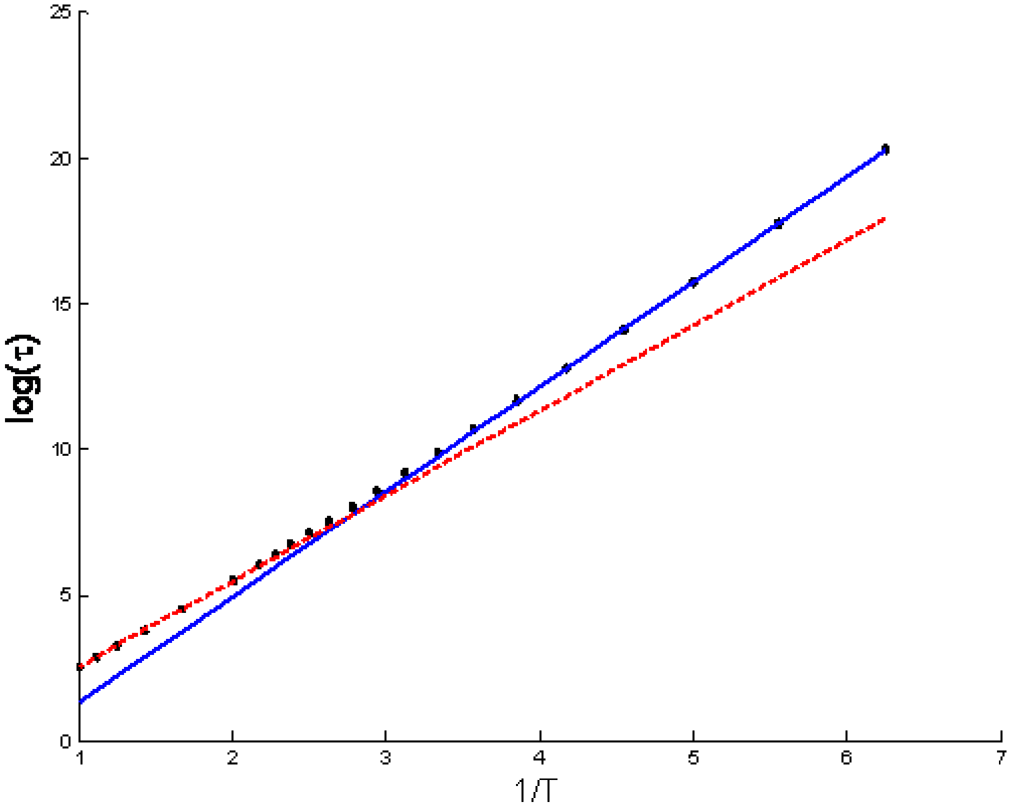

Figure 2.4.4-2: Exponential fits of relaxation time in low and high temperature data Separate Arrhenius fits to the (—) lower temperature ($0.16 < T < 0.2$) and (--) higher temperature ($0.5 < T < 1.0$) data highlights the changes in relaxation time temperature dependence. Some adjacent data points continue to be well fit, but there is gradual change indicating fragile behavior in the window between the two regions.

To highlight that there is a cooperative relaxation temperature regime flanked both at high and low temperature by simple, non-cooperative relaxation, we fit the high and low temperature data to separate Arrhenius fits. Notice in Figure 2.4.4-2 that the activation energy of the two fits is different, however, both are on the order of the energy required to break three bonds ($\text{low } T, E_A = 3.61, \text{ high } T, E_A = 2.92$). At lower temperatures it is elevated, as we would expect. There is no indication of a divergence in the relaxation time of the equilibrium system.

2.5. Supercooled Liquids: Nonequilibrium Glassy States

As expected, the simulation samples prepared using the kMC method and Metropolis MC recipe produce the same results when at high temperatures. However, at lower final temperatures, the simulation samples which are relaxed with kMC develop a change in their dynamics during quenching. We note that if at any specified ‘observation time’ not all samples will have equilibrated, instead they are arrested at a ‘glassy’ state. The structure of these low temperature, non-equilibrium samples is significantly different than those prepared with the Metropolis quench. Because we are able to observe the simulation samples, evolution for very long-times, we notice that there is a change in the relaxation behavior at the fragile-to-strong crossover (FSC). Further, we can continue to investigate temperatures beneath the FSC and find that simulation samples will, given enough time, return to equilibrium.

We first establish that our system has traditional glassy behavior by performing a constant rate quench in Sec. 2.5.1. The simulations are terminated when they reach T close to zero. They are not allowed to relax, but presumably would age, if investigated. Our goal is to demonstrate that our model behaves as a glass former and mimics experimental work.

In Section 2.4, we use the Metropolis MC simulations to prepare equilibrium sample for evaluation. We can determine the relaxation dynamics after equilibration using kMC (see 2.4.4). However, the Metropolis MC method does not give us any information about the dynamics during a quench. Thus, we turn our attention to relaxation during quenching at a ‘constant temperature’ where the simulation is in contact with a heat bath at the final temperature during all steps. Further comparison of the equilibrium samples prepared initially with the Metropolis MC recipe and the simulation samples evolved with kMC, for a period of time at which some samples seem to have equilibrated and others have not is found in Section 2.5.3. Samples quenched with either MC method appear to have the same characteristics as we would expect from the condition of detail balance. However, samples that have not equilibrated indeed have structural characteristics which reflect this.

2.5.1. Constant Rate Quenches

We can observe dynamic changes and thermodynamic changes upon cooling in equilibrated samples. However, we are able to observe a clear signature of a traditional glass transition by inducing kinetic arrest with a rapid quench, similar to those performed in the laboratory.

Using the n-step kMC algorithm, we are able to cool the system at a constant rate. The simulation samples are initialized at a random state as before and at $T = 5$, which is a very high temperature in our system. They are then cooled at the rate $\gamma = {}^{\Delta T}\!/_{\Delta t}$ by performing a MCS using kMC at the current T. The resulting elapsed time is then used to calculate the new T. As the simulation sample cools, each MCS takes longer and results in a larger jump in temperature. At some point, depending on the quench rate, the temperature jump results in the simulation sample leaving an equilibrium quench path. At this point, the sample has arrested and does not find any more satisfied states. The simulation is stopped when the new temperature is negative. Results from various quench rates are shown Figure 2.5.1-1, with the inset providing fits for each data set and the lowest temperature truncated. It is important to note that we repeated simulations with different initial random configurations at each rate. The discrete nature, particularly where there are large temperature drops, leads to clusters of points. To demonstrate that these are due to individual runs, not from a single sample becoming arrested in that area, the inset provides fits to each simulation run separately.

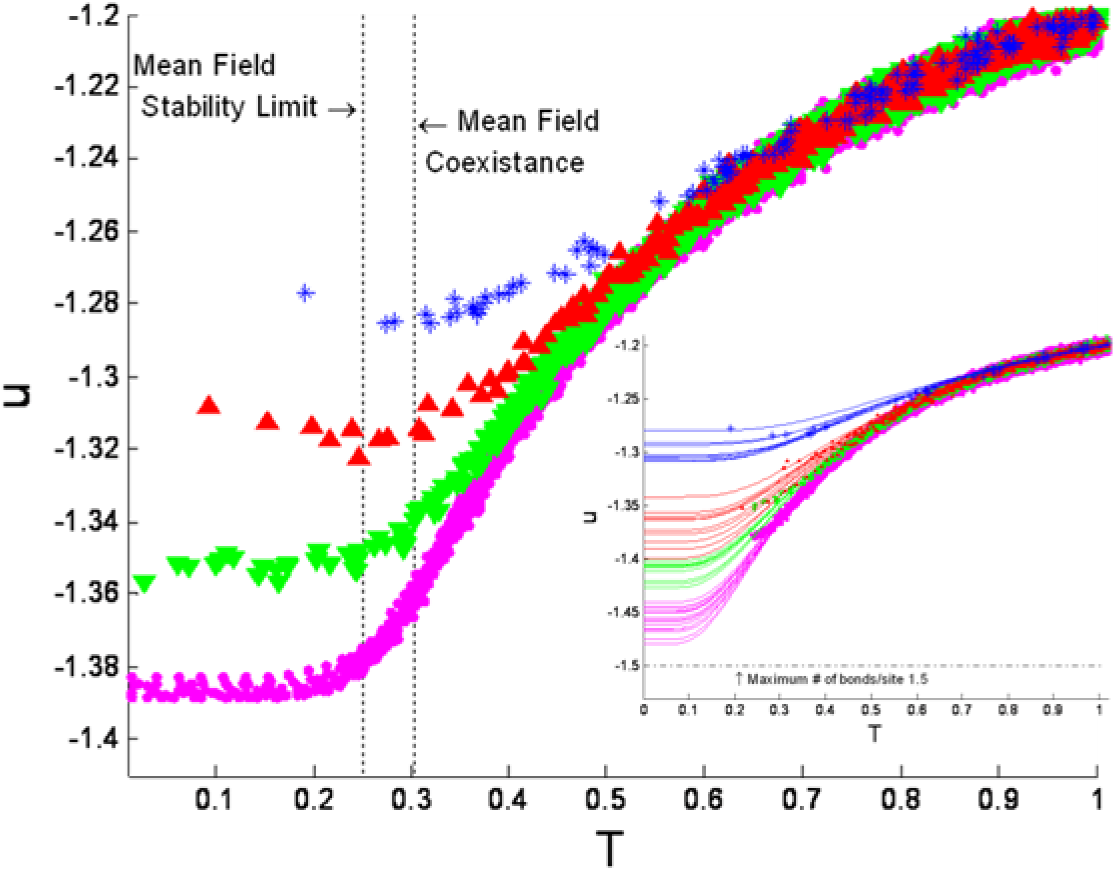

Figure 2.5.1-1: Constant rate kinetic Monte Carlo simulation samples
Energy density as a function of T for 10 independent simulations: γ=0.01(*), 0.001(▲), 0.0001(▼), 0.00001(●). Inset: To emphasize that there are multiple initial conditions simulated each data set is individually fit. We omit the lowest temperature data. The fit is an arbitrary equation similar to Eq. (10) (see Section 2.4.2) without the expectation that the low temperature asympote will be -9/8, intoducing a 4th fit variable: $u = -d - \frac{3}{8}\left((a)\tanh\left(\frac{b}{T}\right) + (1-a)\tanh^2\left(\frac{c}{T}\right)\right)$.

Such behavior is commonly seen in dynamic scanning calorimetry (DSC) measurements in the laboratory. This effect is also captured in several other models[27, 130]. It conforms to the general understanding that a slower cooling rate will prevent the system from falling out of equilibrium at higher temperatures and depress the measured glass transition. Presumably, an infinitely slow quench would describe the supercooled equilibrium state with the same results as can be found in the previous Section. Therefore, we conclude that we do model a glass forming system and that our results are not the due to some unphysical characteristic of this Hamiltonian.

2.5.2. ‘Constant Temperature’ Quenches: Evolution with Time

In the context of the energy landscape paradigm, the physical origin of kinetic arrest is generically represented as an inability to relax when trapped in a potential well. Thus, the glassy system has a higher energy than the equilibrium system due to its large number of unbonded molecules. We perform a ‘constant temperature’ quench by initializing a simulation sample at a random configuration and running the kMC simulation against a constant temperature heat bath. Thus, the energy of the transition states are constant. The exploration of the PEL by the simulation sample leads to a low energy state, which is not discernible from the equilibrium state (as determined by our metrics thus far) if the simulation is run for long enough time.

In Figure 2.5.2-1 the evolution of the energy with time at a given temperature is plotted on a semi-log plot. The range of time scales for the simulation samples to reach their final energy is dramatic. In order to determine whether the low temperature patterns that we see are independent of the choice of initial state or highly dependent on individual quench pattern, additional simulation samples were quenched at $T = 0.16$, 0.14 and 0.12 These temperatures were chosen as the samples evolved sufficiently to see their long-time behavior during the ‘observation time’ of our simulations, but would be most sensitive to their immediate environment on the PEL. There were some deviations in the curves of separate samples quenched under the same conditions as we would expect from diffusion over different regions on the PEL, but they are small; and, overall, the relaxation paths coincide as can be seen in the figure.

Initially, all the samples relax quickly, as they are very far from equilibrium. Following this preliminary growth in bonding, we observe a very interesting trend. When quenched against moderately low temperature baths, above $T \approx 0.3$, the simulation samples follow a single curve as approach they their long-time energy values. We note that these values are very similar to those which are very close to the equilibrium values found by the Metropolis MC, consistent with the hypothesis that these kMC simulations are also in equilibrium. Neglecting the initial portion of the quench, we also find that the simulation samples approach their final equilibrium value through a sequence of states which are also in equilibrium, although at a higher 'effective' temperature. This result is congruent with recent studies of colloidal systems[131, 132].

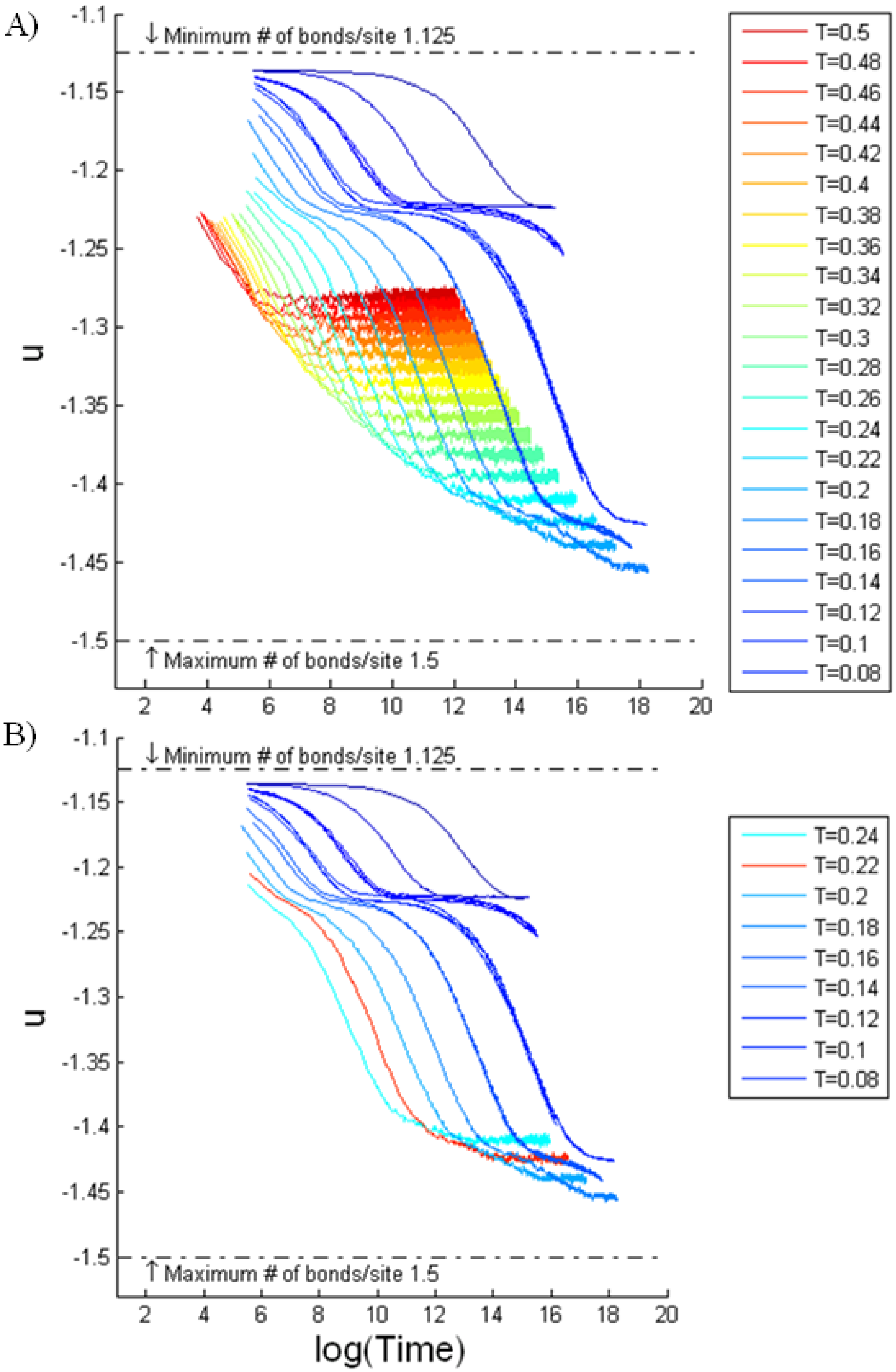

Figure 2.5.2-1: KMC simulation results: 'constant temperature' quench
Starting from a random configuration, kMC was used to evolve samples against a constant heat bath temperature. All quenches, shown in (A) are plotted from high to low by color. A subset of curves are replotted in (B), using new colors for ease of anaylsis by the reader.

In simulation samples quenched against heat baths with lower temperatures, we no longer observe this simple curve. Figure 2.5.2-1 (B) shows a subset of the curves from (A) with a different choice of colors to make inspection of this region easier for the reader. An inflection point can be seen starting at $T_{KMC} \approx 0.24$ such that the simulation sample's energy no longer approaches the equilibrium value in an asymptotic fashion with time. The energy remains relatively constant during two different windows in time, visually appearing as plateaus on the graph. This indicates that there is a kinetic reason these simulation samples become arrested during observations on this time scale, exploring the PEL at that energy for a significant length of time. This multiple step phenomena, in which there are distinctly different dynamics during separate time scales as the simulation sample quenches towards equilibrium, may be reflected in the relaxation dynamics of samples after they have equilibrated. We note that there was indication of such a change in the temperature region same region in Section 2.4.4

Several explanations have been proposed for this phenomena. Caging, in which some molecules are surrounded by immobile molecules that allow changes only on long-time scales has been proposed as an explanation for the development of plateaus in other models[3, 133]. Alternately, this feature may represent regions in which the heat bath temperature is sufficiently low such that the energy required to break one, two, or three bonds becomes significantly different. This would cause the kinetics to change as the sample evolves to lower energy via pathways requiring fewer bonds breaking and more 'diffusion' of vacancies. We speculated in our previous work[1] that this may be the mechanism behind a fragile-to-strong crossover (FSC).

2.5.3. ‘Constant Temperature’ Quenches: Glassy Structure

It is interesting to compare the domain size for the simulations samples quenched using kMC with those for the equilibrium cases created with the Metropolis MC (Section 2.4.3). All the measurements are made at the end of the respective simulations. When the kMC simulations appear to reach equilibrium, we find that the expectation value of the domain size is similar to that of simulation samples equilibrated with the Metropolis MC method. However when the final state of the simulation is not yet at equilibrium and the sample is considered arrested or glassy, the expectation value of the domain size becomes much smaller. Thus for the kMC simulation samples, the domain size does not grow monotonically with lowering heat bath temperature, but instead deviates when the simulation sample is arrested on the observed time scale. Equilibrium simulation samples should be the same regardless of what choice of transition probabilities is chosen, as long as they meet the condition of detail balance, so this is the result we expect. A $T_{kMC,structure} \approx 0.18 - 0.16$ the domain size begins decreasing with temperature. This is the same region in which the final values of the energy no longer reach the equilibrium value, but instead have fewer bonds.

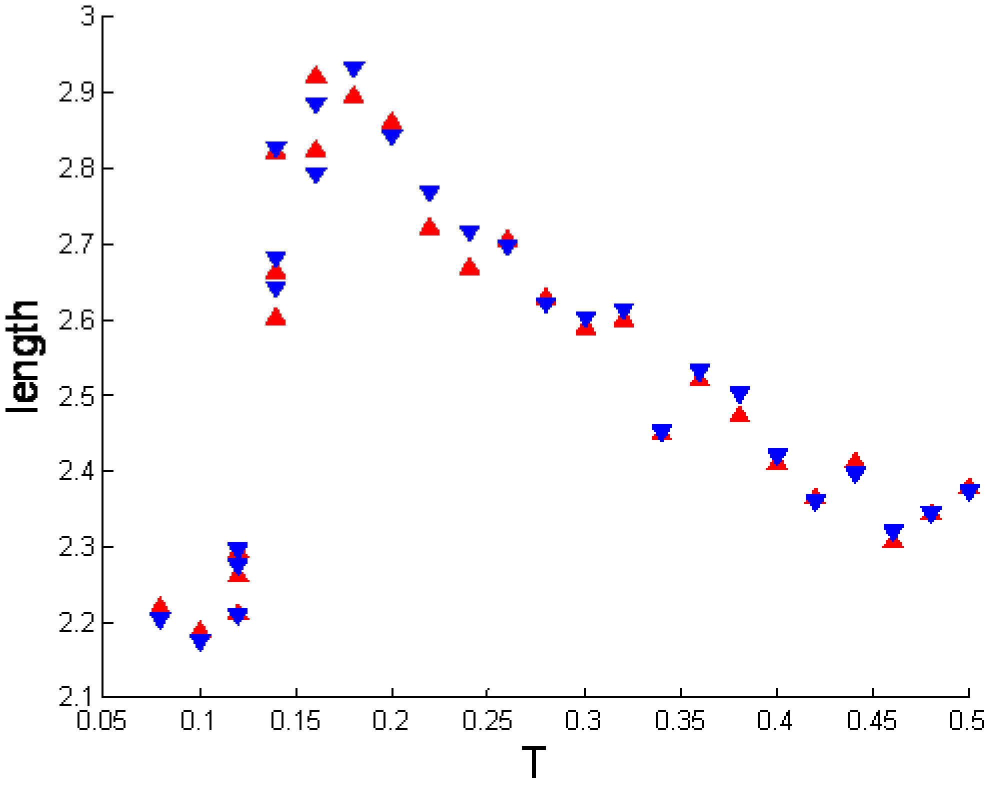

Figure 2.5.3-1: Expectation value of the domain size at different temperatures
The expectation value of the domain size in the direction of the long axis(▲) and perpendicular to the long axis(▼).

We have stated earlier that the formation of these regions is not a thermodynamic property, but instead, the result of the preferred kinetic pathway as the simulation sample traverses the PEL. What is the source of the structural change? We know that the overall energy of the glassy simulation samples is higher than predicted at low temperature as compared with the equilibrium configurations. Thus, it is a requirement that there be a lower density of bonds, which would inhibit large aligned regions. Additionally, it may be that there are pathways on the PEL which are no longer accessible, or are extremely unfavorable due to the separation of time scales between processes which break different numbers of bonds. This comparison demonstrates that there is a distinct difference in the kinetics between the equilibrium and non-equilibrium simulation samples as reflected by the resulting structural features.

2.6. Dynamic Heterogeneity: Evidence of Cooperative Motion

Currently we have two conflicting views of the length scale. First we demonstrated that the equilibrium supercooled liquids have an increasing domain size (Section 2.4.3) starting near the temperature at which we begin to observe cooperativity. This length scale increases in a linear fashion as $T \to 0$, without either diverging, or showing a change at the FSC. We see activated dynamics and a clear stretched exponential bond relaxation function (Section 2.4.4) as the temperature is lowered in the same region the domain size begins increasing. However, we see at the FSC a return to Arrhenious behavior, suggesting length scale has no impact below the FSC. This naturally leads to the question of how these two sets of measurements are related. Particularly, since there seem to be at least some spatially dynamic heterogeneity (SDH) implied by the use of the stretched exponential, characterization of these relationships between length-scale and time-scale are important. In Section 2.4.3, we used the bond relaxation time, τ_{bond} for our analysis of the system dynamics, however, concurrent measurements demonstrated the same trends and similar numeric values in the orientation relaxation time, $\tau_{orientation}$. As the domain size was determined based on orientation, we will monitor the change in the orientation with time during this analysis.

We can quickly see that the dynamics suggest a non-trivial relationship between the length-scale and time-scale. The limitations of our system have not yet made a formal analysis of this system relevant; however, we do find the mathematical description useful in describing our work. The fundamental correlation function now involves a four point correlation function, the change in length scale (two points) and the change in time scale (two points).

We are able to visually establish the presence of spatially correlated dynamics in our model. In Figure 2.6-1, we show a (40 x 40) set of vertices from the larger simulation lattice. We report the time for the molecule at each vertex to change orientation for the first time after an arbitrarily selected time, t_o. To compare each sample despite the disparate time scales at the three temperatures, we choose to represent the time to change orientation at each vertex relative to the distribution of times at that temperature alone. For clarity, we group the molecules into quintiles based on the time for each molecule to change orientation for the first time.

We observe the length scale of spatially correlated motion grows as the temperature decrease. In particular, there are fewer regions which have a checkered appearance, which arises from individual molecules on neighboring vertices changing orientation at time intervals greater than 20% apart. While the choice of the characteristic relaxation time is nontrivial (as discussed below), the increase in the size of dynamic heterogeneities is predicted by kinetically constrained models[28].

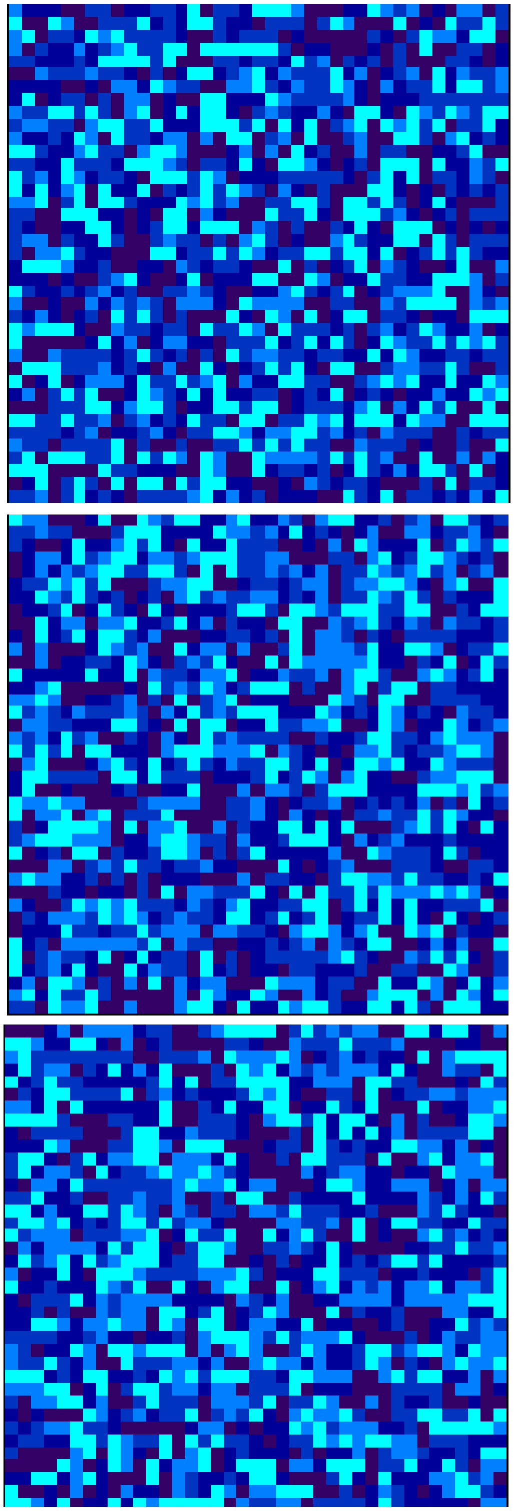

Figure 2.6-1: Representative of supercooled samples, time to first rotation
The time required to for initial rotation of a molecule at each vertex within an equilibrated simulation is roughly distributed in 5 Sections, from shortest to longest, to emphasize the spacial distribution: (■) ~first 20%, (■) ~ 20-40%-,(■) ~40-60%,(■) ~40-60%, (■) ~longest 20%. From left to right $T = 0.4$, 0.3 and 0.2 (each sample is normalized separately).

The representation in Figure 2.6-1 highlights the changes in movement along the PEL that occur as the simulation temperature decreases. At moderate temperatures, the simulation sample can still overcome the energy barriers involving breaking several bonds. Thus, the time for a molecule to change orientation for the first time is not as strongly dependent on the recent changes by its near-neighbors as it will become at lower temperatures. This is similar to the observation that the domain size is smaller at high temperature.

The relaxation time data in the range of $T=0.4$ and and $T=0.3$ suggest fragile dynamics, and therefore, cooperativity. In this regime, the number of bond influences the motion of a molecule. Thus a change in the orientation of a molecule may facilitate or hinder the orientation changes of its near-neighbors. However, we continue to see a growth in the size of the correlated domains as the temperature cools past the FSC to $T=0.2$. This region has Arrhenious dynamics and should not necessarily demonstrate SHD.

We have not yet addressed the question whether there are 'fast' and 'slow' regions. Are there spatial groupings of molecules that continue to remain mobile and change orientation quickly with respect to other regions of the lattice? It is possible to evaluate the mobility of an individual vertex by checking whether the molecule is more likely to change orientation again immediately after it changes for the first time. We do this by recording the time intervals between changes in orientation of the molecule at each vertex.

Evaluating the data for the time between successive changes, we may see that an individual molecule will continue to change orientation many times in an interval, then remain stationary, before eventually resuming a sequence of quick changes. This would be a time-scale of the changes in mobility of an individual molecule, $\tau_{mobility}\left(\vec{i}\right)$. Since the motion of a molecule can facilitate change in its near-neighbors, we may see more, less, or similar spatial heterogeneity in $\tau_{mobility}\left(\vec{i}\right)$ as we do in $\tau_{first\ change}\left(\vec{i}\right)$, the latter represented in Figure 2.6-1. Further, how are either of these values related to the overall relaxation time of the correlation function we previously measured $\tau_{orientation}$?

We have two cases to consider. If the time scale of changes in mobility of the molecules at all vertices is similar, then we can find the average time scale of mobility $\tau_{mobility}\left(\vec{i}\right) \approx \left\langle \tau_{mobility} \right\rangle$. Therefore while there is SHD, the time for a molecule to change orientation for the first time roughly represents the overall correlation time. We find that $\left\langle \tau_{first\ change} \right\rangle = \tau_{orientation}$. Alternately, 'fast' regions stay 'fast' and there are large spatial heterogeneities with respect to mobility. In this case, the relationship between $\left\langle \tau_{first\ change} \right\rangle \neq \tau_{orientation}$ is much more complicated, as the relaxation time of the correlation function scale would be dominated by molecules which require a long-time to change.

Based on the spatial groupings of the time to the first change of a site (Figure 2.6-1) we find compelling evidence of SHD. The question remains how important this feature is to the overall dynamics of the glass. We record the time between changes in orientation for all the molecules from samples equilibrated at the same temperature as those in Figure 2.6-1 to make sure that we capture the time scale for $\tau_{mobility}(\vec{i})$; this data is collected for 10 times the number of MCS required for the change in orientation to occur. Recording the length of time that each molecule spent in the same orientation, the distribution of relaxation times was then fit to a Gaussian curve, shown in Figure 2.6-2. We can compare these reported times to the relaxation time $\tau_{orientation}$.

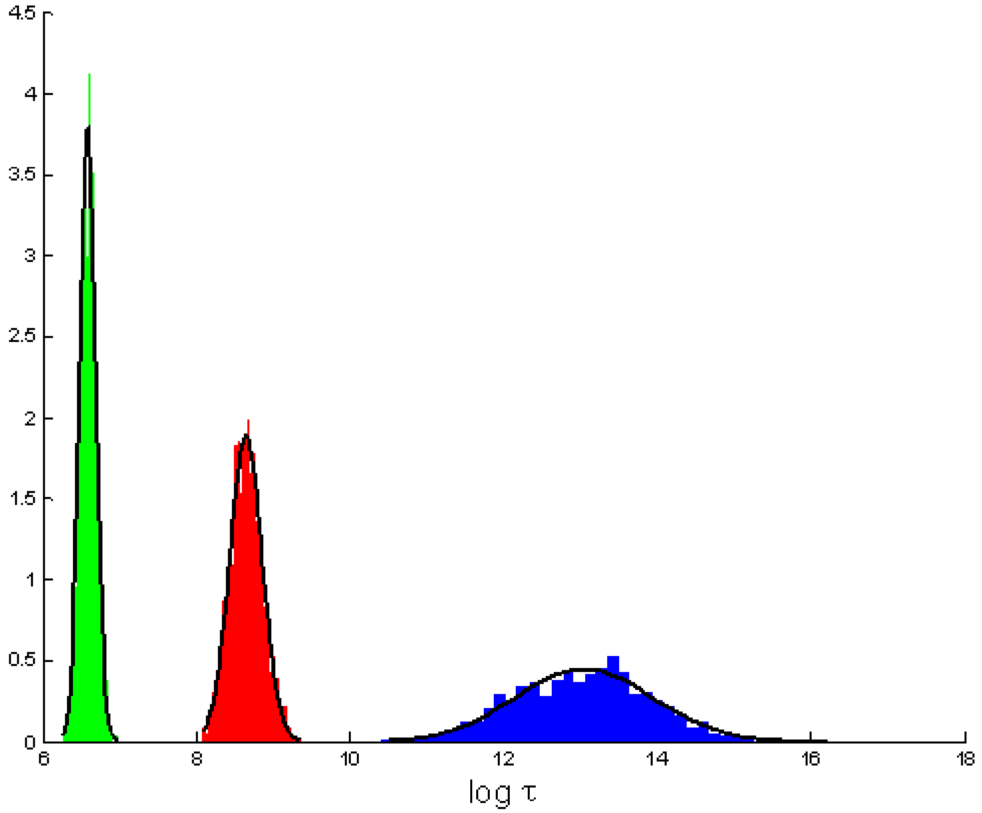

Figure 2.6-2: The distribution of the time for the molecule to change orientation
Tracks the average time it takes for an individual molecule on the lattice to change orientation (units log(t/v_o)) for at each vertex, then plots the histogram. The distribution for each sample is well fit by a Gaussian curve with (🟦) at $T = 0.2$ $(\mu = 13.04 \ \sigma = 0.89)$, (🟥) at $T = 0.3$ $(\mu = 8.64 \ \sigma = 0.21)$, (🟩) at $T = 0.4$ $(\mu = 6.58 \ \sigma = 0.11)$.

We can see this from a rough comparison of the overall relaxation times for the entire lattice and the average time to rotation of individual molecules. We report the values of τ_{bond} in Section 2.4.4, which are very close to the values of $\tau_{orientation}$, we discuss here for logical congruency. The integrated relaxation $\tau_{orientation}$ times are 6.97, 9.77 and 15.75, with decreasing temperature ($T = 0.4$, $T = 0.3$, $T = 0.2$). We note that these are longer than the time it takes for the sites to change for the first time indicating $\tau_{first\ change} < \tau_{orientation}$ and that there is some form of correlation time related to the persistence of the orientation of an individual molecule.

Overall bond percolation, the creation of a geometric network which spans the system, has been shown to occur at temperatures above the glass transition. Indeed, in our system, simulation samples in the fully-dense state will always have a space spanning bond network (Appendix B). Therefore, structural percolation cannot be the signature of the glass transition, nor the sole reason behind the dramatic increase in relaxation times. Alternately, it has been postulated that the increase in modulus at the glass transition is due to percolation of a dynamically slow network of the glass forming molecules, trapping pockets of dynamically fast droplets[87]. This is supported by the idea that the propagation length of mobility is smaller in strong materials than in fragile materials[28] and that the network structure suppress string like motion[134]. While the overall molecule density is constant (every vertex occupied), the bond density is a non-conserved order parameter and may provide the key to unraveling the distributions of fast and slow molecules.

We have attempted a variety of metrics to determine whether there is such a network structure in our systems. In Figure 2.6-3, the average time between changes in orientation for an individual molecule is shown. Those sites that retain the same orientation over a long period of time are shown in red/orange (note time scale on colorbar), so a network of sites which persist for a long-time would appear as a red network. Thus far, we have not identified clear evidence of such behavior. However, this choice would be very sensitive to time scale and our work certainly does not yet exclude the possibility of this dynamic mechanism.

Regions of molecules favoring a specific ordering grow with decreasing temperature (Section 2.4.3). As changes in orientations of highly bonded molecules are strongly disfavored due to the transition states, it may be that these regions persist for kinetic reasons. This result is consistent with a dynamic viewpoint in which the concentration of mobile molecules is also decreasing[28]. This indicates that the overall relaxation of the system -- the time it takes to no longer carry any correlation with the initial state--would reflect the process required for all molecules to have become mobile. If so the overall exchange rate between slow sites and fast sites, $\tau_{mobility}$, becomes the time scale associated with the overall system relaxation[87, 135]. This time scale may be the same as the relaxation times we calculated, or even longer than that associated with $\tau_{orientation}$ or τ_{bond} and not documented by any of our current metrics. Huang and Richert found that $\tau_{exchange} > \tau_{structural}$ for all temperatures in their experimental system[135]. (This would be equivalent to the statement $\tau_{exchange} > \tau_{orientation}, \tau_{bond}$ in our work.) Further, the length scale and relaxation time scale have been shown to be coupled in a non-trivial manner leading to the necessity for a more complex analysis to fully characterize this form of behavior.

In future work, investigation of SHD could be evaluated for this system, however, we would need to exercise caution to consider the system anisotropy with respect to the i and j axis as demonstrated in Section 2.4.3. The susceptibility of four-point correlation functions has successfully been used to quantitatively demonstrate the relationship between correlation length and relaxation time scale in a variety of systems[134, 136]. However these values would be difficult to extract in our simulations due to the length of time required to capture sufficient information to calculate the appropriate variances. Instead, a recent simplification of the values by using several approximations and the results of the fluctuation-dissipation theorem and the specific heat[128, 137, 138] has lead to the development of metrics using relaxation times and thermodynamic variables which may be more accessible[128, 137, 138].

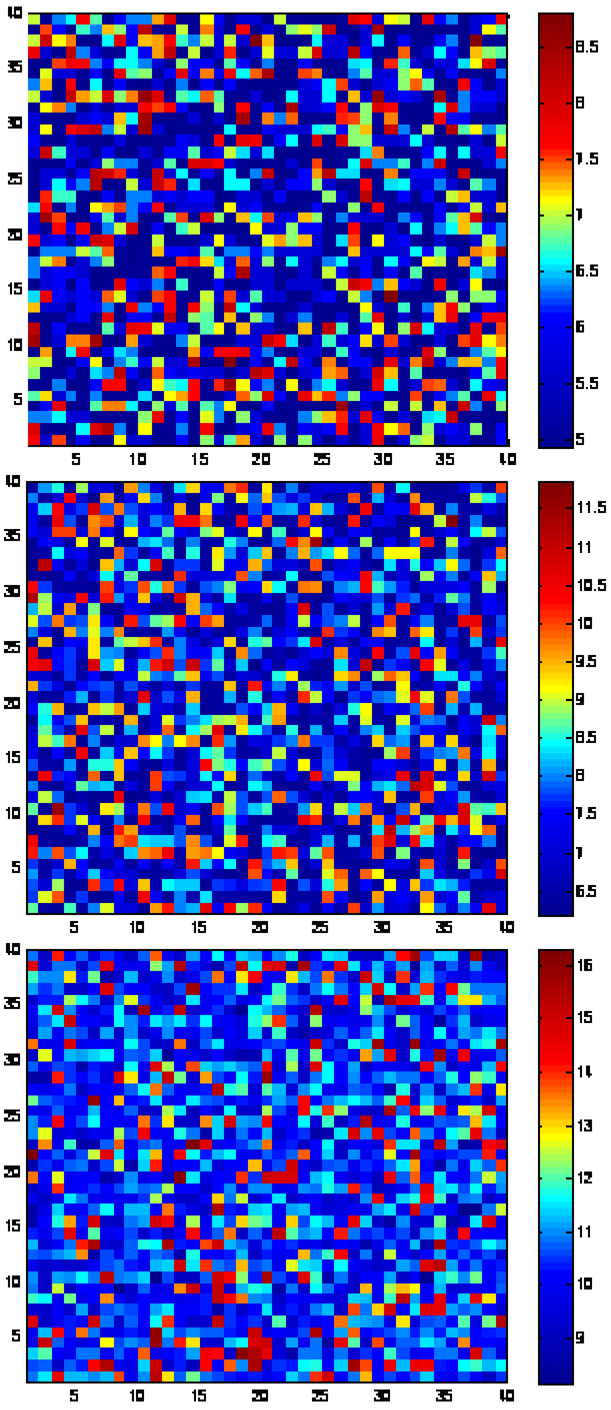

Figure 2.6-3: Representative of supercooled samples, average time to rotation

These figures represent the average time it takes for an individual molecule on the lattice to change orientation (units log(t/v_o)) at each vertex, note color bar is a different scale at each temperature. From top to bottom the temperature is 0.4, 0.3, and 0.2 respectively. The fastest times are blue, the slowest red.

2.7. Discussion

Establishing that the simulation samples quenched with the Metropolis MC method were indeed at equilibrium, due to the reproducibility, path independence and correct limiting behavior of the simulation samples, we are able use these samples as a starting point to evaluate low temperature conditions. Additionally, this provides a backdrop against which the deviation of samples quenched with kMC from the known equilibrium behavior may be clearly illuminated. We hope to extract from this comparison an understanding of the vitrification process in our system, establishing relevant temperatures and properties.

A wide variety of temperatures have been identified within this work and a partial list is included here. The subscripts from Chapter 1 have been extended to provide clarity in the context of this discussion.

Temperature	Value	Section Located
$T_{mf,binodal}$	$\left(3\log(3)\right)^{-1} \approx 0.7$	1.4.3[1]
$T_{mf,spinodal}$	0.25	1.4.3[1]
$T_{o,DMF}$	0.24	1.6.2[1]
$T_{\beta,metropolisMC:FSC}$	$\approx 0.24-0.26$	1.6.3[1]
$T_{o,MetropolisMC}$	0.07	1.6.3[1]
T_{Cv}	0.21	2.4.2
$T_{structure}$	≈ 0.5	2.4.3
$T_{\beta:fragility,onset}$	≈ 0.5	2.4.4
$T_{\beta:FSC}$	$\approx 0.24-0.26$	2.4.4
T_o	0.027	2.4.4
T_a	$\approx 0.46-0.5$	2.4.4
T_x	$\approx 0.22-0.24$	2.4.4
T_{kMC}	≈ 0.24	2.5.2
$T_{kMC,structure}$	$\approx 0.18-0.16$	2.5.3

The comparison of all these reported temperatures, both those derived from an analytic approximation and three different simulation techniques, lead to an interesting conclusion. We are able to distinguish three clear temperature regions, with distinctive kinetic properties based on the underlying thermodynamics. We present a synopsis in this paragraph followed with greater detail. In the high temperature regime where the relaxation is Arrhenius, the influence of the transition states and height of the energy barriers has very little impact. As we move to colder temperatures, we find the onset of an activated regime near $T_{onset} \approx 0.5$. Below this temperature, the simulation sample's movement on the PEL becomes influenced by the transition states. We notice that the domain size begins increasing and the stretching exponent reaches its low temperature plateau. The simulation samples experience cooperative relaxation and the orientation of near-neighbors is very important on the motions. The simulation samples also exhibit both kinetic and thermodynamic fragility. We are able to access very low temperatures and see a return to strong behavior, with an increase in the stretching exponent and Arrhenius temperature dependence in the relaxation time. The fragile-to-strong crossover temperature, $T_{FSC} \approx 0.24 - 0.25$, appears to be related to the thermodynamic details of the system. In the next few paragraphs we will weave together the observations that lead us to this description.

At high temperature, the system will move easily over the PEL and explore large regions easily until the thermal energy is on the same order as the bond energy ($T \approx 1$). Below that temperature, the transition states will begin to have an effect and there will be an onset to activated dynamics. In a mean-field description, our model experiences a first-order transition at $T_{mf,binodal} \approx 0.7$, however we don't find this temperature to be a dramatic transition in our kMC results. Instead, we note that by $T \approx 0.5$, which we identify as T_{onset}, a number of results show a clear change in character and signal entry into an activated regime. Thermodynamically, there is no clear change in the internal energy of the equilibrated structures, although the heat capacity increases strongly in this region. Our best indication of thermodynamic fragility is that the temperature dependence of the relaxation time can no longer be well described with a simple Arrhenius relationship, but becomes super-Arrhenius below T_a. We notice this in all three simulation methods. This observation has been found in other models[139], however we note that the critical temperature suggested by the VF fit is very low, e.g. $T_o = 0.027$, foreshadowing that this function does not describe the approach to an ideal glass transition, which would be barely distinguishable from $T = 0$. In this same intermediate range we find the clear kinetic fragility, as well. The stretching exponential β from the fit of the correlation functions, which has been decreasing with temperature, reaches its lowest values at $T_{\beta: fragility, onset} \approx 0.5$. During the temperature range in which the kMC thermodynamics remain fragile, the value of β remains constant, demonstrating that relaxation of the correlation function is clearly non-exponential. We notice that there is a clear onset of a growing length scale of structures on the lattice at this temperature, $T_{structure} \approx 0.5$. This length scale is kinetically, not thermodynamically determined, but does indicate that the near neighbor orientations, as described by the transition states, are beginning to have a large influence.

There is a second important grouping of temperatures reflecting changes in the neighborhood of $T \approx 0.24$, which we believe reflect the FSC. Under the mean-field approximation, the spinodal is the temperature at which the system becomes unstable with respect to the liquid phase and will be trapped in an energy minima in the absence of thermal fluctuations. During our DMF simulations, we are able to evolve a simulation sample from a homogeneous, supercooled liquid state to a heterogeneous, low energy minima via a very small perturbation. The critical temperature of a VF fit in the DMF simulations $T_{o,DMF} = 0.24$ is very close to the temperature of the mean-field spinodal ($T_{mf,spinodal} = 0.25$). This would indicate complete arrest of the motion on the landscape if the system did not have thermal forcing available to allow it to escape energy minima.

When we consider the results of the kMC, the change in relaxation time with temperature can also be well fit by an Arrhenius function below $T_x \approx 0.22 - 0.24$, indicating a thermodynamically strong glass former. We see that at $T_{\beta:FSC} \approx 0.22 - 0.24$, the stretched exponential now begins to increase with decreasing temperature, becoming kinetically stronger. (This is similarly observed in the previously reported Metropolis MC simulations where $T_{\beta,metropolisMC:FSC} \approx 0.22 - 0.24$ despite the omission of the details of the transition states). We do not observe a dramatic change in the slope of domain size, indicating that there is not a diverging static length scale that at the FSC.

We've established that, for our model, there is an increasing, but not diverging, static length scale for simulation samples equilibrated at decreasing temperature and the entropy remains positive for all temperatures. These observations would seem to indicate that there is not a thermodynamic glass transition for this class of models. Instead, glass transition only occurs when there is insufficient relaxation time to reach an equilibrium state. However, the FSC does have an important thermodynamic signature, the maximum in the heat capacity. Additionally, initial calculations of the minima of the PEL, identified by finding the inherent structure of the simulations (Appendix G), appear to follow the pattern observed in that of liquid silica at the FSC[72]. If we can cool equilibrium liquids below this temperature, and in the absence of other indicators, how does the FSC relate to T_g ?

A purely kinetic description does not explain a subtlety we see when cooling a simulation sample with the kMC methodology. Above the FSC, as a simulation sample cools at constant temperature, the energy will decrease at the same constant rate, regardless of the temperature until it approaches the equilibrium energy of the final temperature. Then it slows and asymptotes into a smooth master curve, terminating at its equilibrium energy. However, at the FSC, the change in energy with time begins to show plateaus, suggesting that the simulation sample is experiencing significant changes as it traverses the energy landscape. There appears to be an inflection point in the curve of time it takes to reach equilibrium. Under the constraints of our simulation time, some of the low temperature samples reach equilibrium while others do not. However there is no indication of a particular reason they could not reach equilibrium should we continue to run the simulation for even longer times. For those samples which reach equilibrium above or below the FSC, the expectation value of the structure length is similar to the equilibrium structures which were equilibrated with the Metropolis MC. Thus there is no indication that the simulation samples are different at equilibrium applying from applying different transition states during MC simulations, a result consistent with the detail balance requirement.

This leads us to a very interesting image of what might be happening in some structural glass systems at very low temperature. Invoking the energy land perspective, one may consider the variety of paths that a simulation sample may traverse in proceeding from one energy minima to another. If a random thermal forcing can create as little as one pair of molecules which are not fully bonded, then the simulation sample can travel from one initially fully satisfied state to another skirting many higher energy regions. This process is diffusive in nature, which suggests the source of the Arrhenius temperature dependence as the simulation samples wander in the ravines which connect the energy minima.

Conceptually, our model is always ergodic, however energy barriers may make the system effectively non-ergodic by inhibiting the complete exploration of the PEL at low temperatures, a feature observed in other kinetically constrained models[27]. In those systems there is explicit frustration which causes the glassy dynamics. While certainly exploring portions of the landscape with high potential energy becomes exceedingly rare at low temperature, even at very low temperature the number of degenerate ground states is greater than exponential. Additionally all of the minima are connected via low potential energy pathways on the PEL, unlike those in other systems. Therefore, we do not see the configurational entropy disappear at finite temperature.

The development of a plateau in the relaxation dynamics from a random configuration to a low temperature minima at the fragile-to-strong crossover is a feature that calls for additional exploration. One possibility is certainly that the population of unbounded molecules peaks in these simulations. It is shown in Appendix E that the distribution of these molecules is a non-monotonic function of temperature. Their presence makes the progress of the simulation exceedingly slow computationally, but this does not have the same dramatic effect on the 'real time' which we document. However, this may hint at underlying structural features that lead to the system becoming trapped at higher energy states for a long length of time. This indicates that documenting the population of molecules which have 0, 1, 2, or 3 bonds may give insight into these issues. When considering only the potential energy landscape, we should recall that it is not the internal energy alone, but the free energy with its entropic component, that describes the equilibrium state[140]. Therefore, we need to consider large, flat regions on the landscape that may describe barriers due to entropy alone, in which case it may never be necessary to take an energetic step up-hill[141].

An alternate idea that involves percolation considers accessibility of regions on the PEL directly[142]. In this theory, transitioning into the glassy state occurs when the possible paths which a simulation sample may follow between minima on the landscape no longer percolate. Because the PEL is hyper-dimensional, the mean-field approximation of this transition becomes exact and predicts the correct behavior at the critical point[142]. We have not formulated our mean-field approximation to address a PEL percolation transition; to do so we would need to include the details of the transition states and consider a time variable. However our static representation may still capture some of this flavor because it does consider the temperature at which amorphous energy minima are preferred with respect to the liquid (random) state, $T_{mf,binodal}$, as well as when the simulation sample will be confined to energetic minima, $T_{mf,spinodal}$. This approach is similar to that described in the Introduction, which describes the simulation sample trajectories that lose ergodicity on time scale of the simulation[108] and those that involve tree representation of movements[110].

Other models with limited valency or 'patchy' interactions have recently been studied. Among the findings, we see that a number of gelformers have transitions influenced by their structural orientation including proteins[143] and colloids[92]. Beyond the scope of this set of materials, valency is also found to be a crucial detail in some materials with a liquid-liquid phase transition, which is not a spatially homogeneous gas/liquid separation, but instead a heterogeneous phase change between two different locally oriented structures [4, 107].

Additionally, the number of bonding sites or patches appears to have more influence on this behavior than the location of the interaction although both contribute to the phase diagram[143]. The overall effect of increasing the valency is to increase both the critical temperature and density when considering phase separation[143]. Our phase diagram is similar to those found both experimentally and in other simulation models. Indeed, without valency limited potentials in colloidal systems there is not a low temperature region that would be able to generate a disordered homogeneous (as opposed to phase separated) arrested state[7, 17]. The lower the valency in these systems, the smaller the force for phase separation as most of the particles are fully bonded so there is no drive towards further density increase. The possibility of finding a region in which the low temperature promotes long-lived bonding opens up exploration of colloidal gels[133, 144].

Currently, in our model we do not have a preference for a crystalline form, however we could easily modify the Hamiltonian by inducing a field

$$\begin{aligned} \beta H &= -\sum_{\langle \vec{i},\vec{i}' \rangle} \beta\varepsilon\left(\sigma_\alpha\left(\vec{i}\right)\sigma_\gamma\left(\vec{i}\,'\right)\right) + \sum_{\vec{i}} \beta\mu_\alpha\sigma_\alpha\left(\vec{i}\right) \\ \text{where } \mu_\alpha &= \begin{cases} 1 \text{ if } \alpha = 1 \text{ or } 3 \\ 0 \text{ otherwise} \end{cases} \end{aligned} \tag{18}$$

or non-equal bond energies:

$$\begin{aligned} \beta H &= -\sum_{\langle i,i' \rangle} \beta\varepsilon_{mn}\left(\sigma_\alpha\left(\vec{i}\right)\sigma_\gamma\left(\vec{i}\,'\right)\right) \\ \text{where } \varepsilon_{mn} &= \begin{cases} \varepsilon_{ll} \text{ if two long axis bonding sites fall on same edge} \langle i,i' \rangle \\ \varepsilon_{ls} \text{ if a short axis and a long axis bonding sites are along edge} \\ \varepsilon_{ss} \text{ if two short axis bonding sites fall on same edge} \langle i,i' \rangle \\ 0 \quad \text{otherwise} \end{cases} \end{aligned} \tag{19}$$

Vogel and Glotzer[134] found that the length scale of clusters did not diverge at the FSC and that there was no clear indication that this temperature was linked to spatially heterogeneous dynamics. However, they point out that the valency would have a strong effect on the spatio-temporal mobility of particle motion because the imposed network structure statistically limits the number of number of near-neighbors which are mobile. Our T-shaped molecule model can easily be extended into higher dimensions (Appendix D) or studied on other lattice structures. Additionally, changing the bonding site number and locations on the molecule does not require any modification of the fundamental techniques.

Our model could be considered one of a class of models which limits the number of near-neighbor bonds via defining the properties of the molecule at the vertex as having fewer bonding regions than the number of edges of the lattice. This leads to viewing the overall state of the system as a composite of the individual occupancy and orientations at each vertex. A conceptually similar Hamiltonian is under very active investigation. A limited valency system is created by restricting the number of bonds via exclusions of states of the system which have too many bonds converging at a single vertex (or too many near-neighbors)[113]. Models similar to ours, in which the valence restriction is a property of the molecule, may prove computationally faster during simulations because we can create 'look-up tables' enumerating, *a priori*, every combination of near-neighbors. Thus the calculation of energy of a state progresses via matrix multiplication. Formulations restricting the number of bonds at a vertex require a step identifying whether the new state is possible, which requires comparisons, inherently slow computationally. One way to side-step these issues is to map the restriction onto a model in which all occupation states are possible, but create an energy penalty for vertexes with large number of near-neighbors. In the limit of an extremely high penalty, we should recover the original exclusion of states. This also suggests a mechanism for proving that the two classes of models may be mapped to each other.

With the simplicity of this model, the possibility of analytic explorations is enticing. It is interesting to note that Sastry et al. found that the Bragg-Williams approximation was better at describing the skewing of the liquid gas spinodal to the low density side of the phase diagram than the Bethe-Peierls approximation in this class of models[113]. However, no explanation for this was proposed. In our model, this skewing was the result of the phase separation between the gas and a heterogeneous liquid phase. It might be that the implementation of the Bethe-Peierls suppresses or excludes consideration of this phase. However, because within their work no explicit discussion of the implementation which would distinguish between an homogeneous and heterogeneous liquid is included, this explanation is tenuous at best. An implementation of the Wertheim perturbation analysis was restricted to valencies above 3 and below 5, severely limiting this approach for exploration of a larger number of systems[144]. With the simulation work in hand, extension of the analytic description of the model can be better approached.

2.8. Conclusions

Our strikingly simple model can be used to describe the low temperature behavior of valence-limited glass formers. Employing the Metropolis MC method, we can cool simulation samples to equilibrium providing the starting states for study of the thermodynamics, dynamics and structure. Consideration of results from the evolution of the simulation samples with a kinetic MC recipe, thus including the effects of transition states on the sample motion on the PEL, yields a picture of three distinct dynamic regimes. At high temperatures the system is free to move without significant impact of the transition states. However, as the system cools, it reaches T_{onset} below which activated events become important, the sample motion that must overcome an energy barrier by concerted thermal activation. In this region we find that the relaxation time exceeds that of a simple Arrhenius dependence and the structural length scale increases. In our model both are hallmarks of a fragile glass former.

Further cooling results in a fragile-to-strong crossover in our system at T_{FSC}. Below this temperature, the stretching exponential increases in value and the relaxation time returns to an Arrhenius behavior with cooling. The FSC resolves the Kauzmann Paradox by demonstrating that the extrapolation of the fragile properties above T_{FSC} is not valid as $T \to 0$. Instead, we find that the configurational entropy does not disappear at low T.

As is found in experimental systems, we can force our system into non-equilibrium conditions by quenching a random sample with the kMC method at a constant rate. However, when a random simulation sample is allowed to cool against a constant temperature bath we observe that it will eventually reach equilibrium. We follow the potential energy as the system cools as a function of time. We see a change in the cooling behavior around the FSC. At higher temperatures, the sample cools rapidly until it asymptotes to the equilibrium temperature. The overlay of this behavior at different temperatures leads to a cooling curve, along which all the samples are at equilibrium at the appropriate potential energy as the time progresses. Near the FSC we note that there is the onset of a plateau at higher potential energies, indicating the simulation sample experiences a multi-step relaxation process where it is no longer at equilibrium as it is cooled. There is no evidence, however, that the samples will not eventually reach equilibrium. It does suggest that on the time scale of experimental and simulated observations, the lattice is arrested at in a non-equilibrium state with higher potential energy. We identify simulation samples that are at this temperature plateau as glasses, indicating that T_{FSC} may often be identified as T_g .

During the simulations which are evolved from an initial, equilibrated state with the kMC method, we observe a peak in the heat capacity at the FSC. Additionally, as we observe the structure of the system, it begins to become aligned due to kinetic reasons starting at T_{onset}, but does not show evidence of a static length scale divergence with temperature. At low temperatures, simulation samples that would be characterized as arrested, glassy states show a significant decrease in static structuring. Our model appears to show significant spatially dynamic heterogeneities, with an increasing correlation length as the temperature decreases. There is evidence that the evolution of the system is dominated by mobile molecules that can change their orientation quickly, and that the time for structural relaxation is determined by the time scale of exchange of mobile and immobile molecules.

The kinetics and thermodynamics of self-assembled structures is a rich field for research today. Our model allows us to explore low temperature conditions at long-times, resulting in insight into the class of limited valency systems. In previous work we have extended this model into a two-phase regime and identified a large variety features in the gel phases upon the addition of solvent. Similar work could lead to a deeper understanding of the phase behavior of physically reversible gels and illuminate the relationship between the glass transition and gelation.

Appendix A: Dimensionless Units

The energy of a bond in our model is not established from a physical system. Therefore, we carefully define it with regard to the thermal energy. For this work, the temperature of the simulation is the variable T which is scaled by

$$T_r \equiv {}^{\varepsilon}\!/_{k} \equiv 1 \tag{1}$$

where ε is the energy of a bond and k the Boltzmann constant. In the stochastic simulations we perform the internal energy u per lattice site is compared to the thermal energy β^{-1} using the definition:

$$\beta u = -\left(\frac{\varepsilon}{kT}\right)\left(\frac{\langle \text{# of bonds} \rangle}{2\text{N}}\right) = -\left(\frac{T_r}{T}\right)\left(\frac{\langle \text{# of bonds} \rangle}{2\text{N}}\right) \tag{2}$$

Reported values of the internal energy are multiplied by k^{-1} as seen by:

$$u = -(\varepsilon)\left(\frac{\langle \text{# of bonds} \rangle}{2\text{N}}\right) = -(kT_r)\left(\frac{\langle \text{# of bonds} \rangle}{2\text{N}}\right) \tag{3}$$

The denominator 2N reflects that each bond is shared by two sites, where there are N sites on the lattice.

We calculate the residual entropy by extracting estimates heat capacity in two ways. One is to estimate the slope of our data and employ the thermodynamic definition:

$$C_V \equiv \left.\frac{\partial U}{\partial T}\right|_V \approx \frac{\Delta u}{\Delta T / T_r} = \left(\frac{kT_r}{2N}\right)\frac{\Delta \langle \text{# of bonds} \rangle}{\Delta T} \tag{4}$$

In the penultimate equality U and T comes from the formal definition; the estimation retains the factor of k^{-1} in our reported quantities as it refers to the definition provided in equation

(3). The alternate definition comes from harnessing the measured susceptibility within our simulation runs:

$$C_V \equiv \frac{\left\langle \left(U - \langle U \rangle\right)^2 \right\rangle}{kT^2} = \frac{\langle U^2 \rangle - \langle U \rangle^2}{kT^2} \tag{5}$$

We derive this from our simulations by calculating:

$$\begin{aligned} C_V &= \frac{1}{k\left(T/T_r\right)^2}\left(\left\langle \left(-\left(\frac{\langle \#\text{ of bonds} \rangle}{2\text{N}} \right) \right)^2 \right\rangle - \left\langle -\left(\frac{\langle \#\text{ of bonds} \rangle}{2\text{N}} \right) \right\rangle^2 \right) \\ C_V &= \frac{kT_r^2}{4N^2}\left(\frac{\left\langle \langle \#\text{ of bonds} \rangle^2 \right\rangle - \left\langle \langle \#\text{ of bonds} \rangle \right\rangle^2}{T^2} \right) = \frac{kT_r^2}{4N^2}\left(\frac{\text{var}\left(\langle \#\text{ of bonds} \rangle\right)}{T^2} \right) \end{aligned} \tag{6}$$

Therefore to return it to the units of N^{-1} so that it scales properly on a per site basis, we multiply by an extra factor of N with the final result:

$$C_V = \frac{kT_r^4}{4N}\left(\frac{\text{var}\left(\langle \#\text{ of bonds} \rangle\right)}{T^2} \right) \tag{7}$$

In Appendix F, we discuss the importance of averaging over only samples which are uncorrelated in time. We take care insure that the observations of the samples used for our analysis are taken at time points much further apart than the relaxation time.

Appendix B: Comparison with Bond Percolation

As we consider the connectivity of our simulation results, it is helpful to relate this to the bond percolation threshold. It has been noted that percolation is a necessary, but not sufficient condition for structural arrest in a reversible gel. Bond percolation is defined as a connected network of bonded sites which spans the lattice. The case in which there is no interaction energy between bonds (the bonds are randomly placed on edges) is equivalent to the high temperature limit in our model. The threshold for bond percolation is defined as the minimum probability that an edge is occupied required for network. This probability p_c is 1/2 on a square lattice and approximately 1/4 on a cubic lattice[145-147]. Converting to the number of bonds per site, the percolation threshold density would be 1 on a square and 3/4 on a cubic lattice. We notice that the dynamic phenomena we observe occur well below the high temperature limits of our model and that the bond densities were larger than the percolation threshold. It is therefore reasonable to assume (although not rigorously proven), that all our simulated samples are percolating networks. This is consistent with the observation that the percolation threshold is above the gelation threshold for reversible bonding systems[40]. The dynamic transitions which we measure are not a direct consequence of percolation.

Appendix C: Landau Theory Calculations in Two Dimension

During the interpretation of our simulation results, it is useful to orient ourselves to the relevant values of the scaled temperature ${}^{T}\!/_{T_r} = {}^{\beta}\!/_{\varepsilon}$ by considering the mean-field results. It is important to acknowledge the simple Landau theory, which expands the energy in terms of an order parameter has severe and well documented limitations. However, the results provide insight into the order parameters in our model and a starting place for our continued analysis. We note that this is a form of the mean-field approximation, as is clearly seen in the values of the results. We note that in our results, there is a locally preferred structure at lower temperature. This is consistent with an order/disorder transition, and reinforces the less obvious lack a macroscopic symmetry breaking with two of the states dominating at all vertices (preponderance in either the (1,3) ┤, ├ or (2,4)┴, ┬). Indeed, in all cases there is little skewing, even when structure on the order of the length scale of the simulation sample size develops. However it is not clear the number of order parameters needed to describe these results.

In this implementation, we define two order parameters, α and δ, to allow for the possibility of two forms of order/disorder symmetry breaking in the system behavior. Both indicate the same limit of stability limit $T = 0.25$. Thus, in our mean-field results presented in Chapter 1, we assert that the orientations not involved in a locally ordered structure will have degenerate probabilities. Employing this assumption we recover the spinodal temperature, $T = 0.25$, further validating that symmetry breaking occurs only in one direction (either ┤, ├ or ┴, ┬).

We use classical Landau theory[148] to identify when the random state becomes unstable relative to the ordered lamella state for the fully-dense lattice. This describes a liquid to crystal phase transition. It is important to note that at this value of T (or conversely temperature), the system will spontaneously order into a lamella. Other satisfied structures might spontaneously form at temperatures near this transition, but they are neglected in this estimate. Thus, the predictions of this analysis would not be inconsistent with observation of a lamella state in a simulation sample at a higher temperature, or a transition to a different energy minima altogether.

At the heart of Landau theory is a functional form of the free energy as an expansion in powers of an order parameter. We can then use the functional form to identify when the free energy minimum transitions from the zero to a finite value of that parameter. Defining an order parameter to distinguish between a glassy and a polycrystalline state remains a fundamental challenge in this field[149]. We recognize that we cannot identify order parameters to discuss generically this transition because of the degeneracy of the potential energy minimum. However, we can identify order parameters for the specific transition from the disordered state to the lamella state, where all the rows (or columns) are identical in one direction and in the opposite direction they alternate. If we assume periodic boundary conditions, we can reduce the lattice to two sites without loss of generality. In this state two molecule orientations (e.g. ┤, ├) will dominate the lattice and the probability of the other two (e.g. ┴, ┬) will be equal everywhere, but smaller. This introduces the first-order parameter, α. A second order parameter, δ, is introduced when we choose either the left-hand or right-hand site to be in state 1 (alternately the top or bottom site to be in state 2).

We use these order parameters to write the free energy expansion. Both α and δ are even functions so no linear term appears in the free energy expansion. The transition occurs when the second order terms change from positive to negative (or the global free energy minimum changes from zero to nonzero). The value of ε required for this transition is 4 (or the temperature of this transition is T =0.25). .

Using the Hamiltonian, we find the internal energy for our model is:

$$\begin{aligned}
\beta H = -\left(\frac{\beta}{2}\right)\sum_{i=1}^{N}\sum_{j=1}^{N}\{\ & p_1(i,j)[\ p_1(i,j+1)+p_2(i,j+1)+p_3(i,j+1)+p_2(i+1,j) \\
&+p_3(i+1,j)+p_4(i+1,j)+p_1(i,j-1)+p_3(i,j-1)+p_4(i,j-1)\ ]+ \\
&p_2(i,j)[\ p_2(i+1,j)+p_3(i+1,j)+p_4(i+1,j)+p_1(i,j-1)+p_3(i,j-1) \\
&+p_4(i,j-1)+p_1(i-1,j)+p_2(i-1,j)+p_4(i-1,j)\ ]+ \\
&p_3(i,j)[\ p_1(i,j+1)+p_2(i,j+1)+p_3(i,j+1)+p_1(i,j-1)+p_3(i,j-1) \\
&+p_4(i,j-1)+p_1(i-1,j)+p_2(i-1,j)+p_4(i-1,j)\ ]+ \\
&p_4(i,j)[\ p_1(i,j+1)+p_2(i,j+1)+p_3(i,j+1)+p_2(i+1,j)+p_3(i+1,j) \\
&+p_4(i+1,j)+p_1(i-1,j)+p_2(i-1,j)+p_4(i-1,j)\ ]\ \} \\
&-\left(\frac{\beta\eta}{2}\right)\sum_{i=1}^{N}\sum_{j=1}^{N}\ p_5(i,j)[\ p_5(i,j+1)+p_5(i+1,j)+p_5(i,j-1)+p_5(i-1,j)\ ]
\end{aligned} \tag{1}$$

With the value of the reduced temperature given in chapter 2 . The free energy is therefore given by:

$$\beta f = \beta u + \sum_{i=1}^{N}\sum_{j=1}^{N}\sum_{k=1}^{4}\ p_{k,i,j}\ln p_{k,i,j} \tag{2}$$

We substitute the following relations to describe the lamella state in terms of one site:

$$\begin{aligned}
p_{2,i,j} &= p_{4,i,j} \\
p_{2,i,j} &= p_{2,i,j+1} = p_{2,i+1,j} \\
p_{1,i,j} &= p_{1,i+2,j} = p_{3,i+1,j} = p_{3,i+3,j} \\
p_{1,i,j} &= p_{2,i,j+1}
\end{aligned} \tag{3}$$

and write the remaining terms of the ordered parameters α and δ:

$$
\begin{aligned}
p_1 &= \tfrac{1}{4}\,(1 + \alpha) + \delta \\
p_2 &= \tfrac{1}{4}\,(1 - \alpha) \\
p_3 &= \tfrac{1}{4}\,(1 + \alpha) - \delta \\
p_4 &= \tfrac{1}{4}\,(1 - \alpha)
\end{aligned}
\qquad (4)
$$

We then expand the free energy in terms of the ordered parameters. This gives:

$$\beta f = \frac{9\beta J}{8} + \ln 4 + \left(\frac{\beta J}{8} + \frac{1}{2}\right)\alpha^2 + (\beta J + 4)\delta^2 + \ldots$$

Thus the onset of instability with respect to the lamella phase is at $T^{-1} = -4$ and both ordered parameters become unstable at the same time. This result foreshadows the general mean-field solution which does not specify which final state of the lattice is preferred (not restricted to the ordered parameter of a single energy minima- that of the lamella). It also supports the results of the DMF simulations which find that even once a minima is found and one orientation is strongly preferred at vertex $\langle \vec{i} \rangle$.

Appendix D: Mean-Field Calculation in Three Dimensions

A natural extension of our work is to consider the model in other lattices forms, either in two dimensions (e.g. hexagonal) or in three dimensions (e.g. cubic). We also can consider other conformations of the bonding sites or additional bonding sites. For example, a molecule with 4 or 5 bonding sites would still be valence-limiting on a cubic lattice (6 edges at each vertex). The complexity this adds to the mean-field calculations is dramatic if we explicitly consider the full Hamiltonian as we did in Chapter 1. During our work, we found the mean-field diagram was a very useful guide for our understanding of the simulations. Others have recently shown that despite the simplicity of this approximation, it provides a more accurate estimate of simulation results than other more detailed calculations. A more detailed discussion of this can be found in Chapter 2.

A further provocative thought is that the glass transition occurs as lack of percolation of mobile regions around glassy states on the potential energy landscape (PEL). The large dimensionality of the PEL exceeds the upper critical dimension limiting a mean field analysis such the mean-field conditions are met and the approximation when used in this way provides the exact results[142]. We have not formulated our approximation to address a percolation transition in accessible portions of the PEL explicitly; however the connection between the ideas is appealing.

As the Hamiltonian becomes larger, we find we can simplify our perspective by considering there are two types of occupied orientations. The first is one in which is part of a locally ordered domain and thus is energetically stabilized. The second is a non-ordered liquid like phase.

In this Section we will consider the same T-shaped molecule, but now on a cubic lattice. Exploration beyond the current T-shape model in 2-dimensions into 3-dimensions or on alternate lattice structures is motivated by both the expectation of more physically relevant systems but also by the increase in accessibility of the equilibrium gel phase. This phase occupies a larger range of densities on the phase diagram as the valency is lowered[7]. Indeed, access to this phase can be shown to require anisotropic interactions[7]. In colloidal gels, represented by potentials that have directional attractive interactions on the smaller than the length scale of the particle, kinetic arrest can be achieved through non-equilibrium routes during phase separation at lower densities (the high density phase becomes an attractive glass) and also via reversible paths at higher density[94, 95, 133].

On the cubic model there are 12 possible orientations for each molecule. We will refer to the probability that the molecule at the vertex is in a locally ordered domain as p_α. Given the density of molecules ρ, and recalling that the other orientations are degenerate as they are still in a liquid-like phase, the value of these probability of the other occupied states are:

$$p_\beta = \frac{(\rho - p_\alpha)}{11} \tag{1}$$

When in the fully-dense region ρ=1. Else, we have used the random dilution approximation by assuming that the interaction with the solvent is neutral. In addition to calculating the phase diagram, we also demonstrate that the model retains the same degeneracy of ground states which we believe to be fundamental to the nature of this class of materials. First we will consider the fully-dense state. At high temperature each orientation is equally probable so:

$$p_\alpha = (1/12) \tag{2}$$

We can calculate the random potential energy by recalling that there are 6 near-neighbors on a cubic lattice, with 3 possible bonds that the molecule at the vertex we are considering could form. The multiplicative factor or 12 arises from the 12 possible orientations and we divide by 1/2 because each bond is shared by two molecules.

$$\beta u_{random} = -\frac{\beta}{2}\left(p_{\alpha} \times 6 \times 3 \times 12 \times p_{\alpha}\right) = \frac{-3}{4}\beta \tag{3}$$

Adding to this the entropy we find

$$\begin{aligned} \beta f_{random} &= \beta u_{random} + s_{random} \\ \beta f_{random} &= -\frac{3}{4}\beta + 12 p_{\alpha} \log(p_{\alpha}) \\ \beta f_{random} &= -\frac{3}{4}\beta + \log(12) \end{aligned} \tag{4}$$

Recall that we are using the same reduced units as described in the other portions of this work. At lower temperatures, there will be a fraction of molecules that may adopt a locally oriented structure. This results in

$$p_{\alpha} > (1/12)\,;\, p_{\beta} = \frac{\left(1 - p_{\alpha}\right)}{11} \tag{5}$$

$$\beta u_{oriented} = -\frac{\beta}{2}\left(3p_{\alpha}^{2} + 30 p_{\alpha}\frac{(1-p_{\alpha})}{11} + 183\left(\frac{(1-p_{\alpha})}{11}\right)^{2}\right) \tag{6}$$

It would be quite difficult to tally by hand the 216 possible combinations, but the use of locally ordered states helps considerably. First, we consider the interactions resulting from the molecule of interest being in a locally preferred orientation, p_{α}. We notice that there must be three bonds between the central molecule and its near-neighbors which are also in the locally preferred orientation by definition resulting in a factor of $3p_{\alpha}^{2}$. Next, we consider the central molecule and the possible bonds it can form with near neighbor molecules which are not in locally preferred orientations. There are 12 orientations at each near neighbor, however, only 6 are oriented toward the center molecule, and one of these configuration must already represent the locally oriented structure. There are three bonds which might form between the central locally oriented structure and these liquid like neighbors. Thus there are 15 possible bonds adding $15p_\alpha \frac{(\rho - p_\alpha)}{11}$.

Now we consider the liquid like states in the from the center molecule. There are 11 states remaining. As before, along the three vertices from which locally oriented bonds are oriented, there are 5 remaining liquid states that can occupy one of the 3 bonds originally between the locally preferred direction and 5 liquid orientations at the near neighbor sites that meet the geometrical requirements. Thus, a first term of $75\left(\frac{(\rho - p_\alpha)}{11}\right)^2$. There are 6 orientations at the central molecule that could present a bond forming direction along the vertice that did not have a bond in the original locally oriented structure. There are the 6 near-neighbors that could take advantage of this. This provides a second term of $108\left(\frac{(\rho - p_\alpha)}{11}\right)^2$ Collecting these terms we find that

$$\begin{aligned}
\beta f_{oriented} &= \beta u_{oriented} + s_{oriented} \\
\beta f_{oriented} &= -\frac{1}{2}\left(3p_\alpha^2 + 30p_\alpha \frac{(1-p_\alpha)}{11} + 183\left(\frac{(1-p_\alpha)}{11}\right)^2\right) \\
&\quad + p_\alpha \log(p_\alpha) + (1-p_\alpha)\log(\left(\frac{(1-p_\alpha)}{11}\right))
\end{aligned} \tag{7}$$

Extension into the solvated region involves merely replacing $1-p_\alpha$ with ρ. We then calculate the chemical potential from the free energy as

$$\beta\mu_{liquid} = \frac{\partial f_{liquid}}{\partial \rho};\beta\mu_{oriented} = \frac{\partial f_{oriented}}{\partial \rho} \quad (8)$$

This allows us to write the grand potential as $w = f - u$. The grand free potential energy describes the relationship between temperature and density. We consider several different coexistence cases. First, we calculate the low density high density coexistence. Then, as temperature lowers, we consider a low density solution in coexistence with a high density locally ordered liquid. These relationships are shown in Figure D-1.

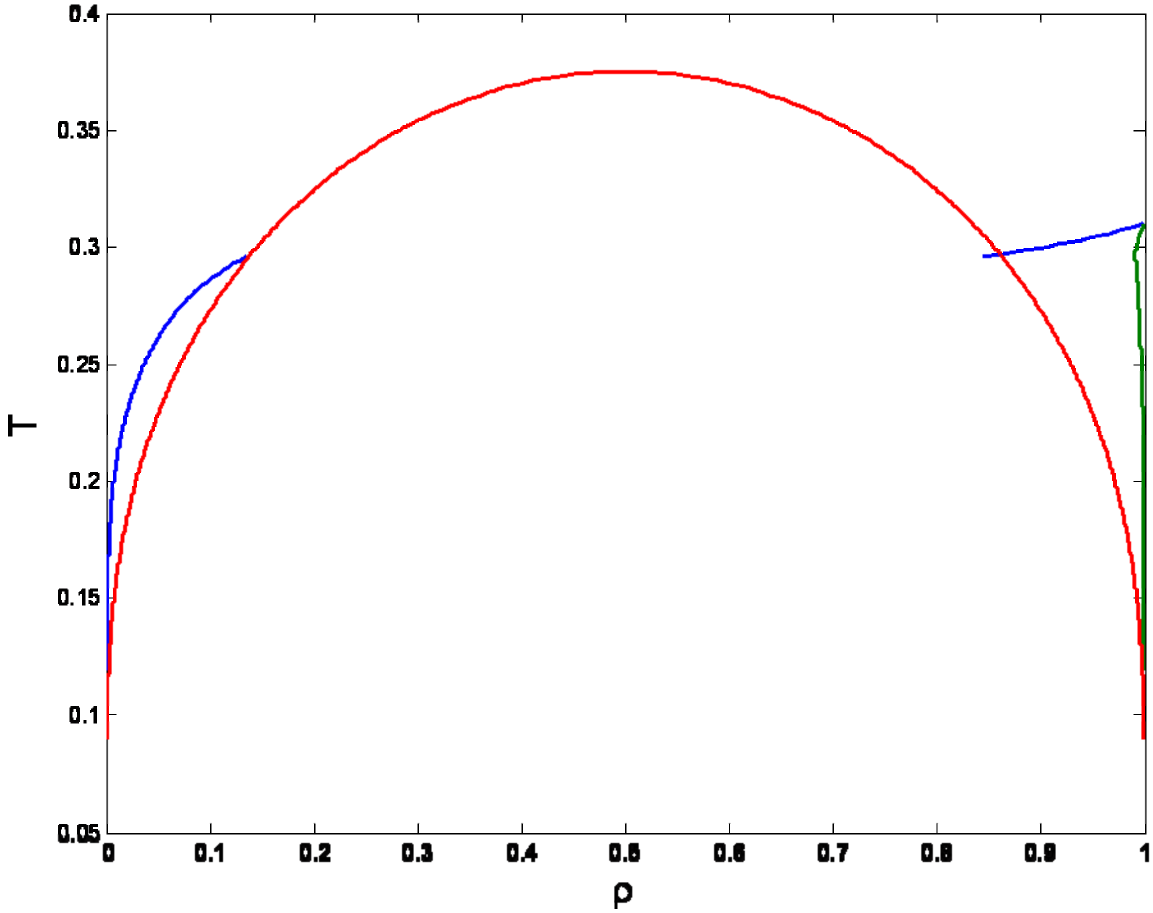

Figure D-1: The three dimensional phase diagram

The red line (——) represents the low density/high density solution coexistence curve. It is superseded by a coexistence between a low density solution represented as a blue line (——) and a high density ordered phase as shown as a green line(——). The fully-dense bimodal is T=0.31 and the spinodal is at T=0.14.

Just as before in the two dimensional case, the quench method whether a continuous quench from a random state, or in a step-wise pattern between previously cooled samples, does not change the average energy of the simulation sample as seen in Figure D-2. This indicates a path independence that further suggests the samples have achieved equilibrium.

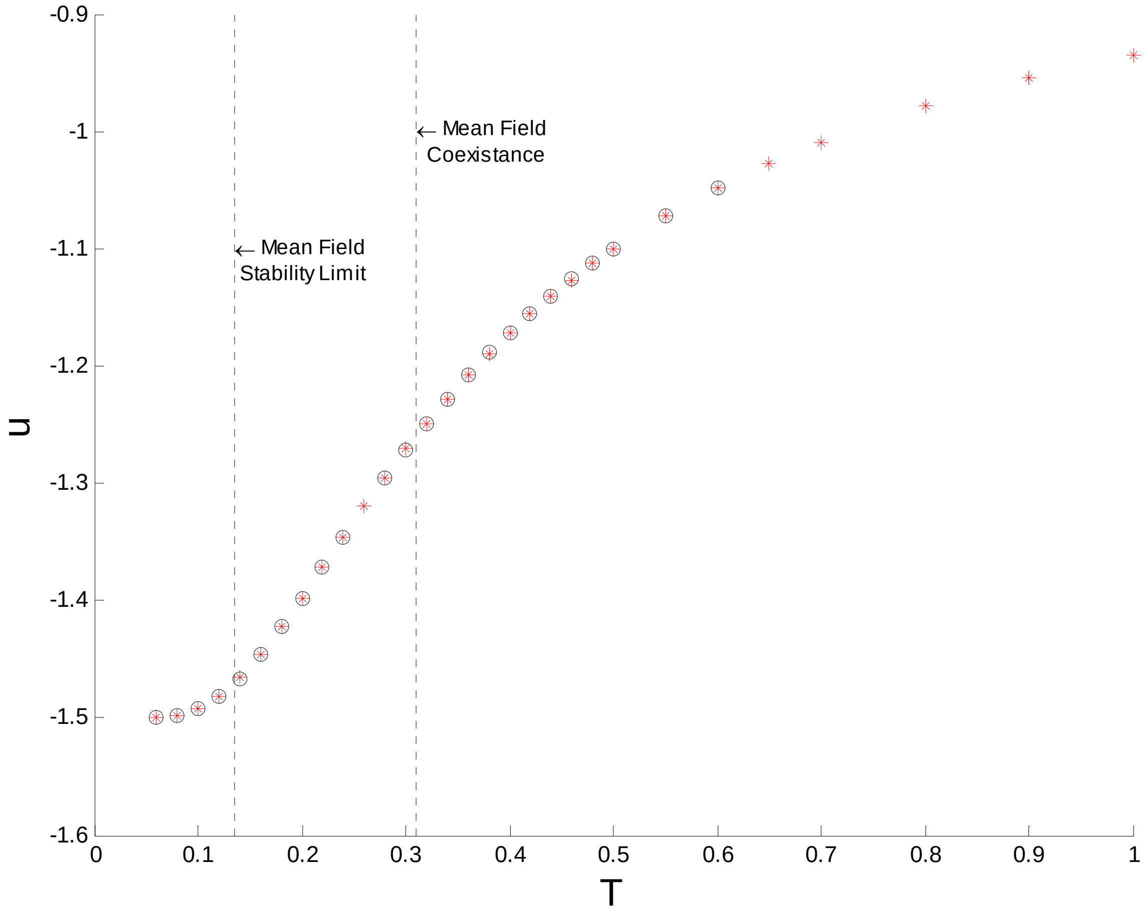

Figure D-2: Simulation results for different quench methods
The Metropolis MC method was used to quench the simulation samples to low temperature based on the choice of path. In the first method, simulation samples were initially in a random configuration and then quenched against the final temperature (o). In the second method, a simulation sample was equilibrated at high temperature and then cooled in a successive series of steps (*). The mean-field bimodal and spinodal are marked as reference temperatures.

We can take an preliminary look at the value of the heat capacity C_v. In our two-dimensional work, we considered three methods of evaluating C_v. In the end, the one we felt was the most representative in the end was fitting the internal energy curve to an analytic fitting function and taking the derivative. We have not shown that in Figure D-3. Instead, we have represented the calculation of C_v using the variance method taking the information directly from the instantaneously quenched simulation samples. As a reference, we also use the quick method of calculating the slope between two measurements with a simple difference method. These results suggest that the C_v maximum is higher than the mean-field spinodal. Whether this is due to the smaller sampling size, not using the preferred method of calculating C_v or some other reason, the impact of this observation on the fragile-to-strong crossover is not evaluated here.

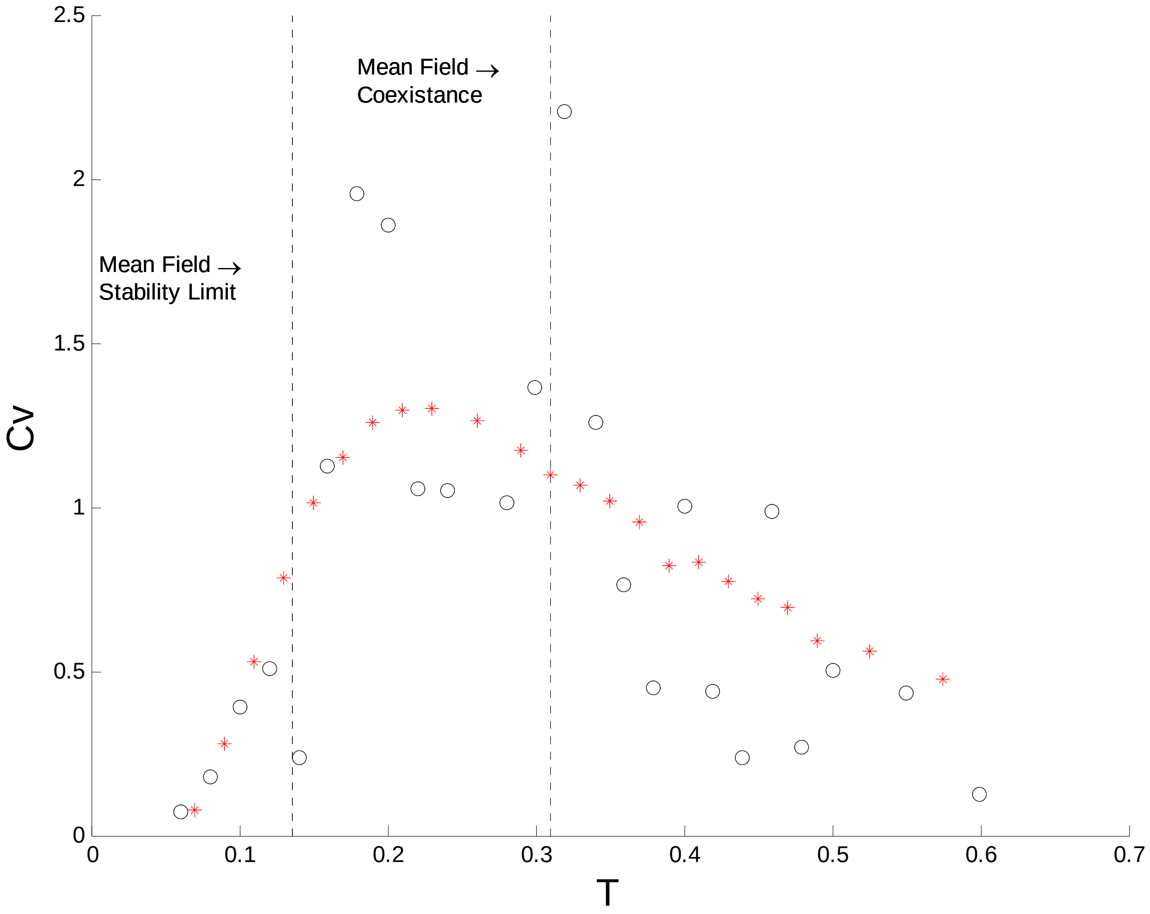

Figure D-3: Heat capacity measurements in the three dimensional model
The heat capacity is calculated by two methods. First, we use the variance from the simulation data itself to calculate the heat capacity (o). As a comparison, we employ a simple difference method to calculate the slope between data from the internal energy (*). The mean-field bimodal and spinodal are once again provided as reference.

One of the key aspects of this model is that it provides a greater than exponential number of ground states connected by very small barriers in energy. Each of the follow groupings is a locally oriented structure that can be tiled across a simulation sample and would result in every bond being satisfied. The boundaries of the tiles all are such that they are interchangeable so that the number of minima is greater than 4^N. There are also other tiling groupings that are not accounted for by combinations of these structures (not shown). Thus, increasing the dimensionality retains this important characteristic.

Figure D-4: Samples of possible locally oriented structures in three dimensions
These four structures could interchangeable be used to tile a large sample. Their boundary conditions match. Each structure is a 4 x 4 x 4 cube.

Appendix E: Stochastic Simulation Techniques

While increases in processor speed and new computational techniques have made simulations a powerful tool in analyzing many systems, they are still plagued by the diversity in size and time scales[110, 150, 151]. Thus, despite the intuitive appeal of molecular dynamics (MD) simulations or off-lattice calculations as incorporating 'more accurate physics', the increased efficiency of on-lattice kMC simulations allow for a much longer time-scale to be evaluated. In the following discussion, we shall parallel the description of MC simulation techniques outlined in Section 2.3.

Master Equation

We can visualize all possible states of the lattice as defining a hyper-dimensional energy surface (albeit discrete) in conformational space. For the purpose of describing this space, the state of the lattice will be identified as a lower case roman character, while the orientation of a specific molecule as a Greek character with a subscript describing its location on the simulation. A specific state m is located at the conformation coordinate $\vec{x}_m$, where $\vec{x}_m \equiv \left\{\sigma_{(1)}, \sigma_{(2)}, \cdots, \sigma_{(N)}\right\}$. The numerical subscripts define the location of the molecule σ on the square lattice. The energy at $\vec{x}_m$ is defined by the Hamiltonian previously described and motion along the surface occurs by the change in orientation of a single molecule. The system is coupled to a thermal bath allowing for transfer between states. This gives us at equilibrium results distributed according to the canonical ensemble; the probability $P_m(eq)$ that the system is located at $\vec{x}_m$, is given by

$$P_m(eq) = \frac{1}{Z}\exp\left(-\beta E_m\right)$$
$$Z = \sum_k e^{-\beta E_k} \tag{1}$$

where k includes all states.

The equilibrium probabilities are not known a priori, instead we use the master equation formalism such that any initial distribution explores conformation space as defined by[115]:

$$\frac{dP_m(t)}{dt} = \sum_k q_{k\to m} P_k(t) - \sum_k q_{m\to k} P_m(t) \tag{2}$$

The transition probabilities, $q_{k\to m}$, specify the choice of motion along the landscape from $\vec{x}_k$ to $\vec{x}_m$. At long-times, steady state should be reached, so the left hand side of (5) must go to zero and the probabilities $P_k(t)$ and $P_m(t)$ adopt their equilibrium value. This results in the condition of detail balance with:

$$q_{k\to m}\exp\left(-\beta E_k\right) = q_{m\to k}\exp\left(-\beta E_m\right) \tag{3}$$

We notice that the choice of transition probabilities is not unique. Our choice of Hamiltonian does not result in an analytically tractable master equation, so we solve for the dynamic and equilibrium properties using MC simulations[46, 116].

Metropolis Monte Carlo

Two different Monte Carlo simulation methods were employed for these studies. First, a simple Metropolis recipe[117] was employed for equilibration of the lattices. In this method, a specific molecule, $\sigma_\alpha(t;\vec{i})$, is chosen at based on a random choice of lattice vertex $\vec{i}$. Then a change in orientation of the molecule from $\alpha \rightarrow \gamma$ is proposed at random. We define the number of bonds that $\sigma_\alpha(t;\vec{i})$ forms with its near-neighbors as $b_\alpha(t;\vec{i})$. The transition state between state m and state n is defined as the difference in the energy between the two orientations is compared with a random number.

$$q_{m \to n} = \begin{cases} 1 \text{ if } e^{(1/T)(b_\gamma(t+1;\vec{i})-b_\alpha(t;\vec{i}))} > u \text{ (attempt accepted)} \\ \text{otherwise } 0 \text{ (attempt rejected)} \end{cases} \tag{4}$$

If the attempt is accepted, the molecule adopts the new orientation, $\sigma_\gamma(t+1;\vec{i})$. Otherwise the original orientation is retained, $\sigma_\alpha(t+1;\vec{i})$. N attempts (where N is the number of vertices on the lattice) is one MCS. The acceptance rate for this method was sufficiently large to cool to very low temperatures relative to the predicted mean-field transition as shown in Appendix C.

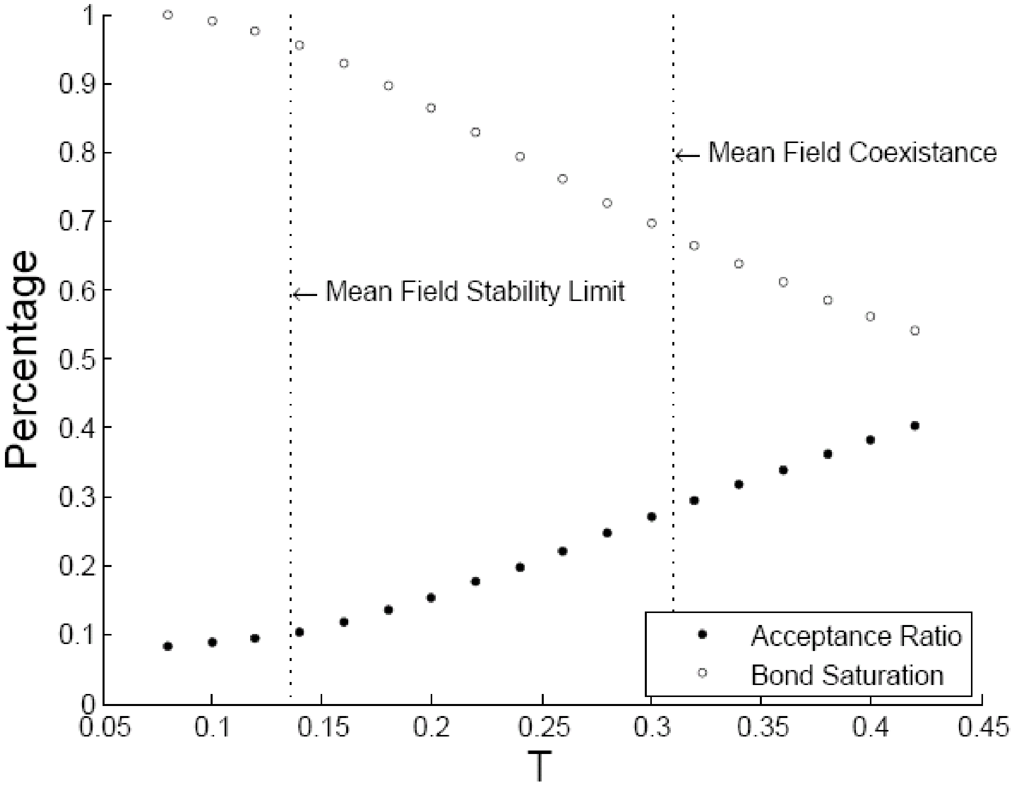

Figure E-1: Metropolis MC acceptance ratio and bond saturation temperature
Despite the 'bond saturation' or the percent of possible bonds which have been formed at low temperature, the 'acceptance ratio' or number of MC attempts which result in a change to the number of attempts made overall, remains relatively large.

Under the Metropolis algorithm, the probability of acceptance is a comparison of the initial and final states only. Although the rate of change of breaking a single bond increases exponentially with decreasing temperature, all transitions to lower or degenerate energy states are accepted. Thus, the method allows for a lattice to explore a large number of configurations quickly from a computational stance. While in our notation we indicate an attempt as an increment in time, $t+1$, the time has no explicit connection to physical time and therefore the dynamics do not have a clear definition. However, we note at equilibrium the distribution of states is expected to be canonical and any method which leads to the correct detail balance is acceptable[118, 119].

Kinetic Monte Carlo:

As we are investigating the properties of the vitrified state, which by definition are time dependent, we need to choose a simulation method which allows us to investigate the dynamics of our system. If the system resides for a considerable length of time within a stable or metastable state and then experiences a very quick (on the time scale of the residence time) transition between such states, the dynamics of the system may be highly dependent on rare transitions. An example of such an event is the difficulty in overcoming high potential energy barriers requiring large activation energies[110, 150]. In such cases, the runtime for a traditional MD simulation is prohibitive; the rare events are separated by an impractical number of MD steps and the sampling necessary to create an accurate thermodynamic ensemble exceeds conventional resources[150]. The wide variety of systems studied that include rare events, and the overall utility of the appropriate kMC simulation results has lead to the development of refined understanding of choice transition states and improved computational techniques [110, 119, 150, 152-161].

In addition to the two conditions described by (5) and (6), extracting dynamic details via kMC simulations requires us to define the of the conformational surface between $\vec{x}_m$ and $\vec{x}_k$ for all states m and k[118, 119]. We then form a dynamical hierarchy of transition rates $r_{m\to k}$ that would reflect the expected behavior of the model system both at equilibrium as well as in non-equilibrium case. The transition probabilities are defined as

$$q_{m\to k} = \frac{r_{m\to k}}{\xi_{\max}} \tag{5}$$

where $\xi_{\max}$ is greater than or equal to the largest transition rate[118]. A wide variety of systems have been studied using this technique[27, 118, 119, 151, 162, 163]. Many examples such of reaction rates have been directly proposed using the general properties of transition state theory or meet its requirements. Transition-state theory proposes that the transition rate $r_{m\to k}$ is dependent on the details of reaching the saddle point $x^*_{m\to k}$ along the path in between $\vec{x}_m$ and $\vec{x}_n$ [115, 163]. It has been noted that the specific form of the transition probabilities influences the non-equilibrium simulation time[156], even leading to incorrect growth exponents[119]. Kang and Weinberg point out that in most cases the energetic barrier from the initial state, $\vec{x}_m$, to the transition state $x^*_{m\to k}$, describes the microscopic transition process[119].

In our model, we neglect any microscopic energetic details of a simulation sample in state m favoring instead a common vibration frequency, ω. The transition probabilities $q_{m\to n}$ reflect of the potential energy difference between $\vec{x}_m$ and $\vec{x}^*_{m\to n}$

$$q_{m\to n} = \omega \exp(-\beta(E^* - E_m)) \tag{6}$$

where ω^{-1} becomes the fundamental time scale. Conveniently, because each state is linked via the rotation of a single molecule σ_m, we define $E^* - E_m$ as the number of bonds that specific molecule had at state m, which are broken to move to the saddle point. With this choice of the transition probability, there is no impact of the final orientation of that molecule on the transition probability and meets the requirements of detail balance.

We have several large separations between time scales on our lattice. The fastest processes are not activated or cooperative events. The exploration of the local minima, the fastest process, has already been reduced to a constant. We accomplished this by incorporating all β-relaxations (exploration of the local minima) into a single thermal variable, ω, which we assume to be temperature independent over the range of our simulations and the same for all wells. This establishes a reference time for our system. The transitions between basins do have a significant dependence on the local topology of the PEL. Even with our simple set of transition rates, at low temperatures the difference in breaking a single bond as opposed to three bonds is very significant. We can see this clearly from the plateaus in Figure 2.5.2. Additionally, in the case of a molecule has no bonds with its neighbors there is also fast event taking place on a time scale distinct from the kinetically activated rotations. This is discussed below and illustrated in Figure E-2 and Figure E-3.

By definition, any kinetic MC simulation uses the current transition rate dependent relationship:

$$\Delta t = \frac{-\log(u)}{\sum_m n_m q_m} \tag{7}$$

where u is a random number, q_i is the transition rate for each possible process, in our case given by equation (6). The number of states which can change due to that process is n_m, for our model this is $\sum_{\vec{i}} b_\alpha(t;\vec{i})$. It is important to remember that while at most only one transition occurs between steps, the 'clock' of elapsed time is running for all molecules in parallel, so we need to include all of them in the time increment.

Because we are investigating the low temperature properties of these simulations, using traditional importance methods of proposing a new state[46] and then accepting or rejecting that move does not improve the simulation time significantly because of the large number of rejected moves. Instead, a residence time or 'n-fold'[118, 120, 121] technique in which an event is selected with the appropriate frequency based on the transition rate and every event is accepted improves the time considerably. The transition probabilities and determination of elapsed real time is the same as any other kMC technique.

This technique is requires that the set of available configuration states and their transition properties are know a priori, [27, 151, 164]. The most computationally intensive portion of the method is creating the list of possible transitions with their relevant rates. We are favored in our case by the limited range of our potential, which makes updating this list reasonable.

To enact this process for our, we evaluate the bond energy at every vertex $b_\alpha\left(t;\vec{i}\right)$ and then grouped the same energies and weight them by the appropriate transition probability as given in (6). Therefore we have the intervals:

$$\left[0,\frac{p_0(t)}{p_{tot}(t)}\right),\left[\frac{p_0(t)}{p_{tot}(t)},\frac{\sum_{m=0}^{1}p_m(t)}{p_{tot}(t)}\right),\left[\frac{\sum_{m=0}^{1}p_m(t)}{p_{tot}(t)},\frac{\sum_{m=0}^{2}p_m(t)}{p_{tot}(t)}\right),\left[\frac{\sum_{m=0}^{2}p_m(t)}{p_{tot}(t)},\frac{\sum_{m=0}^{3}p_m(t)}{p_{tot}(t)}\right]$$
$$\begin{aligned}&where\\&p_{tot}(t)=p_0(t)+p_1(t)+p_2(t)+p_3(t)\\&p_{tot}(t)=\omega n_o(t)+n_1(t)\omega e^{-1/T}+n_2(t)\omega e^{-2/T}+n_2\omega(t)e^{-3/T}\end{aligned}\tag{8}$$

We then generate a random number u and find the corresponding interval. A second random number is chosen to decide which specific monomer will change. The rotation change is proposed by a third random number. Finally the physical time is updated using equation (7). This completes one step. The values of n_m are updated for the new time step and the cycle repeats.

An 'instantaneous' quench rate, in which we initialize a simulation sample in a random configuration and run the kMC simulation at the final temperature shows an extreme example of this behavior. This choice was used in both the results presented in Sections 2.5.2 and 0. The two figures below are representations of the initial portion of the these simulations to demonstrate the effect of the various rates on time progression. One advantage of the residence time kMC technique is that the time between steps changes with the configuration of the lattice. When there are many slow processes, the time step is small.

However if these processes are reduced, the time step becomes larger in a dynamic fashion. In Figure E-2, the ‘physical time’ and is shown after 1000 MCS at a variety of temperatures. Notice that there is a non-monotonic relationship between the progressed time and temperature.

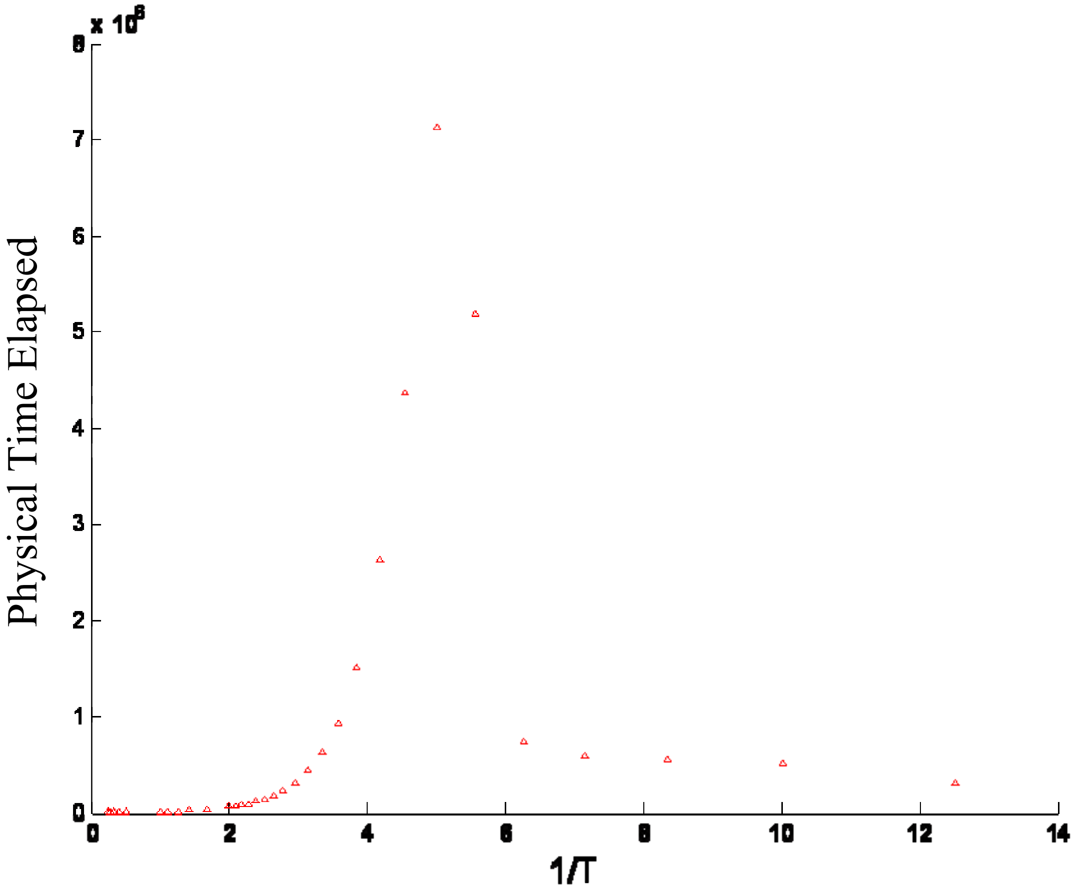

Figure E-2: Physical time at 1000MCS for a variety of temperatures
Despite the same number of successful attempts, the amount of physical time that has elapsed is dramatically different at different temperatures.

For the same ‘snap shot’ in time above, we report the number of monomers we report the fastest process, which would result in the smallest progression in physical time for each MCS.

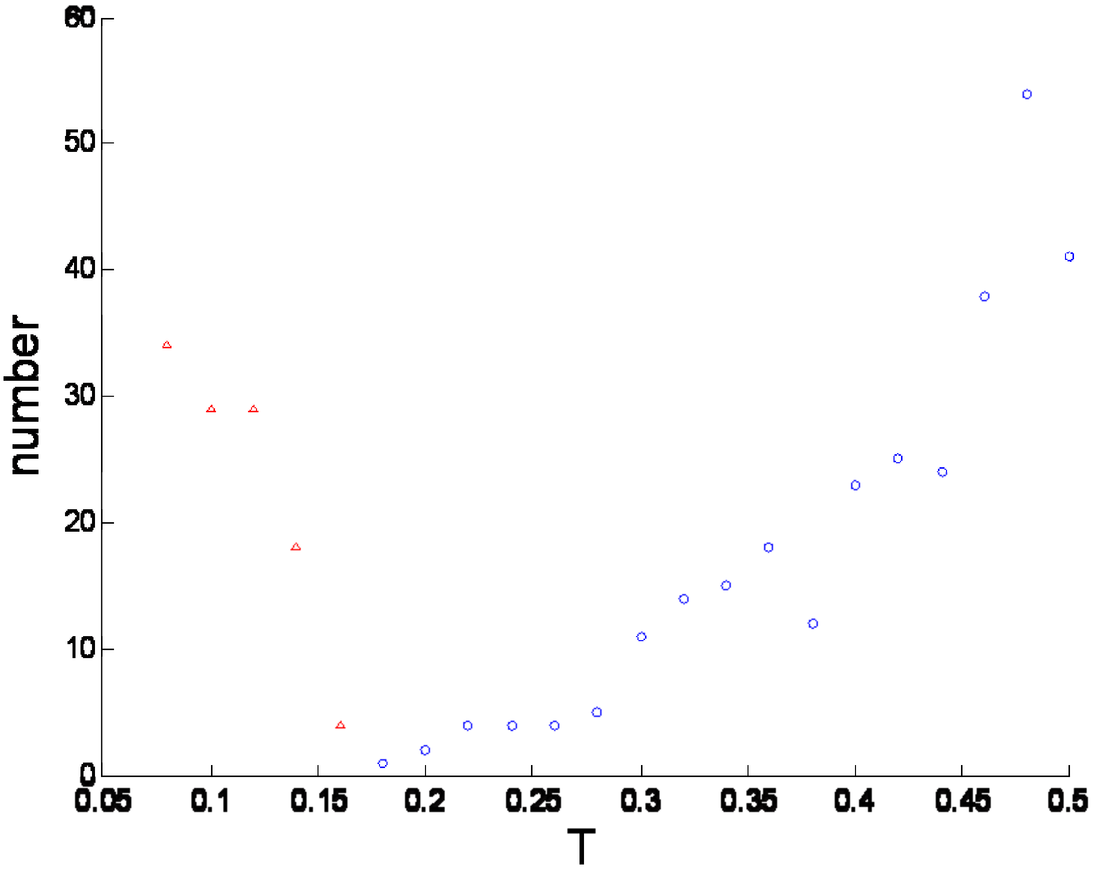

Figure E-3: The number of non-bonded molecules at 1000 MCS as a function of T
Notice that the smallest number of non-bonded molecules after the same number of MC attempts which were successful is the smallest where the elapsed time in Figure E-2 is the largest. This indicates that this fast process was selected with greater frequency. The change in color of symbols indicates whether the simulation was close to its final temperature (o) or still had a long way to progress before it would relax fully (Δ).

The elapsed physical time in each simulation is a dynamic quantity, responding to the distribution of molecules in different bonding states. Thus the accepted simulation step drives will be smaller when there are more fast processes, but then become larger if the number of these processes decreases and the accepted steps are related to the slower, activated events. This is one of the advantages of this technique. There also may be a true dynamic consequence to this pattern of non-bonded states, a relationship that should be explored further in subsequent work.

Appendix F: Calculation of the Heat Capacity from Monte Carlo Simulations

Employing a kinetic Monte Carlo recipe, we can define the relaxation time of a simulation sample by noting that there is a difference of the expectation value of the error when subsequent observations are correlated in time. When deriving the correlation function, we need to exercise great caution in specifying what assumptions are being made. We start our analysis of the correlation function by defining an observable A_t which may be a continuous value such as the energy, or a discrete value such as the state of the lattice sample at time *t*. Properly, an ensemble average would imply averaging over configurational space or time, which are equivalent in an equilibrium system. However we are going to be generous with our definition of ensemble average to include systems which are metastable, that is, are not strictly at equilibrium, but are arrested in a subset of configurational space.

As an MC simulation reflect movement over the PEL, subsequent observations are highly correlated. This provides a difficulty in using the variance, σ, to measure the heat capacity of a simulation because the calculation of expectation value of the variance, $\overline{\delta A^2}$, deviates from σ non-trivially. As we note in our work, the C_v calculation from the derivative of an arbitrarily fit to the energy follows the same trend as the C_v calculated with the measured variance, a relationship shown in Figure F-1. However we also note that as more observations are made, the two values become closer.

How closely does the expectation value of the variance match the actual value as a function of the number of observations? We shall answer that question in two parts. Initially we will ignore the correlated values and see how the accuracy of expectation value of the variance to the relates to the number of measurements during simple sampling. Then we shall address the more complex case of how the variance is related to the correlation (or relaxation) time.

Formally, we start with the assumption that we are measuring independent observations of a quantity A which obeys a Gaussian distribution with mean $\langle A \rangle$ and variance, $\sigma = \langle A^2 \rangle - \langle A \rangle^2$. If we make a set of n observations of the distribution, $\{A_i\}$, the unbiased estimator of the mean is:

$$\overline{A} = \frac{1}{n}\sum_{i=1}^{n} A_i \tag{1}$$

as we have no other information about the sampling or the distribution. Similarly, the deviations from the observations quantity, $\delta A_i = A_i - \overline{A}$, allow us to find the expectation value of the variance.

$$\begin{aligned}\overline{(\delta A)^2} &= \frac{1}{n}\sum_{i=1}^{n}\left(A_i - \overline{A}\right)^2 \\ &= \frac{1}{n}\sum_{i=1}^{n}\left(A_i^2 - 2A_i\overline{A} + \overline{A}^2\right) \\ &= \overline{A^2} - 2\overline{A}\left(\overline{A}\right) + \overline{A}^2 \\ &= \overline{A^2} - \overline{A}^2\end{aligned} \tag{2}$$

If we assume that there is no correlation between measurements, the order of summation of the set may be changed (i.e. indices i and j may be interchanged if this violates no other rule of summation). However we do have the restriction that the observations are not equally weighted, although we do not have further information about the value of the weights. Thus this correlation, that the term A_iA_i has more information than A_iA_j, which provides the first correction to the expectation value.

$$\begin{aligned}\left\langle \overline{\delta A^2} \right\rangle &= \left\langle \frac{1}{n}\sum_{i=1}^{n} A_i^{\,2} - \left(\frac{1}{n}\sum_{i=1}^{n} A_i\right)\left(\frac{1}{n}\sum_{j=1}^{n} A_j\right) \right\rangle \\ &= \left\langle \frac{1}{n}\sum_{i=1}^{n} A_i^{\,2} - \frac{1}{n^2}\sum_{i=1}^{n} A_i A_i - \left(\frac{1}{n}\sum_{i=1}^{n} A_i\right)\left(\frac{1}{n}\sum_{i\neq j=1}^{n-1} A_j\right) \right\rangle\end{aligned} \tag{3}$$

The ensemble average can be moved inside the summations. The individual values $A_i A_j$ and A_i^2 are each replaced by the values $\left\langle A \right\rangle^2$ and $\left\langle A^2 \right\rangle$.

$$\begin{aligned}\left\langle \overline{\delta A^2} \right\rangle &= \left\langle \left\langle A^2 \right\rangle \frac{1}{n}\sum_{i=1}^{n} 1 - \left\langle A^2 \right\rangle \frac{1}{n^2}\sum_{i=1}^{n} 1 - \left\langle A \right\rangle^2 \left(\frac{1}{n^2}\sum_{i=1}^{n}\sum_{i\neq j=1}^{n-1} 1\right) \right\rangle \\ &= \left\langle \left\langle A^2 \right\rangle - \frac{1}{n}\left\langle A^2 \right\rangle - \left(\frac{n(n-1)}{n^2}\right)\left\langle A \right\rangle^2 \right\rangle \\ &= \left(\left\langle A^2 \right\rangle - \left\langle A \right\rangle^2\right)\left(1 - \frac{1}{n}\right)\end{aligned} \tag{4}$$

From the expression (4) we can conclude that improving our estimate of the susceptibility goes as $1/n$ with uncorrelated observations. This shows one computational limit of these methods.

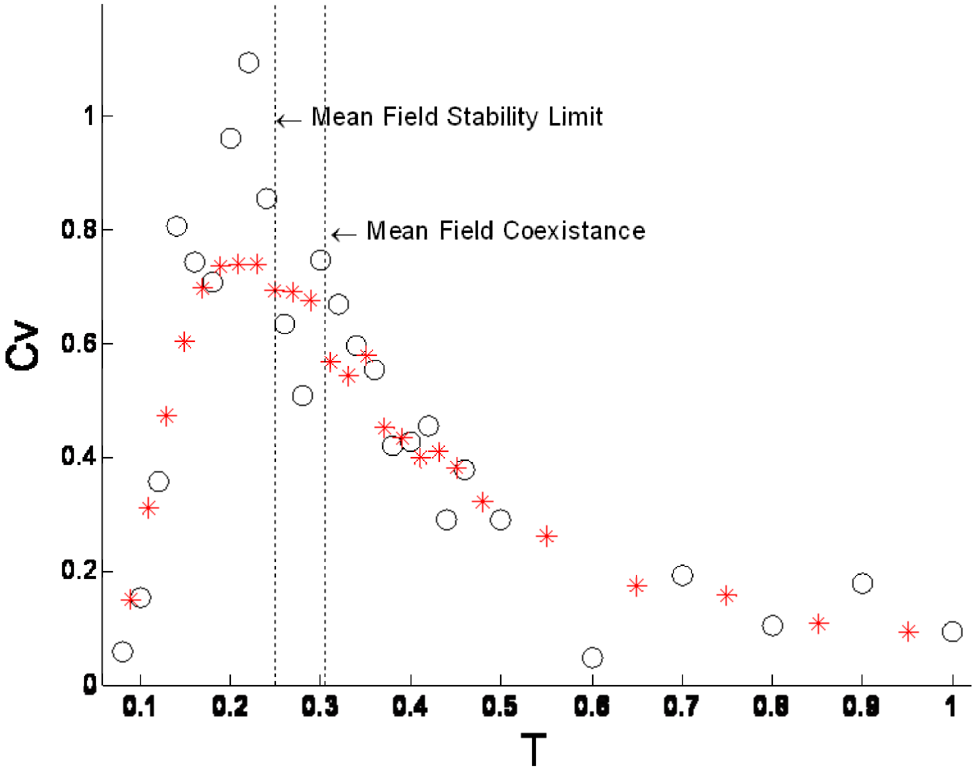

Figure F-1: Specific heat per site calculated by two different methods
The first method was using the slope of u found by simple difference method (*) and using the susceptibility calculated from the variance in the measurements (O)

We can now tighten again our assessment by removing the assumption that subsequent observation are uncorrelated. Returning to equation our original definitions, we remember that the set order is now important, and we cannot interchange indices in sums because they carry information about the order of observation.

$$
\begin{aligned}
\overline{(\delta A)^2} &= \left\langle \left[\frac{1}{n} \sum_{i=1}^{n} \left(A_i - \langle A \rangle \right) \right]^2 \right\rangle \\
&= \left\langle \frac{1}{n^2} \sum_{i=1}^{n} \left(A_i - \langle A \rangle \right) \sum_{k=1}^{n} \left(A_k - \langle A \rangle \right) \right\rangle \\
&= \left\langle \frac{1}{n^2} \sum_{i=1}^{n} \sum_{k=1}^{n} \left(A_i A_k - A_i \langle A \rangle - A_k \langle A \rangle + \langle A \rangle^2 \right) \right\rangle \\
&= \left\langle \frac{1}{n^2} \sum_{i=k}^{n} \left(A_i^2 - 2A_i \langle A \rangle + \langle A \rangle^2 \right) + \frac{2}{n^2} \sum_{i=1}^{n} \sum_{k=i+1}^{n} \left(A_i A_k - \left(\frac{A_i + A_k}{2} \right) \langle A \rangle \right) \right\rangle \\
&= \frac{1}{n} \left[\left\langle A^2 \right\rangle - \langle A \rangle^2 \right] + \frac{2}{n} \sum_{i=1}^{n} \sum_{k=i+1}^{n} \left(\langle A_i A_k \rangle - \langle A \rangle^2 \right)
\end{aligned}
\tag{5}
$$

Next we notice that there is no specific event that breaks the time symmetry between two observations. Thus only the magnitude of $\delta t = |t_k - t_i|$ is important. Therefore, $\langle A_i A_k \rangle =$ $\langle A_0 A_{k-i} \rangle$. Therefore, if we define $t' \equiv k - i$ we can remove one of the summations.

$$
\begin{aligned}
\left\langle \overline{(\delta A)^2} \right\rangle &= \frac{1}{n} \left[\left\langle A^2 \right\rangle - \langle A \rangle^2 \right] + \frac{2}{n^2} \sum_{i=1}^{n} \left[\sum_{k=i+t}^{n} \left(\langle A_i A_k \rangle - \langle A \rangle^2 \right) - \sum_{k=i+1}^{t} \left(\langle A_i A_k \rangle - \langle A \rangle^2 \right) \right] \\
&= \frac{1}{n} \left[\left\langle A^2 \right\rangle - \langle A \rangle^2 \right] + \frac{2}{n} \sum_{t=1}^{n} \left(1 - \frac{t}{n} \right) \left(\langle A_0 A_t \rangle - \langle A \rangle^2 \right)
\end{aligned}
\tag{6}
$$

This already has the form of a response function embedded in it. If we proceed carefully through the integration we find that the integrated response function can be directly related to the expectation value of the response as[46]:

$$
\left\langle \overline{(\delta A)^2} \right\rangle = \frac{\sigma^2}{n} \left(1 + 2 \frac{\tau_A}{\delta t} \right) \tag{7}
$$

Appendix G: Inherent Structures on the Energy Landscape

While there is compelling evidence for the existence of spatial heterogeneity, it is not known if it is a universal characteristic of glassy systems or how it originates. Sastry et al. [165] ran molecular dynamics (MD) simulations of a binary Lennard-Jones mixture. They found that the exploration of the potential energy landscape by the system was distinctly different in the high temperature (above T_g) and low temperature (below T_g) region. In the high temperature region, the average energy was insensitive to temperature; however, the distribution in energy of the inherent structures of the explored basins was high. At low temperature the average energy again changed little with temperature, however the system explored only basins with low energy inherent structures. The transition between these two plateaus in the average energy of the inherent structures was dramatic.[165]

We develop a Metropolis based scheme for exploring the configuration space of the fully-dense lattice. In these simulations we first equilibrate the lattice at a particular temperature. Then we can explore the energy landscape using zero temperature quench[166] and evaluate relaxation time with different correlations. Results indicate that the simulations have glassy dynamics, even using the Metropolis recipe.

We perform a zero temperature quench to identify the inherent structures. During the zero temperature quench, no annealing is possible; the system can never gain potential energy[75]. In our model there are numerous (and often broad) saddles in our potential energy surface. Thus not all basins are uniquely defined. We modified an algorithm used by Glotzer et al. for these non-unique minimizations[166].

After we allow the lattice to equilibrate, we have the lattice continue to explore configuration space using the algorithm above. Every 1000 MCS we identify the inherent structure. First we perform one MCS accepting all states with lower potential energy. If a suggested change in molecule orientation has the same energy it is not accepted. Then we perform a second MCS using the heat bath method[46] suggested by Glotzer et al. The heat bath method accepts all moves with lower potential energy, ½ of the moves with equal potential energy and none of the moves with higher potential energy. These two steps are repeated until the energy no longer decreases between steps or a minimum of 100 times.

Preliminary data shows that the difference in the potential energy of the inherent structures with temperature is very small, on the order of a tenth of a percent, see

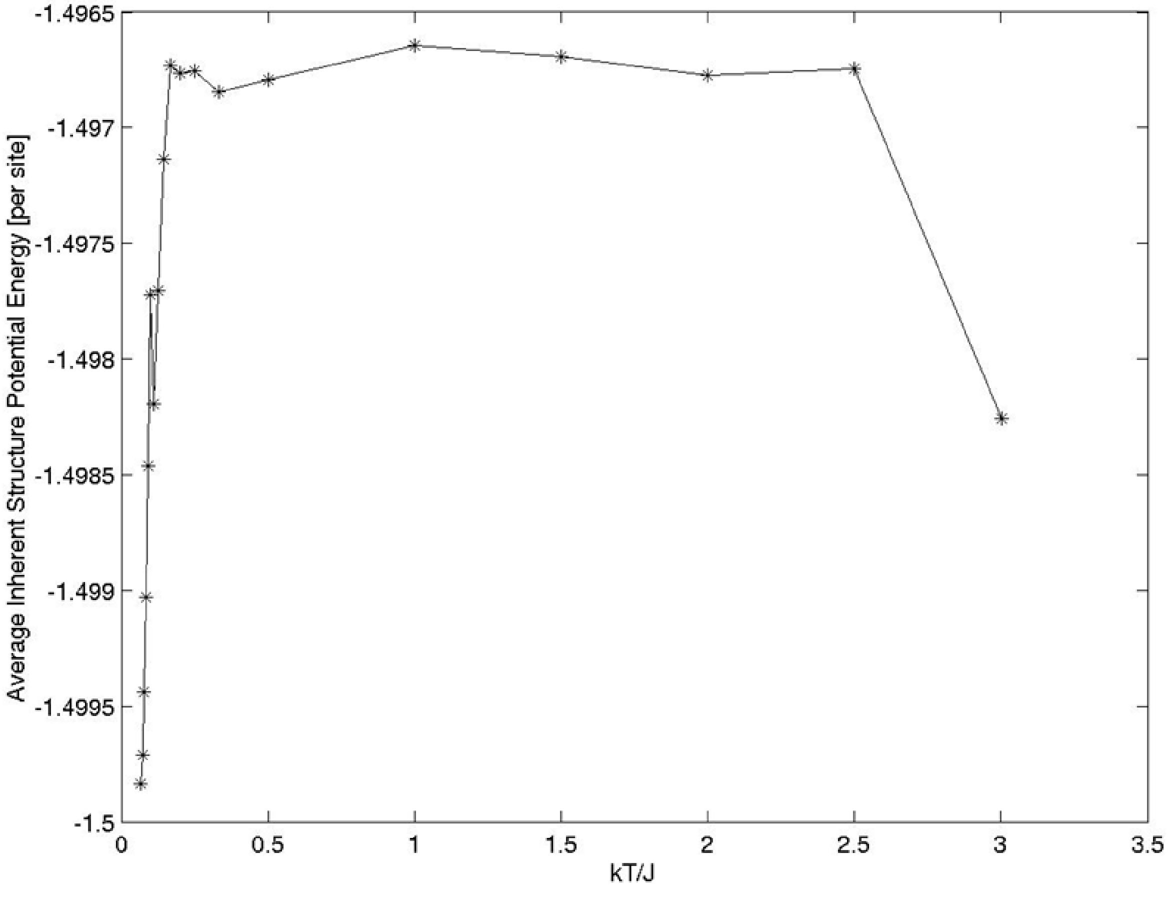

Figure **G-1**. This is smaller than those reported elsewhere. We do not yet have sufficient data to resolve a trend above the error bars. But it is very unlikely that with more data we could see the types of trends shown with both a high and low temperature plateau[165, 166]. This suggests that our data is more consistent with the change in behavior appearing at the FSC as has been documented in silica[72].

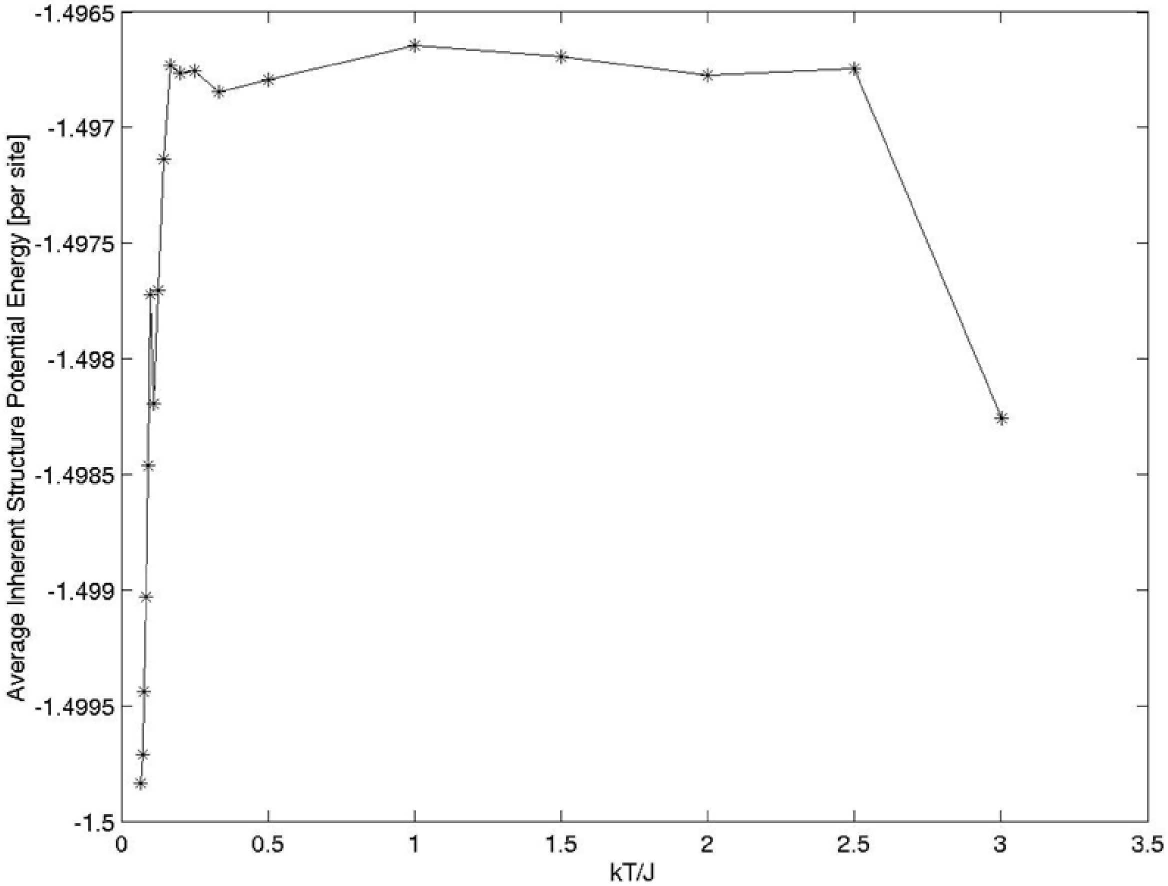

Figure G-1: Average inherent structure potential energy as a function of T
Beginning with an equilibrated Metropolis MC simulation at the T reported. The lattice size is 40 by 40 with a TAM at every site. Average potential energy of the 100 inherent structures is shown. Recall that the random (infinite temperature) potential energy of this model is –1.125 and the potential energy of a fully satisfied structure is –1.5.

Bibliography

1. Witman, J.; Wang, Z.-G., A lattice model of vitrification and gelation. *Journal of Physical Chemistry B* **2006,** 110, (12), 6312-6324.

2. Zaccarelli, E., Colloidal gels: equilibrium and non-equilibrium routes. *Journal of physics. Condensed matter* **2007,** 19, (32), 323101.

3. Largo, J.; Starr, F. W.; Sciortino, F., Self-assembling DNA dendrimers: A numerical study. *Langmuir* **2007,** 23, (11), 5896-5905.

4. Molinero, V.; Sastry, S.; Angell, C. A., Tuning of tetrahedrality in a silicon potential yields a series of monatomic (metal-like) glass formers of very high fragility. *Physical Review Letters* **2006,** 97, (7), 4.

5. Xu, L.; Kumar, P.; Buldyrev, S. V.; Chen, S.-H.; Poole, P. H.; Sciortino, F.; Stanley, H. E., Relation between the Widom line and the dynamic crossover in systems with a liquid-liquid phase transition. *Proceedings of the National Academy of Sciences of the United States of America* **2005,** 102, (46), 16558-16562.

6. Foffi, G.; Sciortino, F., On the possibility of extending the Noro-Frenkel generalized law of correspondent states to nonisotropic patchy interactions. *Journal of Physical Chemistry B* **2007,** 111, (33), 9702-9705.

7. Sciortino, F., Gel-forming patchy colloids and network glass formers: thermodynamic and dynamic analogies. *The European physical journal. B* **2008,** 64, (3-4), 505-509.

8. Douglas, J. F., Theoretical Issues Relating to Thermally Reversible Gelation by Supermolecular Fiber Formation. *Langmuir* **2009,** 25, (15), 8386-8391.

9. Bergenholtz, J.; Fuchs, M.; Voigtmann, T., Colloidal gelation and non-ergodicity transitions. *Journal of Physics-Condensed Matter* **2000,** 12, (29), 6575-6583.

10. Zaccarelli, E.; Foffi, G.; Dawson, K. A.; Buldyrev, S. V.; Sciortino, F.; Tartaglia, P., Static and dynamical correlation functions behaviour in attractive colloidal systems

from theory and simulation. *Journal of Physics-Condensed Matter* **2003,** 15, (1), S367-S374.

11. Sciortino, F.; Mossa, S.; Zaccarelli, E.; Tartaglia, P., Equilibrium cluster phases and low-density arrested disordered states: The role of short-range attraction and long-range repulsion. *Physical Review Letters* **2004,** 93, (5), art. no. 055701.

12. Pham, K. N.; Puertas, A. M.; Bergenholtz, J.; Egelhaaf, S. U.; Moussaid, A.; Pusey, P. N.; Schofield, A. B.; Cates, M. E.; Fuchs, M.; Poon, W. C. K., Multiple glassy states in a simple model system. *Science* **2002,** 296, (5565), 104-106.

13. Dinsmore, A. D.; Weitz, D. A., Direct imaging of three-dimensional structure and topology of colloidal gels. *Journal of Physics-Condensed Matter* **2002,** 14, (33), 7581-7597.

14. Ren, S. Z.; Sorensen, C. M., Relaxations in Gels - Analogies to Alpha-Relaxation and Beta-Relaxation in Glasses. *Physical Review Letters* **1993,** 70, (11), 1727-1730.

15. Ikkai, F.; Shibayama, M., Static inhomogeneities in thermoreversible physical gels. *Physical Review Letters* **1999,** 82, (24), 4946-4949.

16. Gang, H. D.; Krall, A. H.; Cummins, H. Z.; Weitz, D. A., Emulsion glasses: A dynamic light-scattering study. *Physical review. E* **1999,** 59, (1), 715.

17. Foffi, G.; De Michele, C.; Sciortino, F.; Tartaglia, P., Scaling of Dynamics with the Range of Interactions in Short-Range Attractive Colloids. *Physical Review Letters* **2005,** 94, (078301).

18. Del Gado, E.; Fierro, A.; de Arcangelis, L.; Coniglio, A., Slow dynamics in gelation phenomena: From chemical gels to colloidal glasses. *Physical Review E* **2004,** 69, (5).

19. Kauzmann, W., The Nature of the Glassy State and the Behavior of Liquids at Low Temperatures. *Chemical Reviews* **1948,** 43, (2), 219-256.

20. Granasy, L.; Pusztai, T.; Borzsonyi, T.; Warren, J. A.; Douglas, J. F., A general mechanism of polycrystalline growth. *Nature Materials* **2004,** 3, (9), 645-650.

21. Bryngelson, J. D.; Wolynes, P. G., Intermediates and Barrier Crossing in a Random Energy-Model (with Applications to Protein Folding). *Journal of Physical Chemistry* **1989,** 93, (19), 6902-6915.

22. Silbert, L. E.; Ertas, D.; Grest, G. S.; Halsey, T. C.; Levine, D., Analogies between granular jamming and the liquid-glass transition. *Physical Review E* **2002,** 65, (5), art. no. 051307.

23. Mezard, M.; Parisi, G.; Virasoro, M. A., *Spin Glass Theory and Beyond*. World Scientific: Singapore 1987; p xiii, 461 p.

24. Palmer, R. G.; Stein, D. L.; Abrahams, E.; Anderson, P. W., Models of Hierarchically Constrained Dynamics for Glassy Relaxation. *Physical Review Letters* **1984,** 53, (10), 958-961.

25. Fredrickson, G. H.; Andersen, H. C., Facilitated Kinetic Ising-Models and the Glass-Transition. *Journal of Chemical Physics* **1985,** 83, (11), 5822-5831.

26. Jackle, J.; Eisinger, S., A Hierarchically Constrained Kinetic Ising-Model. *Zeitschrift Fur Physik B-Condensed Matter* **1991,** 84, (1), 115-124.

27. Weber, T. A.; Fredrickson, G. H.; Stillinger, F. H., Relaxation Behavior in a Tiling Model for Glasses. *Physical Review B* **1986,** 34, (11), 7641-7651.

28. Garrahan, J. P.; Chandler, D., Coarse-grained microscopic model of glass formers. *Proceedings of the National Academy of Sciences of the United States of America* **2003,** 100, (17), 9710-9714.

29. Aranovich, G. L.; Donohue, M. D., Modeling self-assembly in molecular fluids. *Journal of Chemical Physics* **2002,** 116, (16), 7255-7268.

30. Biroli, G.; Mezard, M., Lattice glass models. *Physical Review Letters* **2002,** 88, (2), art. no. 025501.

31. Cellai, D.; Cuevas, H.; Lawlor, A.; McCullagh, G. D.; Dawson, K. A., Competition between short-ranged attraction and short-ranged repulsion in crowded configurational space: A lattice model description. *Physical Review E* **2004,** 70, (2).

32. Ben-Naim, A. J., *Journal of Chemical Physics* **1971,** 54, 3682-3695.

33. Bell, G. M.; Lavis, D. A., 2-Dimensional Bonded Lattice Fluids 2. Orientable Molecule Model. *Journal Of Physics Part A General* **1970,** 3, (5), 568.

34. Silverstein, K. A. T.; Haymet, A. D. J.; Dill, K. A., A Simple Model of Water and the Hydrophobic Effect. *Journal of the American Chemical Society* **1998,** 120, 3166.

35. Girardi, M.; Figueiredo, W., A trimer model for water. *Journal of Chemical Physics* **2004,** 120, (11), 5285.

36. Poole, P. H.; Sciortino, F.; Grande, T.; Stanley, H. E.; Angell, C. A., Effect of Hydrogen Bonds on the Thermodynamic Behavior of Liquid Water. *Physical Review Letters* **1994,** 73, (12), 1632.

37. Dellavalle, R. G.; Andersen, H. C., Molecular-dynamics simulation of silica liquid and glass. *Journal of Chemical Physics* **1992,** 97, (4), 2682.

38. Debenedetti, P. G., *Metastable Liquids:Concepts and Principles*. Princeton University Press: Princeton, 1996.

39. Stillinger, F. H.; Debenedetti, P. G., Alternative view of self-diffusion and shear viscosity. *Journal of Physical Chemistry B* **2005,** 109, (14), 6604.

40. Kumar, S. K.; Douglas, J. F., Gelation in physically associating polymer solutions. *Physical Review Letters* **2001,** 8718, (18), art. no. 188301.

41. Grant, M. C.; Russel, W. B., Volume-Fraction Dependence of Elastic-Moduli and Transition-Temperatures for Colloidal Silica-Gels. *Physical Review E* **1993,** 47, (4), 2606-2614.

42. Kumar, S. K.; Panagiotopoulos, A. Z., Thermodynamics of reversibly associating polymer solutions. *Physical Review Letters* **1999,** 82, (25), 5060-5063.

43. Shibayama, M.; Ikkai, F.; Moriwaki, R.; Nomura, S., Complexation of Poly(Vinyl Alcohol) Congo Red Aqueous-Solutions .1. Viscosity Behavior and Gelation Mechanism. *Macromolecules* **1994,** 27, (7), 1738-1743.

44. Singh, Y., Hard-sphere glass and the density-functional theory of aperiodic crystals. *Physical Review Letters* **1985,** 54, (10), 1059.

45. Kawasaki, K., In *Phase Transitions and Critical Phenomena*, Domb, C.; Lebowitz, J. L., Eds. Academic Press: New York, 1972.

46. Landau, D. P.; Binder, K., *A Guide to Monte Carlo Simulations in Statistical Physics*. Cambridge University Press: New York, 2000.

47. Wang, Z.-G., Mean-Field Approximations and Coupled Maps for Kinetic Lattice Models. *Physical Review A* **1992,** 45, (2), 692-700.

48. Barker, A. A., Monte Carlo Calculations of Radial Distribution Functions for a Proton-Electron Plasma. *Australian Journal of Physics* **1965,** 18, (2), 119.

49. Marconi, U. M. B.; Tarazona, P., Dynamic density functional theory of fluids. *Journal of Chemical Physics* **1999,** 110, (16), 8032-8044.

50. Fraaije, J. G. E. M., Dynamic Density-Functional Theory for Microphase Separation Kinetics of Block-Copolymer Melts. *Journal of Chemical Physics* **1993,** 99, (11), 9202-9212.

51. It is not apparent that in the crystal-like state the probabilities of the three non-preferred orientations should be equal as there is not a symmetry breaking event in the direction transverse to the lamella direction. However our calculations found that this assumption holds for all temperatures.

52. Klein, W., Clusters and fluctuations at mean-field critical points and spinodals. *Physical Review Letters* **2000,** 85, (6), 1270.

53. Bagchi, B.; Cerjan, C.; Rice, S. A., *Journal of Chemical Physics* **1983,** 79, 5595.

54. Woodcock, L. V., Glass-Transition In The Hard-Sphere Model And Kauzmann Paradox. *Annals Of The New York Academy Of Sciences* **1981,** 371, (OCT), 274-298.

55. C.-Z. Zhang and Z.-G. Wang. Phys. Rev. E. Submitted.

56. Reichl, L. E., *A Modern Course in Statistical Mechanics*. 2nd ed.; John Wiley & Sons: New York, 1998.

57. The coefficent 9/8 in the energy term arises from multiplying the probability that two arms of molecules on adjacent sites are touching, multiplied by one half of the coordination number (3/4*3/4*4/2).

58. Rubinstein, M.; Dobrynin, A. V., Associations leading to formation of reversible networks and gels. *Current Opinion in Colloid & Interface Science* **1999,** 4, (1), 83-87.

59. Guenet, J.-M., *Thermoreversible Gelation of Polymers and Biopolymers*. Academic Press: San Diego, 1992.

60. Press, W. H.; Teukolsky, S. A.; Vertterling, W. T.; Flannery, B. P., 13.8 Spectral Analysis of Unevenly Sampled Data. In *Numerical Recipes in Fortran 77: The Art of Scientific Computing*, 2nd ed.; Cambridge University Press: New York, 2001; Vol. 1, pp 569-577.

61. Cahn, J. W., On spinodal decomposition. *Acta metallurgica* **1961,** 9, (9), 795.

62. Stabile glassy colloidal clusters that appear not to aggregate or coalescence have been observed experimentally; D. A. Weitz, private communication

63. De Gennes, P.-G., *Scaling Concepts in Polymer Physics*. Cornell University Press: Ithaca, N.Y., 1979.

64. Angell, C. A.; Ngai, K. L.; McKenna, G. B.; McMillan, P. F.; Martin, S. W., Relaxation in glassforming liquids and amorphous solids. *Journal of Applied Physics* **2000,** 88, (6), 3113-3157.

65. Debenedetti, P. G., Truskett, T. M., Lewis C.P., Theory of Supercooled Liquids and Glasses. In *Advances in Chemical Engineering ; 28. Molecular Modeling and Theory in Chemical Engineering*, Chakraborty, A., Ed. Academic Press: San Diego, Calif., 2001.

66. Sciortino, F., Potential energy landscape description of supercooled liquids and glasses. *Journal Of Statistical Mechanics-Theory And Experiment* **2005**.

67. Angell, C. A., Structural Instability and Relaxation in Liquid and Glassy Phases near the Fragile Liquid Limit. *Journal of Non-Crystalline Solids* **1988,** 102, (1-3), 205-221.

68. Xia, X. Y.; Wolynes, P. G., Microscopic theory of heterogeneity and nonexponential relaxations in supercooled liquids. *Physical Review Letters* **2001,** 86, (24), 5526-5529.

69. Adam, G.; Gibbs, J. H., On Temperature Dependence of Cooperative Relaxation Properties in Glass-Forming Liquids. *Journal of Chemical Physics* **1965,** 43, (1), 139.

70. Onuki, A., *Phase Transition Dynamics*. Cambridge University Press: Cambridge, 2002.

71. To reach cooler temperatures, we started with a high temperature simulation, which reaches equilibrium relatively quickly. This was then used as the starting point for the next coolest temperature. Working in this stepwise fashion colder and colder temperatures were reached.

72. Saika-Voivod, I.; Poole, P. H.; Sciortino, F., Fragile-to-strong transition and polyamorphism in the energy landscape of liquid silica. *Nature* **2001,** 412, 514.

73. Tanaka, F., Thermoreversible gelation driven by coil-to-helix transition of polymers. *Macromolecules* **2003,** 36, (14), 5392-5405.

74. Stillinger, F. H.; Debenedetti, P. G., Energy landscape diversity and supercooled liquid properties. *Journal of Chemical Physics* **2002,** 116, (8), 3353-3361.

75. Stillinger, F. H.; Weber, T. A., Hidden Structure in Liquids. *Physical Review A* **1982,** 25, (2), 978-989.

76. Stillinger, F. H.; Weber, T. A., Packing Structures and Transitions in Liquids and Solids. *Science* **1984,** 225, 983-989.

77. This argument is based on an exchange dynamics for the lattice. However, a flip (rotation) dynamics (as employed here in the DMF) would yield the same result. With a concentration of unpaired molecules being $\exp(-\beta\varepsilon)$, the probability that a randomly chosen satisfied molecule is turned into an unpaired one in unit time is

simply $\omega\exp\text{-}(\beta\varepsilon)$. The time it takes for the lattice to relax is such that $\tau\omega\exp(-\beta\varepsilon)\sim 1$, or $\tau\sim\omega\text{-}1\exp(\beta\varepsilon)$.

78. Monasson, R., Structural Glass-Transition and the Entropy of the Metastable States. *Physical Review Letters* **1995,** 75, (15), 2847-2850.

79. Nussinov, Z.; Rudnick, J.; Kivelson, S. A.; Chayes, L. N., Avoided critical behavior in O(n) systems. *Physical Review Letters* **1999,** 83, (3), 472-475.

80. Mezard, M.; Parisi, G., Statistical physics of structural glasses. *Journal of Physics-Condensed Matter* **2000,** 12, (29), 6655-6673.

81. Schmalian, J.; Wolynes, P. G., Stripe glasses: Self-generated randomness in a uniformly frustrated system. *Physical Review Letters* **2000,** 85, (4), 836-839.

82. Puertas, A. M.; Fuchs, M.; Cates, M. E., Comparative simulation study of colloidal gels and glasses. *Physical Review Letters* **2002,** 88, (9), art. no. 098301.

83. Dawson, K. A., The glass paradigm for colloidal glasses, gels, and other arrested states driven by attractive interactions. *Current Opinion in Colloid & Interface Science* **2002,** 7 218-227.

84. Sciortino, F., Disordered materials - One liquid, two glasses. *Nature Materials* **2002,** 1, (3), 145-146.

85. Stillinger, F. H.; Weber, T. A., Computer-Simulation of Local Order in Condensed Phases of Silicon. *Physical Review B* **1985,** 31, (8), 5262-5271.

86. Bhat, M. H.; Molinero, V.; Soignard, E.; Solomon, V. C.; Sastry, S.; Yarger, J. L.; Angell, C. A., Vitrification of a monatomic metallic liquid. *Nature* **2007,** 448, (7155), 787.

87. Zondervan, R.; Kulzer, F.; Berkhout, G. C. G.; Orrit, M., Local viscosity of supercooled glycerol near T-g probed by rotational diffusion of ensembles and single dye molecules. *Proceedings of the National Academy of Sciences of the United States of America* **2007,** 104, (31), 12628-12633.

88. Bedrov, D., Structural and dynamic heterogeneity in a telechelic polymer solution. *Polymer* **2004,** 45, (11), 3961.

89. Saksaengwijit, A.; Reinisch, J.; Heuer, A., Origin of the fragile-to-strong crossover in liquid silica as expressed by its potential-energy landscape. *Physical Review Letters* **2004,** 93, (23).

90. Largo, J.; Tartaglia, P.; Sciortino, F., Effective nonadditive pair potential for lock-and-key interacting particles: The role of the limited valence. *Physical Review E* **2007,** 76, (1), 4.

91. Liu, H.; Kumar, S. K.; Douglas, J. F., Self-assembly induced protein crystallization. *Physical Review Letters* **2009,** 103, 018101.

92. Akcora, P.; Liu, H.; Kumar, S. K.; Moll, J.; Li, Y.; Benicewicz, B. C.; Schadler, L. S.; Acehan, D.; Panagiotopoulos, A. Z.; Pryamitsyn, V.; Ganesan, V.; Ilavsky, J.; Thiyagarajan, P.; Colby, R. H.; Douglas, J. F., Anisotropic self-assembly of spherical polymer-grafted nanoparticles. *Nature Materials* **2009,** 8, (4), 354-U121.

93. Terech, P.; Weiss, R. G., Low Molecular Mass Gelators of Organic Liquids and the Properties of Their Gels. *Chemical Reviews* **1997,** 97, (8), 3133-3160.

94. De Michele, C.; Tartaglia, P.; Sciortino, F., Slow dynamics in a primitive tetrahedral network model. *Journal of Chemical Physics* **2006,** 125, (20), 8.

95. De Michele, C.; Gabrielli, S.; Tartaglia, P.; Sciortino, F., Dynamics in the presence of attractive patchy interactions. *Journal of Physical Chemistry B* **2006,** 110, (15), 8064-8079.

96. de Arcangelis, L.; Del Gado, E.; Coniglio, A., Complex dynamics in gelling systems. *European Physical Journal E* **2002,** 9, (3), 277-282.

97. Ediger, M. D., Spatially heterogeneous dynamics in supercooled liquids. *Annual Review of Physical Chemistry* **2000,** 51, 99-128.

98. Angell, C. A., Water-II is a strong liquid. *Journal of Physical Chemistry* **1993,** 97, (24), 6339-6341.

99. Ashwin, S. S.; Sastry, S. In *Low-temperature behaviour of the Kob-Andersen binary mixture*, 2003; Iop Publishing Ltd: 2003; pp S1253-S1258.

100. Middleton, T. F.; Wales, D. J., Comparison of kinetic Monte Carlo and molecular dynamics simulations of diffusion in a model glass former. *Journal of Chemical Physics* **2004,** 120, (17), 8134-8143.

101. Sastry, S.; Angell, C. A., Liquid-liquid phase transition in supercooled silicon. *Nature Materials* **2003,** 2, (11), 739-743.

102. Saika-Voivod, I.; Sciortino, F.; Poole, P. H., Free energy and configurational entropy of liquid silica: Fragile-to-strong crossover and polyamorphism. *Physical Review E* **2004,** 69, (4).

103. Goldstein, M., Viscous liquids and glass transition- a potential energy barrier picture. *Journal of Chemical Physics* **1969,** 51, (9), 3728-&.

104. Stillinger, F. H., A topographic view of supercooled liquids and glass-formation *Science* **1995,** 267, (5206), 1935-1939.

105. Matyushov, D. V.; Angell, C. A., Gaussian excitations model for glass-former dynamics and thermodynamics. *Journal of Chemical Physics* **2007,** 126, (9), 19.

106. Tanaka, H., General view of a liquid-liquid phase transition. *Physical Review E* **2000,** 62, (5), 6968-6976.

107. Angell, C., Glass formation and glass transition in supercooled liquids, with insights from study of related phenomena in crystals. *Journal of Non-Crystalline Solids* **2008,** 354, (42-44), 4703-4712.

108. Hedges, L. O.; Jack, R. L.; Garrahan, J. P.; Chandler, D., Dynamic Order-Disorder in Atomistic Models of Structural Glass Formers. *Science* **2009,** 323, (5919), 1309-1313.

109. Lecomte, V.; Appert-Rolland, C.; van Wijland, F., Thermodynamic formalism for systems with Markov dynamics. *Journal of Statistical Physics* **2007,** 127, (1), 51-106.

110. Wales, D. J.; Bogdan, T. V., Potential energy and free energy landscapes. *Journal of Physical Chemistry B* **2006,** 110, (42), 20765-20776.

111. Ediger, M. D., Supercooled liquids and glasses. *Journal of Physical Chemistry* **1996,** 100, (31), 13200-13212.

112. Elmatad, Y. S.; Chandler, D.; Garrahan, J. P., Corresponding States of Structural Glass Formers. *Journal of Physical Chemistry B* **2009,** 113, (16), 5563-5567.

113. Sastry, S.; La Nave, E.; Sciortino, F., Maximum valency lattice gas models. *Journal of statistical mechanics* **2006**, (12), P12010.

114. Each vertex has four edges along which bonds may form. The probability that there is a bonding site from the monomer along a specific edge is 3/4; in the limit of high temperature there is no correlation in orientation of neighboring monomers. Each bond is shared by two monomers. This results in 4 x 3/4 x 3/4 x 1/2 =9/8 bonds/vertex.

115. Zwanzig, R., *Nonequilibrium Statistical Mechanics*. Oxford University Press: Oxford ; New York, 2001.

116. Smit, B.; Frenkle, D., *Understand Molecular Simulation*. 2nd ed.; Academic Press: San Diego, 2002; Vol. 1.

117. Metropolis, N.; Rosenbluth, A. W.; Rosenbluth, M. N.; Teller, A. H.; Teller, E., Equation of State Calculations by Fast Computing Machines. *Journal of Chemical Physics* **1953,** 21, (6), 1087-1092.

118. Fichthorn, K. A.; Weinberg, W. H., Theoretical Foundations of Dynamic Monte-Carlo Simulations. *Journal of Chemical Physics* **1991,** 95, (2), 1090-1096.

119. Kang, H.; Weinberg, W. H., Dynamic Monte-Carlo with a Proper Energy Barrier-Surface-Diffusion and Two-Dimensional Domain Ordering. *Journal of Chemical Physics* **1989,** 90, (5), 2824-2830.

120. Bortz, A. B.; Kalos, M. H.; Lebowitz, J. L., New Algorithm for Monte-Carlo Simulation of Ising Spin Systems. *Journal of Computational Physics* **1975,** 17, (1), 10-18.

121. Gillespie, D. T., General Method for Numerically Simulating Stochastic Time Evolution of Coupled Chemical-Reactions. *Journal of Computational Physics* **1976,** 22, (4), 403-434.

122. Di Marzio, E. A.; Yang, A. J. M., Configurational entropy approach to the kinetics of glasses. *Journal of Research of the National Institute of Standards and Technology* **1997,** 102, (2), 135-157.

123. Karmakar, S., Growing length and time scales in glass-forming liquids. *Proceedings of the National Academy of Sciences of the United States of America* **2009,** 106, (10), 3675-3679.

124. Simon, S. L.; McKenna, G. B., Experimental evidence against the existence of an ideal glass transition. *Journal of Non-Crystalline Solids* **2009,** 355, 672-675.

125. Mauro, J. C.; Gupta, P. K.; Loucks, R. J.; Varshneya, A. K. In *Non-equilibrium entropy of glasses formed by continuous cooling*, 2009; Elsevier Science Bv: 2009; pp 600-606.

126. Goldstein, M., On the reality of residual entropies of glasses and disordered crystals. *Journal of Chemical Physics* **2008,** 128, (15), 7.

127. Ediger, M. D.; Harrowell, P.; Yu, L., Crystal growth kinetics exhibit a fragility-dependent decoupling from viscosity. *Journal of Chemical Physics* **2008,** 128, (3), 6.

128. Capaccioli, S.; Ruocco, G.; Zamponi, F., Dynamically correlated regions and configurational entropy in supercooled liquids. *Journal of Physical Chemistry B* **2008,** 112, (34), 10652-10658.

129. Kuhlmann, C., Kinetic Ising model in two and three dimensions with constraints. *Physica Status Solidi - B - Basic Solid State Physics* **2005,** 242, (12), 2401-2411.

130. Sastry, S., Signatures of distinct dynamical regimes in the energy landscape of a glass-forming liquid. *Nature* **1998,** 393, (6685), 554-557.

131. Sciortino, F.; De Michele, C.; Douglas, J. F., Growth of equilibrium polymers under non-equilibrium conditions. *Journal of Physics-Condensed Matter* **2008,** 20, (15), 10.

132. Corezzi, S.; De Michele, C.; Zaccarelli, E.; Tartaglia, P.; Sciortino, F., Connecting Irreversible to Reversible Aggregation: Time and Temperature. *Journal of Physical Chemistry B* **2009,** 113, (5), 1233-1236.

133. Zaccarelli, E.; Buldyrev, S. V.; La Nave, E.; Moreno, A. J.; Saika-Voivod, I.; Sciortino, F.; Tartaglia, P., Model for reversible colloidal gelation. *Physical Review Letters* **2005,** 94, (21).

134. Vogel, M.; Glotzer, S. C., Temperature dependence of spatially heterogeneous dynamics in a model of viscous silica. *Physical Review E* **2004,** 70, (6), 13.

135. Huang, W.; Richert, R., Dynamics of glass-forming liquids. XI. Fluctuating environments by dielectric spectroscopy. *Journal of Chemical Physics* **2006,** 124, art. no. 164510.

136. Coniglio, A., Dynamical heterogeneities: from glasses to gels. *Journal of Physics-Condensed Matter* **2008,** 20, (49), 494239.

137. Berthier, L.; Biroli, G.; Bouchaud, J. P.; Cipelletti, L.; El Masri, D.; L'Hote, D.; Ladieu, F.; Pierno, M., Direct experimental evidence of a growing length scale accompanying the glass transition. *Science* **2005,** 310, (5755), 1797-1800.

138. Dalle-Ferrier, C.; Thibierge, C.; Alba-Simionesco, C.; Berthier, L.; Biroli, G.; Bouchaud, J. P.; Ladieu, F.; L'Hote, D.; Tarjus, G., Spatial correlations in the dynamics of glassforming liquids: Experimental determination of their temperature dependence. *Physical Review E* **2007,** 76, (4), 15.

139. Sastry, S., Liquid limits: Glass transition and liquid-gas spinodal boundaries of metastable liquids. *Physical Review Letters* **2000,** 85, (3), 590-593.

140. Chan, H. S.; Dill, K. A., Protein folding in the landscape perspective: Chevron plots and non-Arrhenius kinetics. *Proteins-Structure Function and Genetics* **1998,** 30, (1), 2-33.

141. Dill, K. A., Polymer principles and protein folding. *Protein Science* **1999,** 8, (6), 1166-1180.

142. Lois, G.; Blawzdziewicz, J.; O'Hern, C. S., Percolation Model for Slow Dynamics in Glass-Forming Materials. *Physical review letters* **2009,** 102, (1), art. no. 015702.

143. Liu, H.; Kumar, S. K.; Sciortino, F., Vapor-liquid coexistence of patchy models: Relevance to protein phase behavior. *Journal of Chemical Physics* **2007,** 127, (8), 5.

144. Bianchi, E.; Largo, J.; Tartaglia, P.; Zaccarelli, E.; Sciortino, F., Phase diagram of patchy colloids: Towards empty liquids. *Physical Review Letters* **2006,** 97, (16), 4.

145. Stauffer, D.; Aharony, A., *Introduction to Percolation Theory*. 2nd ed.; Taylor & Francis Inc.: Bristol, PA, 1994.

146. Vyssotsky, V., CRITICAL PERCOLATION PROBABILITIES (BOND PROBLEM). *Physical review* **1961,** 123, (5), 1566.

147. Domb, C.; Sykes, M. F., Cluster Size in Random Mixtures and Percolation Processes. *Physical Review* **1961,** 122, (1), 77.

148. Callen, H. B., *Thermodynamics and an Introduction to Thermostatistics*. 2nd ed.; John Wiley & Sons, Inc.: 1985.

149. Truskett, T. M.; Torquato, S.; Debenedetti, P. G., Towards a quantification of disorder in materials: Distinguishing equilibrium and glassy sphere packings. *Physical Review E* **2000,** 62, (1), 993-1001.

150. Dellago, C.; Bolhuis, P. G., Transition Path Sampling and Other Advanced Simulation Techniques for Rare Events. In *Advanced Computer Simulation Approaches for Soft Matter Sciences Iii*, Springer-Verlag Berlin: Berlin, 2009; Vol. 221, pp 167-233.

151. Battaile, C.; Srolovitz, D. J.; Butler, J. E., A kinetic Monte Carlo method for the atomic-scale simulation of chemical vapor deposition: Application to diamond. *Journal of Applied Physics* **1997,** 82, (12), 6293-6300.

152. Gilmer, G. H., COMPUTER-MODELS OF CRYSTAL-GROWTH. *Science* **1980,** 208, (4442), 355-363.

153. Hanggi, P.; Talkner, P.; Borkovec, M., Reaction-rate theory- 50 years after Kramers. *Reviews of Modern Physics* **1990,** 62, (2), 251-341.

154. Grunwald, M.; Dellago, C.; Geissler, P. L., Precision shooting: Sampling long transition pathways. *Journal of Chemical Physics* **2008,** 129, (19), 8.

155. Voter, A., Classically Exact Overlayer Dynamics - Diffusion of Rhodium Cluster on RH(100). *Physical review. B, Condensed matter* **1986,** 34, (10), 6819-6829.

156. Ray, L. A.; Baetzold, R. C., A Monte-Carlo estimation of surface-diffusion by simulating laser-induced thermal-desorption. *Journal of Chemical Physics* **1990,** 93, (4), 2871-2878.

157. Mayawala, K.; Vlachos, D. G.; Edwards, J. S., Computational modeling reveals molecular details of epidermal growth factor binding. *Bmc Cell Biology* **2005,** 6, 11.

158. Voter, A. F.; Doll, J. D., Dynamic corrections to transition-state theory for multistate systems- surface self diffusion in the rare-event regime. *Journal of Chemical Physics* **1985,** 82, (1), 80-92.

159. Maragliano, L.; Fischer, A.; Vanden-Eijnden, E.; Ciccotti, G., String method in collective variables: Minimum free energy paths and isocommittor surfaces. *Journal of Chemical Physics* **2006,** 125, (2), 15.

160. Voter, A. F.; Montalenti, F.; Germann, T. C., Extending the time scale in atomistic simulation of materials. *Annual Review of Materials Research* **2002,** 32, 321-346.

161. Geissler, P. L.; Dellago, C.; Chandler, D.; Hutter, J.; Parrinello, M., Autoionization in liquid water. *Science* **2001,** 291, (5511), 2121-2124.

162. Despa, F.; Wales, D. J.; Berry, R. S., Archetypal energy landscapes: Dynamical diagnosis. *Journal of Chemical Physics* **2005,** 122, (2), 8.

163. Grote, R. F.; Hynes, J. T., Reactive Modes in Condensed Phase Reactions. *Journal of Chemical Physics* **1981,** 74, (8), 4465-4475.

164. Chatterjee, A.; Vlachos, D. G., An overview of spatial microscopic and accelerated kinetic Monte Carlo methods. *Journal of Computer-Aided Materials Design* **2007,** 14, (2), 253-308.

165. Sastry, S.; Debenedetti, P. G.; Stillinger, F. H.; Schroder, T. B.; Dyre, J. C.; Glotzer, S. C., Potential energy landscape signatures of slow dynamics in glass forming liquids. *Physica a-Statistical Mechanics and Its Applications* **1999,** 270, (1-2), 301-308.

166. Glotzer, S. C.; Jans, N.; Poole, P. H., The potential energy landscape of the +/- J Ising spin glass. *Journal of Physics-Condensed Matter* **2000,** 12, (29), 6675-6682.